Effect of Silica Nanoparticles on Interfacial Tension and Crystallization of Poly(lactic acid) in Supercritical Carbon Dioxide

by

Kaveh Sarikhani

A thesis
presented to the University of Waterloo
in fulfillment of the
thesis requirement for the degree of
Doctor of Philosophy
in
Chemical Engineering

Waterloo, Ontario, Canada, 2016

AUTHOR'S DECLARATION

I hereby declare that I am the sole author of this thesis. This is a true copy of the thesis, including any required final revisions, as accepted by my examiners. I understand that my thesis may be made electronically available to the public.

ABSTRACT

Effect of Silica Nanoparticles on Interfacial Tension and Crystallization of Poly(Lactic Acid) in Supercritical Carbon Dioxide

Kaveh Sarikhani

In this thesis, the effect of silica nanoparticles on two of the most important parameters in the foaming of poly (lactic acid) (PLA) was studied: interfacial tension and crystallization. According to classical nucleation theory, the nucleation rate is inversely related to the exponential cubic power of interfacial tension, similarly the critical nucleation cell size to interfacial/surface tension. A decrease in surface tension decreases the energy barrier for cell nucleation and consequently increases the number of cells, leading to an exponential increase in cell density and smaller cell size. Solid nanoparticles, such as those made of silica, can be adsorbed at the interface and decrease the interfacial tension between polymer melt and surrounding fluid. They can also prevent coalescence through repulsion between two similar particles at the interface of two growing cells or increase in elasticity of the interface. Furthermore, nanoparticles can act as nucleating agents for the foaming of polymers by increasing local stress variations around the particles. In particular, nanoparticles can improve PLA crystallization, which is one of the approaches to address the low melt strength of PLA, one of the barriers for PLA foaming. In addition to melt strength, crystallization and crystallinity can further improve the mechanical properties of PLA.

At first, the interfacial behavior of the PLA/ supercritical carbon dioxide (CO_2) under foaming conditions was studied using Axisymmetric Drop Shape Analysis Profile (ADSA-P). The results showed a decrease in interfacial tension with increasing temperature and pressure, and a decrease in dependency of interfacial tension on temperature at high pressures.

As the next step, the interfacial tension of PLA composites made with surface- modified silica is studied. The interfacial tension between PLA and supercritical CO_2 decreased as a result of nanoparticles' adsorption to the interface. There was a minimum at 2 wt. % loading of the nanoparticles and the interfacial tension curve reached a plateau afterwards. The lateral capillary force of the adsorbed aggregates of the nanoparticles to the PLA-CO_2 interface was considered the reason for the observed increase in interfacial tension. Contact angle measurements at high pressures showed the affinity of the surface-modified nanoparticles to the polymer-supercritical CO_2 interface. A comparison of calculated binding energy of the nanoparticles to the PLA-CO_2 interface with thermal energy (k_BT) showed that the adsorption was irreversible.

Last, the crystallization behavior of PLA/surface-modified silica nanocomposites under isothermal, non-isothermal, and isothermal with compressed CO_2 conditions were studied. A significant improvement in crystallization rate was observed after introduction of amine-modified silica nanoparticles. A modified Hoffman-Lauritzen nucleation theory showed that the low surface energy of the modified nanoparticles and interfacial energy between polymer/nanoparticle facilitated the crystallization. Avrami exponents obtained from isothermal investigation of the nanocomposites indicated the sporadic formation of three-dimensional spherulites in the PLA matrix, which shift into the range of two-dimensional at higher temperatures. In the presence of compressed CO_2, crystallization rate increases, but at pressures higher than 21 bar no significant effect was observed. Nanocomposites of PLA samples with lower molecular weight and higher stereoregularity also showed a significant increase in crystallization rate with no change in crystallization mechanism in presence of the nanoparticles.

ACKNOWLEDGEMENTS

I would like to thank my supervisor, Professor Pu Chen, for his continuous guidance, patience, and support during my PhD and his commitment towards development of the spirit and skill of research in me.

I would also like to pass my great appreciation to my co-supervisors, Professor Chul B. Park and Professor Russell Thompson for their insightful comments, guidance, and encouragement throughout my PhD. Many thanks to all my friends and colleagues at the University of Waterloo and the members of Biomedical Engineering and Energy Storage Group for their help and support especially to Kazem Jeddi, Rasool Nasseri, Hamed Shahsavan, and Madjid Soltani.

I cordially acknowledge the financial support from the Natural Sciences and Engineering Research Council (NSERC) through the Network for Innovative Plastic Materials and Manufacturing Processes (NIPMMP), Ontario Centers of Excellence, and Canada Research Chairs (CRC).

A warm thank you to my co-op students: Sukrit Rajpal, Chunghwan (Christian) Park, Han Kyul (Sue) Oh, and Victor Lotocki for their assistance and help in the lab.

Last but not least, my special feeling of gratitude to my loving parents and brothers for their love, support, and presence throughout my whole life.

DEDICATION

To my beloved parents for their endless love and support

Table of Contents

LIST OF TABLES

LIST OF FIGURES

1. CHAPTER 1: INTRODUCTION AND THESIS OBEJCTIVES

1.1 Introduction

Foams are interesting materials consisting of a dispersion of voids in a dense continuum [1]. Among foams, polymeric foams have attractive mechanical, energy-absorbing, and thermal-insulation properties [2]. Foams are made of either chemical blowing agents or physical blowing agents. Although the former have drawbacks such as environmental issues and processing limitations, physical blowing agents have been promising in producing microcellular polymer foams (polymeric foams with micron size cells). Among physical blowing agents, supercritical fluids such as carbon dioxide (CO_2) and nitrogen are both suitable candidates to substitute for conventional physical blowing agents like chloroflurocarbons (CFCs) [3]. Two steps are involved in polymer foaming using physical blowing agents: nucleation and growth, which includes absorption of enough gas molecules in polymer in order to reach a thermodynamically unstable threshold to be able to nucleate a bubble bigger than a critical size and then growth of the bubbles [1].

In order to improve the foaming behaviour of microcellular foams, both phenomena can be addressed: increasing the number of nucleating sites through incorporation of particles with a higher modulus to enhance nucleation through lowering the energy barrier for nucleation of cells caused by fluctuation in pressure and stress around particles [4] and improving cell growth by modification of rheological properties such as melt strength via improvement in crystallization. Moreover, the particle's surface geometry can also be a determining factor in improving cell nucleation [5]. All the above-mentioned enhancements can be satisfied by engineering a nanoparticle of a specific size and geometry and modifying it to not only act as a nucleating site, but to be able to adsorb to the interface and improve the crystallization of the polymer.

On the other hand, based on classical nucleation theory (CNT), the nucleation rate is inversely related to the exponential cubic power of surface tension [6]; lowering surface tension decreases the energy barrier for cell nucleation and exponentially increases the number of cells leading to higher cell densities. Additionally, lower surface tension leads to smaller cell size since critical cell size is directly related to surface tension [1]. Considering these facts, one may manipulate the surface tension of polymer composites using an

appropriate modification on the nanoparticle surfaces and/or various shapes [7,8] of nanoparticles to dictate their location at the interface between polymers and supercritical carbon dioxide. This aim can be achieved by incorporating a CO_2 philic functional group on the surface of the nanoparticles [9] and amphiphilic characteristics of the particles to induce the nanoparticles' migration to the interface. Eventually, with desired design of nanoparticles and appropriate modification of nanoparticles, one can achieve higher solubility of CO_2 in the matrix, which leads to higher solubility of CO_2 or preventing the solubility reduction as a result of vitrified polymers in composites. Furthermore, to decrease the bubble size a higher percentage of carbon dioxide is required to increase the bubble pressure against suppressing surface tension force during bubble growth [10]. Incorporation of nanoparticles decrease the surface tension, and their adsorption to the interface could possibly prevent coalescence because of their steric and electrostatic stabilization [11]. In addition, the adsorbed film of the particles is shown to increase the surface modulus as a result of interactions between the adsorbed molecules [12].

Beside microcellular polymeric foam applications, nanoparticle modification and control over their localisation at the interface can be used in Pickering emulsions [13–15].

1.2 Thesis Objectives

Based on previous works, the goal of the current study is to study the effect of silica based nanoparticles on interfacial tension and crystallization behavior of PLA under compressed carbon dioxide. It was shown that PLA is a potential sustainable material with processing challenges during foaming. In this work, surface-modified silica nanoparticles are used to change interfacial behavior and crystallization of PLA/ CO_2 system.

As discussed earlier, interfacial tension and crystallization of polymer materials are two key factors determining foaming of polymers. Herein, the synthesis of silica nanoparticles with a desired shape, size, and surface chemistry is designed in order to study their effect on interfacial tension and crystallization of PLA. It is shown that the nanoparticles with tuned surface properties can be adsorbed to the interface and decrease the interfacial tension between melted polymer and supercritical fluids. The nanoparticles can also act as a nucleating agent for nucleating step of the foaming. The decrease in surface tension decreases the energy barrier for cell nucleation and consequently increases the number of cells, leading to an exponential increase in cell densities and smaller cell sizes. Furthermore,

the irreversible adsorption of the nanoparticles to the PLA/CO_2 interface can prevent coalescence phenomena. The nanoparticles improve crystallization behavior of the PLA. Improvement in crystallization for polymers with slow crystallization rate (such as for PLA) is an effective route and hence to increase the melt strength to create a stable bubbles during growth step in foaming.

1.3 Thesis Organization

This thesis is divided into six chapters. The first two chapters include an introduction and the literature review on the subject of study. The Chapters 3 to 5 each presents the scientific results relating to one of the objective questions. And each chapter consists of a published or submitted article. The structure of the main part of the thesis and a brief review for each chapter are as follows:

Chapter 3 discusses the effect of supercritical carbon dioxide on interfacial tension of PLA in the melting point window and under foaming processing conditions using the pendant drop method. The study of PLA interfacial tension in that temperature window is of practical application as most polymeric foams form and stabilize in that temperature range. The results show a decrease in interfacial tension with increasing temperature and pressure with a reduction in interfacial tension dependency on temperature at high pressures due to a reduction in CO_2 solubility at high temperatures. Furthermore, the relationship between the interfacial tension and the density-difference of polymer-supercritical CO_2 mixtures is studied by the generalized Macleod equation. The stability range for the melted drop can also be clarified by the dimensionless Bond number to have both valid and accurate interfacial tension measurements.

In chapter 4, interfacial behavior of PLA-silica nanocomposites in a CO_2 environment is investigated in detail at high temperature and high pressures. We observed a nonlinear trend in interfacial tension values with increasing amount of nanoparticles. The reason for an increase in interfacial tension at higher contents of the nanoparticles was attributed to the lateral capillary forces of the adsorbed aggregates of the nanoparticles to the PLA/CO_2 interface; the interfacial tension increased due to attractive lateral capillary forces originating from the perturbation of the PLA/CO_2 interface by particles. The compatibility between the nanoparticles and PLA at high pressures of CO_2 decreased based on contact angle results. In

addition, binding energy calculations showed irreversible adsorption of the nanoparticles to the interface.

In chapter 5, a detailed study was performed on the dispersion and crystallization of the surface – modified silica nanoparticles in PLA matrices. Contact angle measurement at low and high temperatures showed that nanoparticles with amine modification had lower surface energy and higher work of adhesion led to a higher level of dispersion. A better dispersion means more individual nucleating sites across the matrices. Furthermore, it was shown that based on Lauritzen–Hoffman secondary nucleation theory, lower surface energy led to an improvement in crystallization through reduction in energy barrier for nucleation. The crystallization behavior of PLA/surface-modified silica nanocomposites at different loadings of amine-modified silica (1, 2, and 8 wt. %) under both isothermal and non-isothermal conditions is studied. In order to consider crystallization improvement for foaming processes, isothermal crystallization under compressed CO_2 was also investigated. A significant improvement in crystallization rate was observed after introduction of amine-modified silica nanoparticles. The Avrami equation was used to investigate the mechanism of the crystallization. An increase in isothermal crystallization led to an Avrami exponent in the range of two-dimensional structures, due to the formation of a less packed crystal structure at higher temperatures. High-pressure DSC results also showed an increase in crystallization rate at 15 bar compared with the atmospheric pressure condition. However, an increase in pressure up to 21 bar had no significant effect on crystallization rate. The PLA samples with lower molecular weight and lower D-content also showed a significant increase in crystallization rate but with no change in crystallization mechanism with a presence of the nanoparticles.

In Chapter 6 concluding remarks and suggested recommendations for future work are presented. Briefly, the chapters and the relationship between the chapters are shown in the following flowchart:

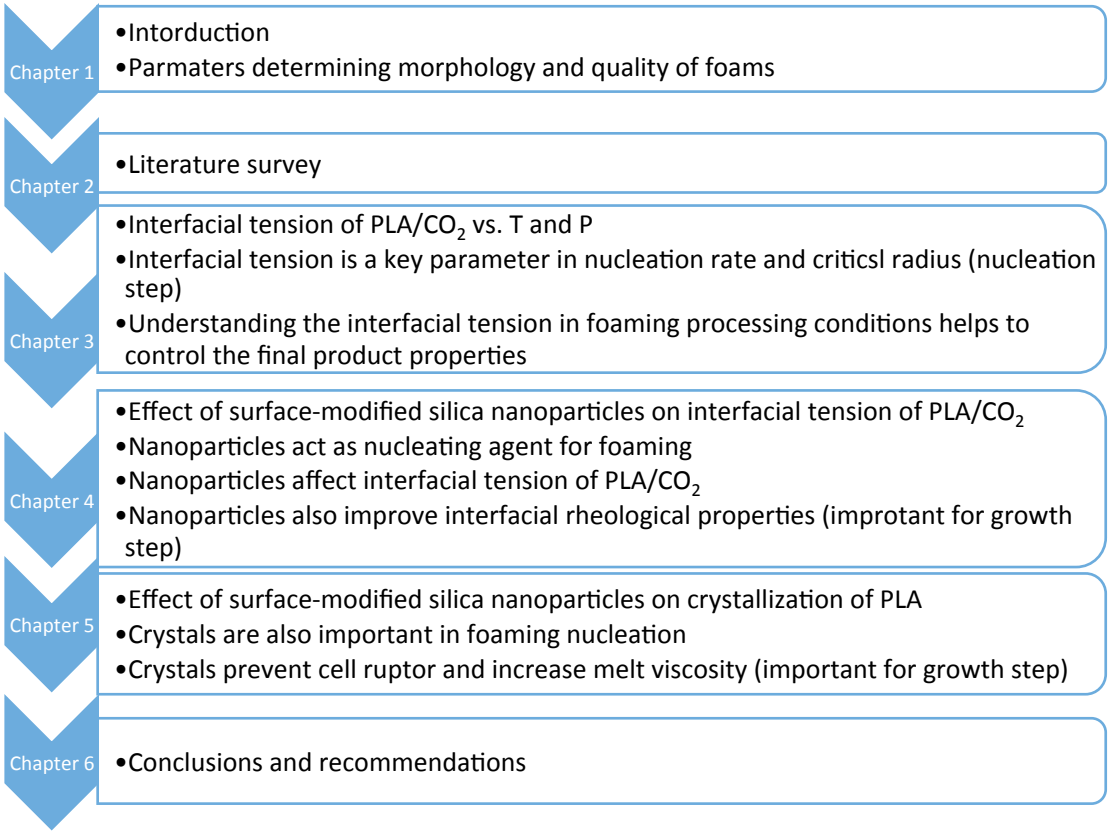
Chapter 1
•Intorduction
•Parmaters determining morphology and quality of foams
Chapter 2
•Literature survey
Chapter 3
•Interfacial tension of PLA/CO_2 vs. T and P
•Interfacial tension is a key parameter in nucleation rate and criticsl radius (nucleation step)
•Understanding the interfacial tension in foaming processing conditions helps to control the final product properties
Chapter 4
•Effect of surface-modified silica nanoparticles on interfacial tension of PLA/CO_2
•Nanoparticles act as nucleating agent for foaming
•Nanoparticles affect interfacial tension of PLA/CO_2
•Nanoparticles also improve interfacial rheological properties (improtant for growth step)
Chapter 5
•Effect of surface-modified silica nanoparticles on crystallization of PLA
•Crystals are also important in foaming nucleation
•Crystals prevent cell ruptor and increase melt viscosity (important for growth step)
Chapter 6
•Conclusions and recommendations

2. CHAPTER 2: LITERATURE REVIEW

2.1 Foaming of Poly Lactic Acid (PLA)

2.1.1 Poly Lactic Acid (PLA)

Poly lactic acid or polylactide (PLA) is a biodegradable and biocompatible thermoplastic polyester derived from lactic acid produced from sustainable resources [16]. PLA was first produced by Carothers as a low molecular weight product by heating lactic acid in vacuum, in 1932 [17]. Lactic acid is the building block of PLA which is also the side product of PLA hydrolytic degradation. Lactic acid is a naturally occurring organic acid that can be produced by fermentation of sugars such as cornstarch and sugarcane [18].

Lactic acid (2-hydroxypropionic acid) is a chiral molecule with two enantiomers of L- and D-lactic acid. The L-lactic acid has an advantage over the D-form as it provides the polymer with high mechanical strength [17]. In Figure 2-1, three stereoforms of lactide namely L-lactide, D-lactide, and meso-lactide are shown [17,18].

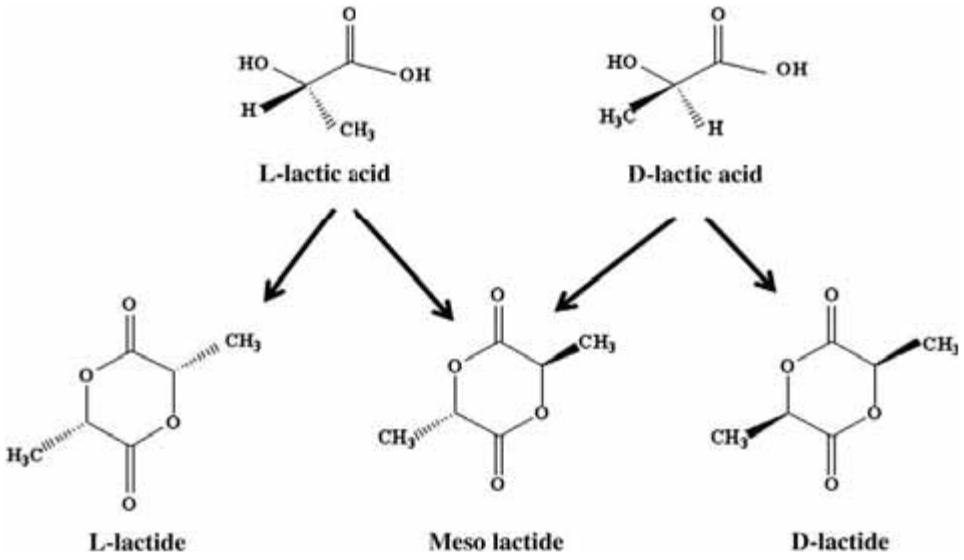

Figure 2-1. Three stereoforms of lactide: L-lactide, D-lactide, and meso-lactide [18]

Thanks to its biocompatibility and low immunogenicity, nontoxic degradation, and good mechanical properties, PLA has been used in pharmaceutical and biomedical applications such as implants, drug delivery, and tissue engineering scaffolds [19].

2.1.2 Foaming of Polymers

Polymeric foams are made from polymers using either chemical or physical blowing agents. In foams with physical blowing agents the gas is directly injected into the polymer melt or polymer composite melt, but in chemical blowing agents the gas is produced through chemical decomposition. Foams made from using of chemical blowing agents have processing and environmental drawbacks. Foam processing with a physical blowing agent involves the saturation of the polymer at a certain pressure and temperature using a certain gas or supercritical fluid. The mixture of polymer/gas is subjected to a sudden thermodynamic instability (such as temperature increase or pressure drop) and consequently the gas escapes the mixture, causing a cellular structure formation. If the cell membranes around a bubble remain unchanged the foam is closed-cell, but if the membrane ruptures the foam is an open one. [20].

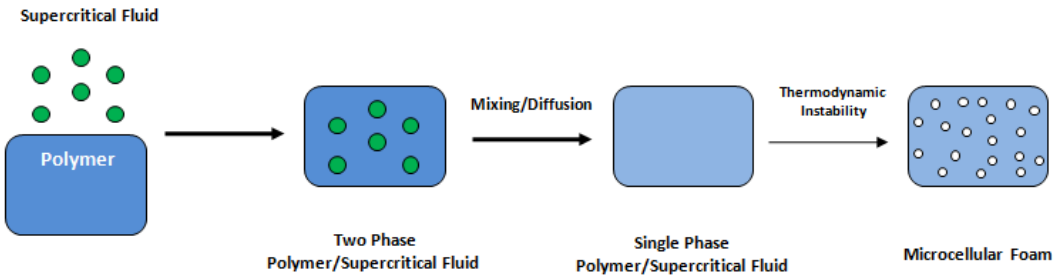

Figure 2-2. Schematic of polymer foam production using supercirtical fluid as a physical blowing agent.

According to classical nucleation theory [6,21,22], the nucleation rate N depends on:

$$N = Cf \exp\left(-\frac{16\,\pi\,\gamma^3}{3\,k\,T\,\Delta P^2}\right) \qquad 2\text{-}1$$

where C is a function of gas concentration, f is the frequency factor of gas molecules joining the nucleus, γ the surface/interfacial tension, T is the temperature, and ΔP is the pressure related to supersaturation developed in the polymer. As can be seen, the nucleation and foaming of polymers is strongly influenced by the polymer's surface/interfacial tension. Nucleation rate is inversely related to the exponential cubic power of surface/interfacial tension; lowering surface tension decreases the energy barrier for cell nucleation and exponentially increases the number of cells leading to higher cell densities

Foaming involves the introduction of a gaseous phase into a melt, then foaming by the gas, and afterwards solidifying the melt before the bubbles collapse. Gas bubbles have a spherical shape as the spherical form has the lowest surface energy for a given volume. There must be sufficient gas molecules together to overcome the resistance of the surrounding matrix. In the other words, the size of the bubbles should reach a critical bubble radius (R_{cr}) to have a stable growing bubble in system:

$$R_{cr} = \frac{2\gamma}{(P_b - P)} \qquad 2\text{-}2$$

where γ is the surface/interfacial tension, P_b is the bubble pressure, and P is the surrounding pressure. For the case of bubbles smaller than the critical radius, the surface tension force is high and causes the gas clusters to collapse. In the ultimate equilibrium state P_b is equal to P, and R_{cr} becomes an infinity; a spherical bubble cannot be made as any bubble size is smaller than the infinite critical radius. After passing the equilibrium state, the bubbling process may happen when the system reaches another equilibrium through a series of non-equilibrium states. When an instability like a drop in pressure happens and surrounding pressure becomes less than the bubble pressure, the system reaches to an equilibrium through bubbling. In other words, in the bubbling phenomenon the system creates a significant amount of interfacial area for diffusion to dissipate any energetic inequalities. For very small sizes of bubbles, the bubble pressure is relatively high to be able to endure the surface tension force. The high bubble pressure makes the foaming process unstable even though the buoyancy force is low. The unstable bubbles grow and expand in size and evidently dissipates the pressure gradient across the interface. For systems with low resistance the buoyancy force is significant and therefore the bubbles accumulate on top of

the liquid (like soda or soapy water systems). The bubble walls will rupture when the bubbles collide because of the material drainage and thinning of the cell walls [1].

2.1.3 **PLA Foams**

PLA foams are promising candidates to replace petroleum based foams products such as polystyrene (PS) foam due to their competitive material and processing costs, and mechanical properties. In addition, PLA foams have biodegradable and biocompatible characteristics which make them an attractive replacement for commodity and synthetic foam products for solving global waste disposal concerns [16]. The applications of PLA foams would be in commodity applications such as packaging, shock-absorbing, construction, thermal and sound insulation [23]. The majority of PLA foams are produced using physical blowing agents. The foam structure is produced by a thermodynamic instability and ejection of the dissolved gas from the PLA/gas mixture and followed by cell stabilization by solidification of the product as the temperature drops below T_g.

PLA foams are produced through various processing methods such as extrusion, foam injection molding, and expanded PLA (EPLA) bead method [24–26]. In extrusion and injection molding methods, normally a low-density PLA foam with simple geometries or a high-density foam with three dimensional complex geometries are produced. However, bead foaming results in low-density foam with three dimensional complex geometries [24,27].

2.2 Surface /Interfacial tension of polymers under Supercritical Fluids

The interfacial tension of polymers and supercritical fluids is the subject of many works. A supercritical fluid is defined as " any substance, the temperature and pressure of which are higher than their critical values, and which has a density close to or higher than its critical density " [28]. Supercritical carbon dioxide (CO_2) is an economic, non-toxic, non-flammable, and environmentally friendly solvent in polymer blending, synthesis, coating, and polymer foaming [3,29,30]. In microcellular foaming using physical blowing agents, the surface tension between a polymer melt and a fluid is a principal factor in determining cell nucleation and growth.

There are various methods to measure the surface/interfacial tension of liquids and melts. Pendant and sessile drop methods for measuring surface tension have numerous advantages, such as, using small quantities of liquids/melts, operating at various temperatures and pressures, and being useful for both dynamic and steady-state surface/ interfacial tensions. In recent years, there have been some attempts at measuring the surface tension of polymers at various temperatures and pressures. The relationship between the equilibration time and steady state surface tension and a polymer chain structure is investigated by Kwok et al. [31]. They have shown that the surface tension increase initially due to chain relaxation occurs in relatively shorter times and then reduces because of relaxation or rearrangements of polymer chains. These two phenomena become more significant if the temperature is lowered. Different equilibration measurement time was demonstrated for polyethylene and polypropylene; the observations are believed to occur because of different steric side groups, but the molecular weight has a more significant role in equilibration time.

Both polypropylene-polystyrene (PP-PS) and PP interfacial tension under supercritical CO_2 have been investigated [22]. It was observed that the interfacial tension in both cases decreases remarkably; however, it reaches a plateau at high pressures. In the case of PS and CO_2, the values of interfacial tension converge for various temperatures at higher pressures, leading to disappearance of the effect of temperature at higher pressures. This phenomenon occurs because of the counterbalance between the interfacial tension reduction effect of temperature and solubility reduction at higher temperature (less CO_2 means less reduction in interfacial tension). Moreover, the effect of supercritical CO_2 on PP and PS compatibility, regardless of PP's molecular weight, was a sharp decrease in interfacial tension after 50 atm due to possibly shielding of the undesirable contact between two polymers.

Park et al. [32] measured the surface tension of polystyrene under supercritical CO_2 at different pressures and temperatures. In order to estimate (Pressure-Volume-Temperature) PVT data to calculate the density of their system, they used the Sanchez-Lacombe (SL) equation of state (EOS). They also found an exponent of 2.5 for the Macleod equation. They also investigated [33] the effect of processing conditions such as pressure and temperature on the interfacial tension of polystyrene. They used self-consistent field theory to explain the surface tension trend with processing conditions. In another work from this group [34], the effect of the molecular weight of PS under supercritical nitrogen was explored. Monodispersed polystyrene with higher molecular weight had higher interfacial tension and

more dependency on temperature and pressure than low molecular weight ones. Furthermore, polydisperese polystyrene had higher surface tension than monodispersed one, probably because of the possibility of finding polystyrene chains with higher molecular weight than those of monodisperse one.

Wei et al. [35] investigated the effect of various temperatures and pressures on the surface tension of high density polyethylene (HDPE) under supercritical nitrogen. Although their model of surface tension had coefficients consistent with those of polystyrene, no interaction term between temperature and pressure was observed. On the other hand, unlike amorphous polymers, the trend for HDPE as a semi-crystalline polymer was anomalous below the melting-point temperatures at which the polymer crystallizes; the surface tension dropped first and then diminished to reach a plateau. The authors concluded that crystals formed in the polymer melt possibly acted as nanoparticles to decrease the surface tension. The reduction in surface tension depends on the rate of temperature change: the faster the temperature changes, the less the change in surface tension. In another study, Thompson et al. [36] carried out an investigation based on self-consistent field theory (SCFT) to demonstrate the effect of nano-sized polymeric crystals on surface tension. Their calculations showed that nanocrystals can be selectively located at the polymer surface. They also suggested that preferential location of nanocrystals will provide a narrower boundary with a smaller "spatial extent" than the polymer chains, a phenomenon that leads to lower internal energy and consequently lower surface tension.

Lia et al. [6] considered the effect of long-chain branching on the density and interfacial tension behaviour of poly (propylene) PP in supercritical CO_2. The densities of the systems were calculated using the Sanchez-Lacombe (SL) equation of state (EOS), Simha-Somcynsky (SS) EOS, and experimental data. The density differences measured by SS EOS are identical to those of measured experimentally. The deviation of density difference obtained from SL EOS with experimental values is higher when pressure and/or temperature increases. The results showed higher interfacial tension, lower solubility, and a lower swelling ratio for branched PP because the greater force requires creating new interface and expanding the polymer as a result of entanglements of long chain branches and the polymer's higher melt elasticity.

Surface/interfacial tension of polylactide acid (PLA) and specifically at high temperatures is scarcely reported in literature. In one work [37], the CO_2 solubility and the pressure–

volume–temperature (PVT) behavior of PLA were investigated using a magnetic suspension balance (MSB) instrument. It was shown that as the temperature increased, the swelling and the solubility decreased, while an increase in pressure results in higher swelling and solubility values. The effect of D-lactic acid content (D-content) on the solubility of CO_2 and swelling was not significant. Mahmood et al. [38], measured the interfacial tension and density of PLA/CO_2 mixtures using a sessile drop method at high-pressures and high-temperatures. It was shown that the density difference between of the mixture and the CO_2 decreased with increasing the gas pressure. Temperature dependency of interfacial tension was related to CO_2 pressure. In the other words, at lower pressures the interfacial tension decreased with an increase in temperature, but at a higher pressures it was the opposite way. The reason was attributed to hydraulic pressure and polymer swelling effect of CO_2 which act in a competing manner. PLA samples with different D-content showed no significant effect on density difference and interfacial tension of PLA.

2.3 Self-Assembly and Adsorption of Nanoparticles at Fluid-Fluid Interfaces

Colloidal particles, whether with homogeneous surface chemistry or heterogeneous (Janus particles) (Figure 2-3), are surface active and similar to a surfactant can spontaneously adsorb to the interface between two immiscible fluids (liquid–gas or liquid–liquid) [39]. The adsorption to curved interfaces was first reported by Pickering [40] and Ramsden [41] about a century ago [42].

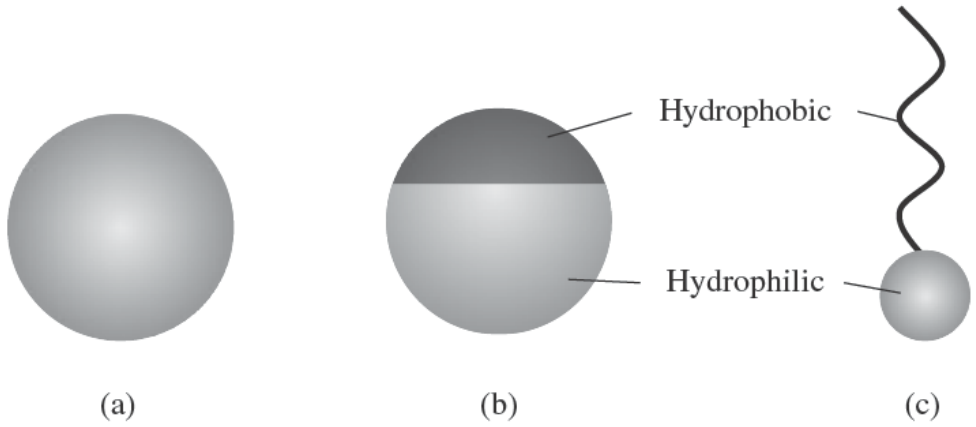

Figure 2-3.Schematic of (a) homogeneous, (b) heterogeneous or amphiphilic (Janus) colloidal particles and (c) a surfactant molecule [39]

Particles at fluid interfaces are available in various natural systems and technological processes [43,44] including food science, cosmetics, oil production and renewable energies [45,46]. Adsorption of particles at fluid interfaces is also a new route to produce new materials based on the assembly of the particles at interfaces. The presence of particles at the interface and its effectiveness in stabilization of fluid-fluid interfaces depends on the surface chemistry, size, shape, roughness and wettability of the particles. Wettability is a key factor characterized by the three-phase contact angle and is analogous to the hydrophilic– lipophilic balance (HLB) in surfactants [47]. Wettability of particles mainly depends on the surface chemistry of the particle and on the chemical nature of the two phases at the interface. The surface of the particles can be modified either by surface physisorption or chemisorption of molecules. For physisorption cases, the adsorption of surface active agent (e.g. long-chain surfactant or short-chain alcohols) to the particles' surface occur because of electrostatics, hydrogen bonds, and van der Waals interactions [48,49], but in chemisorption, like silanization of silica surfaces, chemical modification happens by covalent bonding between surface active agent and particle's surface [50]. Another interesting route to tune the wettability is through Janus-type particles. These particles have assymetrical wettability with particular physico-chemical properties and structure of the layers at the fluid interfaces [8,51]. In general, unlike micrometer particles, unmodified nanoparticles are not surface active in Pickering emulsions or foams, because they do not spontaneously adsorb to the interface and consequently do not significantly reduce surface tension [52,53]. However, the emulsification properties of particles can be enhanced through surface modification of the

nanoparticle [13,54,55]. Alvarez et al. [55] studied the interfacial dynamics and rheology of silica nanoparticles grafted by poly(2-9 dimethylamino) ethyl methacrylate) PDMAEMA at both air-water and oil-water interfaces. At oil-water interface, the nanoparticles with a higher grafted density had a much lower equilibrium surface tension and faster dynamics. The dynamics was much faster in higher concentrations of particles with high grafting density. It has been shown that particles with high grafting density had faster interfacial penetration than those with medium grafting density. The grafting density of polymers on the particle's surface determines the dynamic and conformational relation of nanoparticles at the interface. In other words, despite the lower bulk diffusion of nanoparticles with higher grafting density, each such particle carries more chains to the interface: the higher number of chains transported to the interface and also relaxation of chains at the interface determines the cohesion pressure.

The geometry of particles is also among the determining factors in the interfacial behaviour of liquid-liquid interfaces. Ruhland et al. [8] investigated the effect of polymeric Janus particles' geometry and shape on orientation and structure formation at liquid-liquid interface through both experimental and simulation approaches. Janus discs showed maximum reduction in interfacial tension, and the Janus cylinders led to the lowest equilibrium interfacial tension, and the spheres had low surface activity. They also observed different adsorption kinetics: spherical particles of small size (50 nm) had a fast adsorption regime at the beginning due to a higher diffusion coefficient, while for anisotropic particles, the kinetic was slow. The simulation results showed that the disc-shaped particles had two minima in their energy profile. The value of energy barrier for removal from the interface for spherical, cylindrical, and global minimum of disc shapes were 5×10^{4} kT, 1×10^{6} kT, and 1.5×10^{6} kT respectively. The results indicate that the energy barrier for expulsion from the interface is strong for particles with large cross-sectional areas such as cylinders and discs. The authors concluded that the difference in dynamic interfacial behaviours of particles emerges from dissimilar packing behaviours, forms, and shapes which are the factors that determine the energy barrier values and adsorption steps.

Since the localization of nanoparticles at an oil-water interface and its adsorption energy are functions of contact angle and interfacial tension of the oil, water, and particle, the contact angle of nanoparticles at the interface has been widely investigated [50,56]. In one study [57], the relationship between the effect of the chain length and structure of polymers

in soft core-shell nanoparticles on liquid-liquid interfacial behaviour, contact angle, and inter-particle distance has been addressed. The core-shell nanoparticle was composed of iron oxide grafted by linear and dendritic poly (ethylene glycol) (PEG). It has been observed that linear PEG nanoparticles have faster adsorption than dendritic ones: one reason for this finding is that the dendritic nanoparticles have higher surface charges, leading to a repulsive electrostatic barrier upon adsorption at the interface. The other reason is that rigid dendritic shells make particles resemble hard spheres having adsorption energy in range of 20 k_BT or less (reversible adsorption and desorption) compared to adsorption energies of thousands of k_BT (irreversible) for the case of linear polymers. Although the hydrophilicity and contact angle of the nanoparticles are independent of molecular weight and the architecture of PEG chains, the equilibrium interfacial tension of water/n-decane is inversely proportional to the molecular weight of polymer at the shell. X-ray reflectivity results show that the interparticle distance between dendritics is much larger than their shell due to long-range repulsion of surface charges. At saturation, this distance is also larger than the thickness of linear polymers due to stretching of the polymer chains and different conformations at the interface.

The effect of surface charge (pH, ionic strength, and temperature) on adsorption of gold nanoparticles capped with n-dodecanethiol to the oil/water interface was also investigated [58]. It was shown that the lower the thickness of the double layer, the higher the chance of the nanoparticles being adsorbed at the interface. For all pH values, at the beginning of the dynamic IFT measurement, nanoparticles experience free diffusion, while at equilibrium the diffusion is hindered. They showed that at very low concentrations of salt, the chance of adsorption of ions at the interface is low, so the oil-water interface is not disturbed. On the other hand, at high ionic strengths, Na^+ ions screen the negative charge on the surface of nanoparticles. This phenomenon leads to diminishing the double layer thickness and consequent adsorption of higher concentrations of nanoparticles at the interface. Studies on temperature effects also revealed that at higher temperatures the adsorption density decreases and the area per particle increases leading to an increase in interfacial tension.

Thompson et al. [59] illustrated the effect of the size and volume fraction of nanoparticles in their distribution in diblock copolymer domains. In the case of a high-volume fraction of large particles, the exclusion of chains-ends from the centre of one region provides room for nanoparticles to self-assemble at the centre, leading to a nanosheet at the

centre. However, for a low-volume fraction of nanoparticles, the number of nanoparticles is not enough to form a well-organized structure at the centre. The distinct structures formed in various volume fractions can be explained in terms of entropic contributions, where in a low volume fraction, the chains should stretch to be around the particles, leading to entropic penalty due to loss in conformational entropy. However, for higher-volume fractions, the loss in translational entropy is counterbalanced by the free energy gain by the polymer. The scenario is completely different for small particles: the nanoparticles tend to self-assemble at the interface of two regions. From entropy point of view one can say that for small particles the stretching of chains is not significant and a more uniform dispersion of particles increases the entropic free energy of each block, leading to positioning of particles at the interface.

Besides factors affecting the entropy of the systems such as the size and volume fraction of the nanoparticle-block copolymer systems, one can meet the aim of localization through an enthalpic point of view. Chiu et al. [60] controlled the localization of nanoparticles through manipulation of surface chemistry. They observed that gold nanoparticles coated with a homopolymer of one of the two diblocks under investigation, with a core-shell size of around 8 nm, were localized in the rich domain with the same block to lower their enthalpy. In their observations, the nanoparticles segregated around the centre of the same domain. To accommodate the nanoparticles, chain ends near the centre moved instead of stretching, a phenomenon that has a higher entropic penalty than the translational entropy of nanoparticles. In order to localise the nanoparticles at the interface, the nanoparticle should be covered by homopolymers of both blocks. The adsorption at the interface happened when the difference of interfacial energies of the nanoparticles with each homopolymer was much less than the interfacial energy of the diblock copolymer.

In another study, the surface tension of silica and titanium dioxide dispersions as a function of concentration has been investigated [61]. For both dispersions, two distinct regions were observed one at the low and the other at the high concentration of particles. At low concentrations, the surface tension decreased when the concentration increased, while after a minimum of around 5-7 wt%, surface tension increased to a constant value. The minimum was higher in SiO_2 dispersions, than in TiO_2 ones, and it happened at higher concentrations of particles. The reduction in surface tension was related to a thermodynamically favourable phenomenon of adsorption due to lowering the energy of the

system and raising its entropy. However, at a higher concentration of particles at the interface the attractive capillary force between particles increased, leading to an increase in the work needed to deform the interface, and as a result, an increase in the surface tension. Since the contact angle and density of both particles are roughly the same, the only reason for the difference in their surface tension values is their unlike size and surface-to-volume ratio. The TiO_2 particles are smaller and higher numbers of them are expected to be at the interface.

The presence of nanoparticles at liquid-liquid or liquid-vapour interfaces provides a line at the contact of the three phases (nanoparticle and the two other fluids). This line of tension is defined as "an excess positive or negative energy per unit of length to the total surface energy" [62]. Although the line of tension has only a small value, it has a significant role in wetting phenomena such as adsorption of spherical solid particles at the interface [63]. From a thermodynamic point of view, a positive line of tension makes the three-phase system unstable, leading to a decrease in the length of the line of tension, and consequently a drying/ wetting transition [63–65]. This transition is a function of a dimensionless parameter consisting of the ratio of the line of tension to the product of surface tension of two liquid phases and the radius of particle. The shape and orientation of nanoparticles at the interface was investigated by Faraudoa et al. [65]. They found a critical value for the aspect ratio of non-spherical particles using the generalized Young's equation, beyond which the particles could not adsorb to the interface. The results showed that spherical and oblate particles adsorbed to the interface, while particles with a higher aspect ratio did not have tendency to move toward the interface. It has been shown that a small deviation from a spherical shape with an aspect ratio between 1 and 1.9 results in stabilization even though elongated particles are less stable than spherical and oblate ones. The most stable condition arose from an oblate form with a symmetry axis parallel to the normal of interface. The stability for other shapes and orientations are as follows: sphere, prolate with perpendicular, prolate with parallel and oblate with perpendicular symmetry axes to the normal of the interface had less stability at the interface. The results highlighted the importance of the shape of nanoparticles in their self-assembly at liquid-fluid interface.

2.4 Foam Stabilization with Particles

Pickering foams and emulsions are stabilized by particles. In some systems, surfactants with the dual function of foaming agent and particle hydrophobizing agent may also be added [66].In the food industry, many colloids are stabilized, at least in part, by adsorption of particulate material to oil–water (emulsions) or air–water (foams) interfaces. Examples of Pickering emulsions and foams in food industries include casein micelles (in homogenized milk), egg-yolk lipoprotein granules (in mayonnaise), fat crystals (in spreads and margarine), and partially aggregated emulsion droplets or fat crystals at bubble interfaces (in whipped creams) [67]. Small solid particles, surfactants, and proteins prevent the collapse of the foam by adsorbing at interfaces and acting as a surface active agent [44,68]. Figure 2-4 [69] shows the possible configurations of the particles in solid stabilized emulsions and the mechanism responsible for their stabilization. Nanoparticles can be used for stabilization of viscous CO_2-in-water foams for utilization in enhanced oil recovery (EOR) and geologic CO_2 storage (GCS) applications [70]. Proteins are widely used as a foaming agents because they strongly adsorb to the gas–water interface, and have good steric and electrostatic stabilization. Furthermore, the adsorbed film of the particles have high surface rheological moduli as a result of interactions between the adsorbed molecules [11].

Another well-known example of particle –stabilizing of foams is the floatation method (for extraction of minerals). In floatation, the mineral particles adhere to air bubbles which have already created by frothing agents (surface active agents) and collectors. In addition to the role of frothing agent to delay or prevent the coalescence of bubbles, mineral particles contribute in stabilization of bubbles [66]. Particle-stabilized aqueous foams are also made using zirconium phosphate [71], surface modified iron particles [72], silica [68,73,74], polymeric latex [75], cellulose [76], and graphite and quartz particles [77].

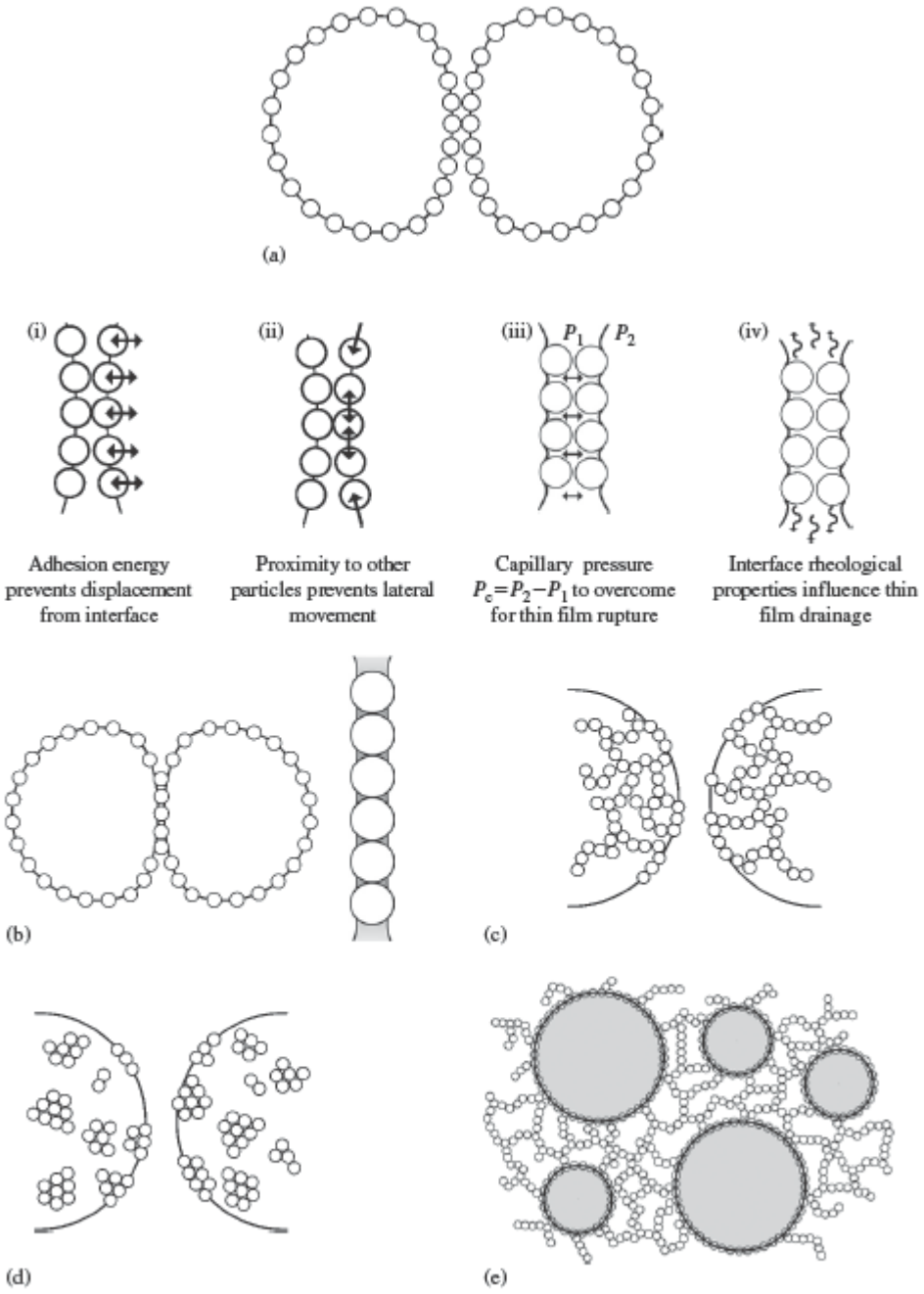

Figure 2-4. Possible configurations of the particles in solid stabilized emulsions (a-e, and the mechanism responsible for stability of the emulsions (i- iv) [69]

Alargova et al.[78] demonstrated that particles with non-spherical shape can act as an effective foam stabilizer in the absence of any additives. They have shown that extreme foam stability even under drying or vacuum treatment was obtained using polymer rodlike particles due to the strong particle attachment to the bubbles, microrod entanglement and

formation of rigid hairy shells around the bubbles. Madivala et al.[79] also investigated the effect of aspect ratio of both hydrophilic and hydrophobic ellipsoidal particles on the stability of oil-in-water and water-in-oil emulsions. In another system [80], the foaming behaviour of platelet clay particles coated with fluorinating agents were studied for different air and oil mixtures. The foaming depends both on oil surface tension and the surface energy of the particles. Pickering oil/air foams were formed for liquids with higher surface tensions with three-phase contact angles between 65 and 125°. For oils with surface tensions above 27 $mN.m^{-1}$, oil drops were stabilised with particles in air and the resulting products were dry oil powders.

2.5 Effect of Particles on PLA Crystallization

In foaming of PLA, cell coalescence and cell rupture occur during cell growth step because of insufficiency in low melt strength [81], consequently, gas loss as a result of cell rupture during foam expansion results in significant shrinkage in the final product [10,16]. Numerous solutions are suggested for improvement the low melt strength of PLA including using chain extenders, branching the chains [81,82], and mixing with fillers and additives [83–85]. Among all the solutions, improvement in PLA's crystallization kinetics during processing and foaming is considered as an effective way to improve the viscoelastic properties to create better cell nucleation and growth through formation of a network of nucleated crystals [86–88]. Furthermore, promoting the crystallization of the polymers can lead to heterogeneous cell nucleation around the crystals [89], since the crystals can create local stress variations around themselves [88,90]. Based on classical nucleation theory, the presence of an interface reduces the free energy for nucleation and consequently increases the nucleation rate. It was shown that presence of spherulites in a PLLA matrix enhanced the cell nucleation and the number of nucleated cells increased significantly as the spherulite density increased [91]. The reason for the observed phenomena is the ejection of CO_2 from the spherulites and its accumulation at the crystalline/amorphous interface [91].

Despite the advantages of crystallization on foam processing, there must be a balanced amount of crystals in the systems; high modulus and stiffness because of very high level of crystallinity restrain foam expansion [92]. Furthermore, gas solubility would decrease significantly as gases cannot easily dissolve in the crystalline phase [93].

Since PLA has low nucleation and slow crystallization kinetics in homogeneous conditions [94], it is necessary to improve PLA crystallization kinetics by adding nucleation sites (nucleating agents) and increasing chain mobility through plasticization (short length molecules or CO_2). The nucleating agents decrease the crystallization half-time and the energy barrier for nucleation. Minerals and fillers are among the physical nucleating agents for crystallization [87]. Silica is a promising additive to improve crystallization of PLA. There are reports showing its efficacy on promoting the crystallization. In one study, the effect of silica nanoparticles on non-isothermal crystallization kinetics of PLA was studied [95]. It was shown that silica promoted the crystallization nucleation while it also increased the crystallization activation energy. In the other words, the nanoparticles hindered the movement of the molecular segments of PLA and decreased the crystal growth rate. However the overall crystallization rate increased denoting the effect of silica on crystallization nucleation of PLA was more dominant than the crystal growth.

In another study [96], crystallization behavior of in-situ polymerized PLA/silica composites of silica and silane-modified silica nanoparticles were studied. Both crystallinity and crystallization rates were higher in the presence of silica and it was even faster when the surface of silica was modified. Isothermal crystallization evaluations using the Avrami equation also showed faster crystallization with kinetics of crystallization constant of two orders of magnitude greater for the modified silica.

It was also claimed that for nanoparticles with higher compatibility with the matrix, the nucleating effect of silica was more significant and the melting point was slightly higher than PLA. Nofar et al. [85] studied the effect of different fillers on the crystallization kinetics of PLA at atmospheric pressure and under CO_2 pressures. Their results showed that PLA/talc composites had faster nucleation and growth rate with high crystallinity and more perfection in the crystals. In the PLA/nanocomposites (silica and clay) the final crystal nucleation density was higher than talc, but the nucleation was slower probably because of higher surface area and hindering effect of the nanoparticles on PLA chain mobility and crystal growth because of more molecular entanglement. The hindering effect was more notable in clay compared with silica possibly due to a longer aspect ratio of the clays. The crystallization kinetics increase at low pressures of CO_2 as a result of an increment in molecular mobility of PLA.

3. CHAPTER 3: EFFECT OF PRESSURE AND TEMPERATURE ON INTERFACIAL TENSION OF POLY LACTIC ACID MELT IN SUPERCRITICAL CARBON DIOXIDE

K. Sarikhani, K. Jeddi , R.B. Thompson , C. B.Park , P.Chen [*1]

Graphical Abstract

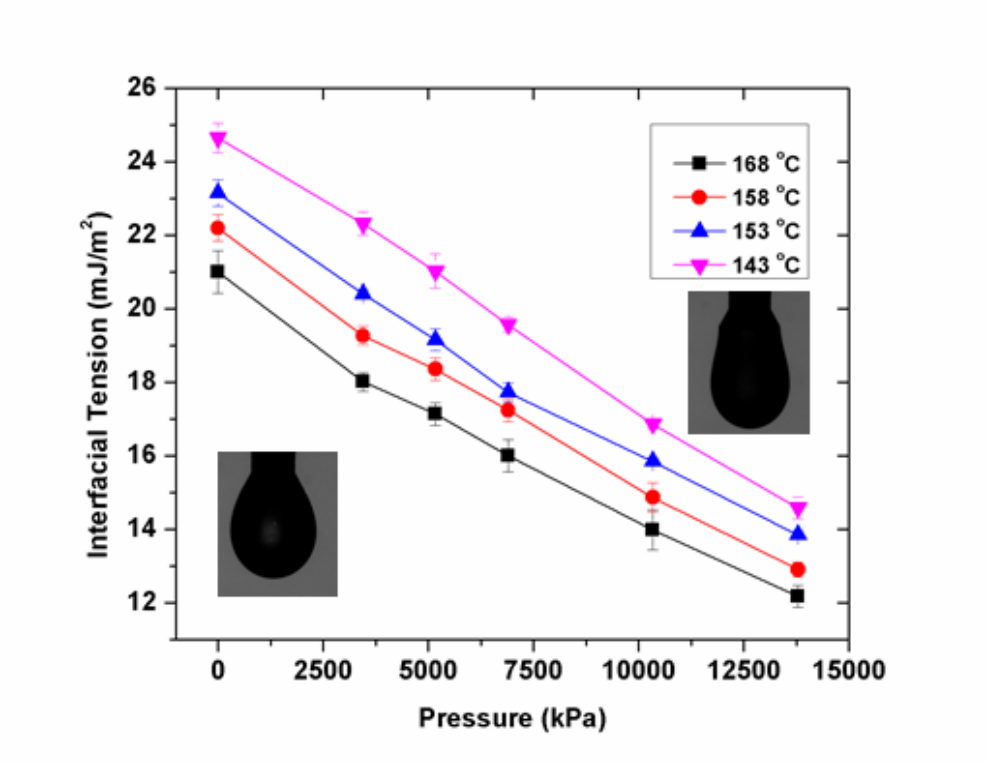

[*] Published in Thermochimica Acta 609 (2015) 1–6.

3.1 Summary

In this chapter the interfacial tension of poly lactic acid (PLA) melt is measured in supercritical carbon dioxide (CO_2) at processing temperatures and pressures using Axisymmetric Drop Shape Analysis Profile (ADSA-P). Interfacial tension is a key parameter in nucleation rate as well as critical bubble size. The results from this chapter are important from processing prospective and are obtained to both have a comparison with PLA composites (Chapter 4) and to find the range of stability for the melted drop.

The results are published in *Thermochimica Acta* (2015). The co-authors include professor Pu Chen as supervisor, professors Chul B. Park and Russell Thompson as co-supervisors, and Kazem Jeddi who assisted me in performing some replica experiments of the interfacial measurements.

3.2 Introduction

The interfacial and surface tension of polymers is a key thermodynamic parameter in various applications such as polymer blending [97], wetting [98], dispersion of particles or fibres in polymers [99], and polymer foaming [6]. Numerous methods can be used to measure the interfacial tension of polymers. Among them, Axisymmetric Drop Shape Analysis (ADSA) is a powerful and precise technique for the measurement of surface tensions and contact angles of liquids and solids. The technique can be applied for various systems such as pendant drop, sessile drop, and captive bubbles [100]. Generally, ADSA methods work based on the numerical fit between the profile obtained from the shape of drops or bubbles and the theoretical drop shape from the Laplace equation of capillarity [101].

Even though the importance of surface tension and interfacial tension of polymer melts is evident in many applications, data related to high-pressures and high-temperatures are rarely reported in the literature because of the high viscosities, difficulties of forming the drop in high temperatures, thermal degradation, and lack of PVT data at high temperatures and high pressures.

In foam materials, the interfacial tension between a dense continuum and the dispersed voids plays a critical role in the structure and properties of final products [1]. Among foams, polymeric foams have attractive mechanical, energy-absorbing, and thermal-insulation

properties [2]. One promising polymer in the foam industry is polylactide (PLA); a biodegradable and biocompatible polyester derived from lactic acid [29]. Because of its high modulus, high strength and appropriate clarity, this aliphatic thermoplastic polyester can be seen as a potential replacement for petroleum-based synthetic polymers [87]. Besides its decent mechanical properties, PLA has significant environmental merits compared with other commodity polymers, including its renewable agricultural source, the consumption of carbon dioxide during its production, its compostability and recyclability [29,102].

Polymeric foams are made of either chemical blowing agents or physical blowing agents. The former have drawbacks such as environmental issues and processing limitations. On the other hand, physical blowing agents have shown promise in producing microcellular polymer foams. Among physical blowing agents, supercritical fluids such as carbon dioxide (CO_2) and nitrogen are both suitable candidates to substitute for conventional physical blowing agents like chlorofluorocarbons (CFCs) [103]. Two steps are involved in polymer foaming using physical blowing agents: nucleation and growth. The first step includes absorption of enough gas molecules in the polymer matrix to reach a thermodynamically unstable threshold to be able to nucleate a bubble bigger than a critical size. The second involves growth of the bubbles [1].

In order to improve the foaming behaviour of microcellular foams, one can increases the number of nucleating sites through manipulating surface tension. Based on classical nucleation theory (CNT), the nucleation rate is inversely related to the exponential cubic power of surface tension [6,22]; lowering surface tension decreases the energy barrier for cell nucleation and exponentially increases the number of cells, leading to higher cell densities. Additionally, lower surface tensions lead to a smaller cell size since critical cell size is directly related to surface tension [1]. For the above mentioned reasons, a study of the effect of processing conditions (temperature and pressure) on the interfacial tension of PLA and the blowing agent (CO_2) is indispensable. Despite the importance of foaming and blending of biodegradable polymers such as PLA with supercritical CO_2 ($SCCO_2$), there is very scarce data for interfacial and surface tension of PLA at high temperatures and high pressures [104]. Mahmood et. al [104], have reported the interfacial tension of PLA and supercritical CO_2 using a sessile drop method at temperatures higher than melting point for PLA with different D-contents. In the current work, surface tension measurement of a different grade of PLA with different molecular weight and D-content is measured using a different method

(pendant drop). Surface tension of PLA at high temperatures and the interfacial tension of PLA and $SCCO_2$ are investigated in the melting point window and under foaming processing conditions using the pendant drop method. The study of PLA interfacial tension near the melting point seems essential because not only do most polymeric foams form and stabilize in temperatures in the range of the melting point, but also the solubility of supercritical CO_2 in the polymer may vary at temperatures around and below the melting point of the polymers. The results shows that unlike polymers with high level of crystallinity (such as high-density polyethylene (HDPE)) [35,36], no anomalous behaviour in interfacial tension due to crystallization is observed in PLA.

3.3 Materials and Methods

3.3.1 Materials

In this work, PLA under the trade name of PLA-2002D with M_n = 100 kg/mol and D-content of 4.5 % was kindly provided by NatureWorks. Carbon dioxide chromatographic grade (purity 99.99 %) was purchased from PRAXAIR, Canada.

3.3.2 Solubility Measurement

The solubility of CO_2 in the PLA melts was obtained using a Magnetic Suspension Balance (MSB) from Rubotherm GmbH as the schematic shows in

Figure 3-1. Details about the experimental apparatus and procedure can be found in previous publications [105–107], however, a brief overview of the solubility measurement is as follows. At vacuum (P=0) and temperature T, polymer pellets were weighed as W (0, T) from the balance readout. After adjustment of pressure and completion of gas sorption in the polymer by reaching saturation point, the weight of the saturated polymer melt was recorded from the readout on the MSB, and was defined as W (P,T) at pressure (P) and temperature (T). Then, using the obtained weights, the amount of gas dissolved in the polymer melt, Wg, was calculated as below [108]:

$$W_g = W(P,T) - W(0,T) + \rho_{CO_2}(V_B + V_P + V_S) \qquad 3\text{-}1$$

where the density of the gas, ρ_{CO_2} was obtained using a MSB [106]; V_B is the volume of the sample holder, V_P is the volume of the neat polymer (without gas dissolution and volume

swelling) at pressure *P* and temperature *T*. The latter was obtained from the mass and specific volume (V_{sp}) based on Tait's PLA equation. The term V_S is the swollen volume of the polymer melt due to gas dissolution.

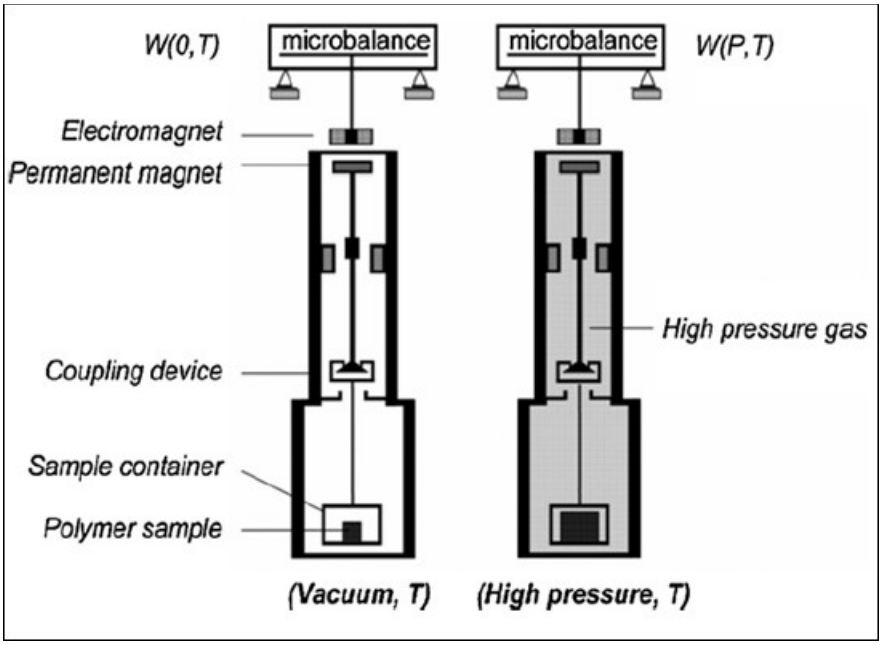

Figure 3-1.A schematic of the magnetic suspension balance (MSB) [109]

If the volume of swollen polymer (V_S) is not considered, the apparent solubility $X_{apparent}$ is as follows:

$$X_{apparent} = \frac{W(P,T) - W(0,T) + \rho_{CO_2}(V_B + V_P)}{mass\ of\ sample} \qquad 3\text{-}2$$

It is obvious that the apparent solubility is less than the actual solubility. The corrected solubility, $X_{corrected}$, considering the buoyancy effect , can also be calculated:

$$X_{corrected} = X_{apparent} + \frac{\rho_{gas} V_S}{mass\ of\ sample} \qquad 3\text{-}3$$

Theoretically, an approximation of the swollen volume can be obtained using the following calculation:

$$V_S = [(1 + X) + v_{p,mixture} - v_{p,pure}] \times m \quad (3\text{-}4)$$

where X is the gas solubility in the polymer melt from the Simha Somcynsky (SS) equation of state (EOS), m is the initial weight of the polymer, $v_{p,pure}$ is the specific volume of pure polymer that can be obtained from Tait's equation, and $v_{p,mixture}$ is the specific volume of the polymer/gas mixture at equilibrium that can be calculated using the EOS.

More details about the PVT behavior of the polymer-CO_2 mixture can be found in the literature [107,110]. In brief, it is as follows. Each measurement at each pressure is recorded until the volume of the polymer-CO_2 mixture becomes unchanged. The swollen volume was determined by the ratio between the final equilibrium volume and the initial volume from Tait's equation:

$$S_w = \frac{V(T,P,t_{eq})}{V(T,P,t_{in})} = \frac{V(T,P,t_{eq})}{m_{sample}\upsilon(T,P)} \quad (3\text{-}5)$$

where $V(T,P,t_{eq})$ is the measured equilibrium volume of the polymer-CO_2 mixture at temperature T, pressure P, and equilibrium time t_{eq}. $V(T,P,t_{ini})$ is the volume of the PLA sample under the same conditions, taken from Tait's equation.

3.3.3 **Surface Tension Measurement**

Axisymmetric drop shape analysis profile (ADSA-P) technique was used to measure the surface tension of PLA at various temperatures and pressures ranging from 143 to 168 ° C. The surface tension of the polymer samples was measured by fitting the shape and dimensions of the menisci, obtained through image capturing, to the theoretical drop profile based on the Laplace equation of capillarity:

$$\Delta P = \gamma\left(\frac{1}{R1} + \frac{1}{R2}\right) \quad (3\text{-}6)$$

In order to provide processing conditions for surface tension measurements, a high-temperature and high-pressure chamber was designed as explained previously [32,35]. The optical viewing chamber is a stainless steel cylinder equipped with an electrical band heater and temperature controller. The chamber is a hollow cylinder, with an inner diameter of 30

mm and length of 25 mm, and two optical-quality sapphire windows (Meller Optics, Inc.) that make it possible to observe the pendant drop of polymer melt during the experiment.

Before starting the experiments, the accuracy of the technique was tested using a drop of pure water, and the value of 72.12 ± 0.11 mJ/m^2 was consistent for all the measurements. This agrees with a well-established literature value of water surface tension at 23 ° C [111]. A small amount of polymer, ~ 0.004-0.006 g, was attached to the tip of a stainless steel rod with a diameter of 1 cm and a polished tip to avoid asymmetric drop formation. The method used here has advantages over using drops formed by heating polymer in the capillary tube of a syringe: it eliminates the capillary rise and necking effects, besides allowing for a known system density. To measure the density of the polymer-gas mixture, the volume of one drop was obtained from the pendant drop profile using ADSA software [112] and used to calculate the density of polymer melts at different pressures and temperatures, after the initial weight of the polymer and amount of absorbed supercritical carbon dioxide had been obtained by solubility measurements. The density is an input for surface tension measurement and is introduced through the capillary constant: $C = \frac{\Delta\rho\, g}{\gamma}$, where C is the capillary constant, $\Delta\rho$ is the density difference between the polymer and the supercritical fluid, γ is interfacial tension, and g is gravity's acceleration. The simultaneous measurement of interfacial tension includes introduction of the density of the sample after measurement of its volume. The results can be recalculated using the new density through the capillary constant [112–114].

3.3.4 Differential Scanning Calorimetry

The thermal behavior of PLA at atmospheric pressure was performed using Differential Scanning Calorimeter (DSC), Q2000 (TA Instruments). The PLA sample was heated from room temperature to 200 °C at a heating rate of 10 K/min and then equilibrated at 190 °C for 5 min to eliminate the thermal history. Then the sample was cooled to 10 °C at a rate of 2 K/min and eventually the sample was reheated to 190 °C at a rate of 10 K/min.

3.4 Results and Discussions

3.4.1 Stability of Polymer Melt Drops

Due to the importance of crystallization on surface tension through preferential adsorption of crystallized polymer particles at interfaces [35,36], the presence of any crystals

in the system should be shown. Figure 3-2 shows isothermal differential scanning calorimetry of the PLA melt at 143 °C. No peak is observed after more than 2.5 hours of experiment denoting the absence of crystals at the lowest temperature of the interfacial tension measurements.

In order to find the desired size of the polymer melt drop for pendant drop measurements, the stability of the drops can be investigated through a dimensionless Bond number, as shown in the Equation 4-7:

$$Bo = \frac{\Delta\rho\, g\, R^2}{\gamma} \qquad 3\text{-}7$$

where $\Delta\rho$ is the density difference between PLA-$SCCO_2$, g is gravitational acceleration, R is the average radius of curvature of the drop, and γ is the interfacial tension between the two phases . Since Bond number is the ratio between buoyancy forces and surface forces, it can determine the range of stability of the drop as well as the validity of surface tension measurements [115]. With this in mind, polymer drops with a wide range of weights at different pressures were formed. Figure 3-3 shows the range of stability of polymer melt drops based on Bond number. Bond numbers for drops with surface tension value discrepancies of a maximum 2% from the average are shown. The lower and higher limit for polymer melt drops are 0.37 and 0.48, respectively. It turns out that for polymer drops with Bond number beyond 0.48, breakage and necking phenomena were happened, and for Bond numbers below 0.37 the accuracy of measurements were questionable due to the formation of "close to spherical" drops and an imbalanced ratio between buoyancy forces and surface forces [115,116].

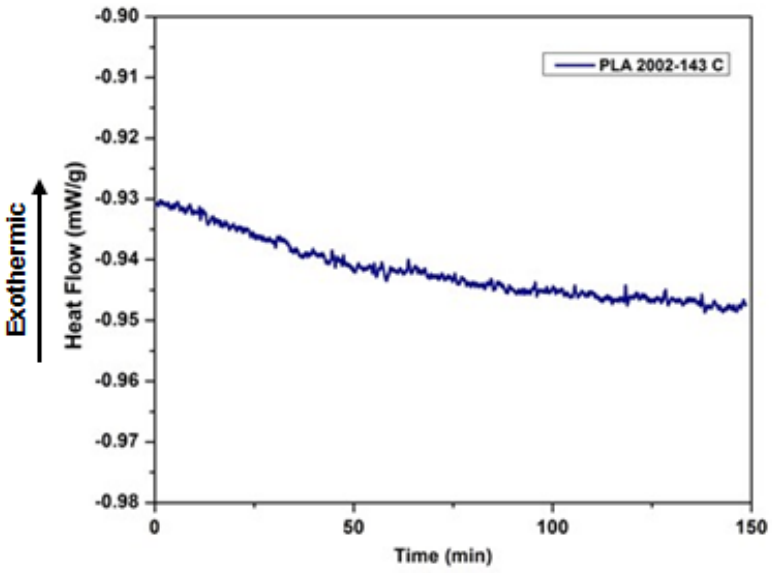

Figure 3-2.Isothermal differential scanning calorimetry of PLA 2002 sample at 143 °C

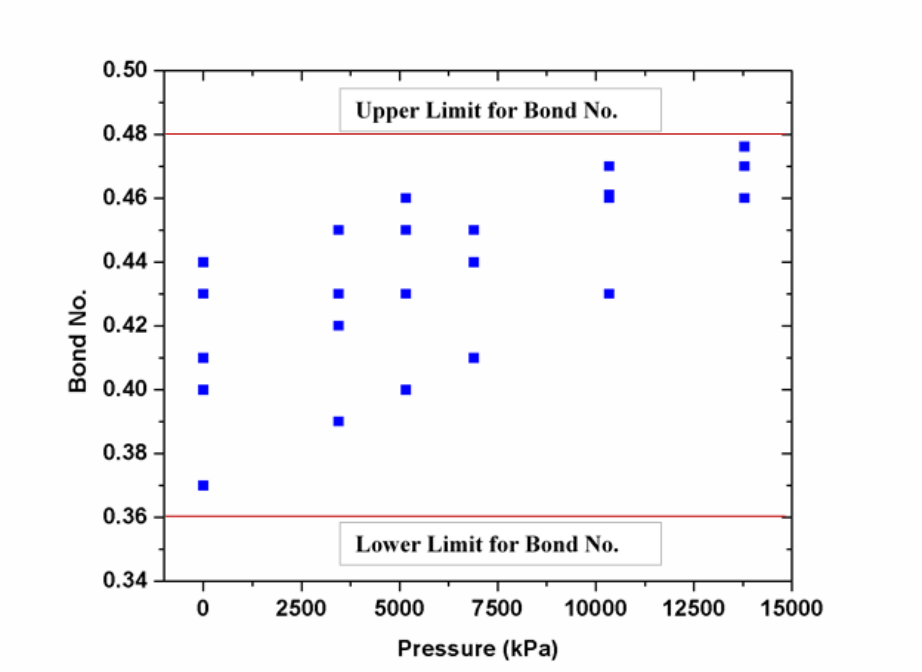

Figure 3-3. Bond number vs. pressure reflecting the range of stability of polymer drops.

3.4.2 **Solubility Measurements**

Like surface tension, solubility is another determining factor in microcellular foam processing and polymer blending [107,117,118]. Knowing solubility, as well as surface tension in the processing range of temperature and pressure, one can decide on the processing window of the desired polymer. Figure 3-4 presents the solubility data in the pressure range of 3450 to 13790 kPa for temperatures of 140, 150, 160 ° C. As can be seen from the graph, at a constant temperature, an increase in pressure increases the solubility due to higher dissolution of gas molecules at high pressures. On the other hand, as temperature increases the solubility of CO_2 decreases; although there is more free-volume for adsorption of gas molecules at elevated temperatures, the rate of desorption for physisorption is higher [119]. Moreover, a reduction in the polymer viscosity leads to less resistance in retention of gas molecules in polymer melt. Beside the importance of solubility results in the processing of polymers with supercritical CO_2, they can be used to simultaneously determine the density of the mixture at high temperatures and pressures; the amount of dissolved carbon dioxide is added to the initial weight of polymer.

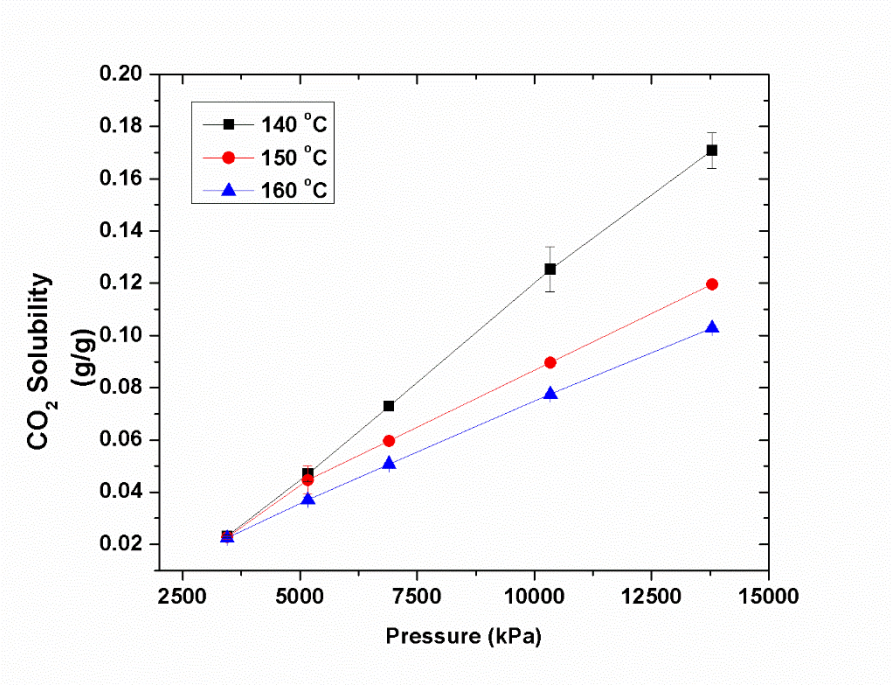

Figure 3-4. Solubility data of PLA at pressures from 3450 to 13790 kPa and 140,150, and 160 ° C

3.4.3 **Effect of Pressure and Temperature on Interfacial Tension**

Figure 3-5 shows the variation of PLA interfacial tension as a function of temperature and pressure. The interfacial tension decreases when both temperature and pressure increase. The reduction in interfacial tension of the polymer and supercritical CO_2 caused by increasing temperature happens because of a change in the overall internal energy of the system. It has been shown that the internal energy of mixture of polymers and gases (supercritical CO_2) is dominant in determining the overall internal energy [33]. Thus, the polymer-gas internal energy determines the reduction in surface tension at higher temperatures. Surface tension can be obtained from a derivative of the free energy with respect to surface area. Free energy is defined as F= U- TS, where F is free energy, U is internal energy and S is entropy. The entropic contribution improves the mixing of the polymer-gas system, while an increase in internal energy promotes segregation of the polymer and gas. An increase in temperature leads to a reduction in the effective interaction between polymer and gas molecules, and so the internal energy decreases. On the other hand, a reduction in internal energy makes entropy a relatively larger contributor in the free energy and improves mixing across the interface. The interface then becomes more diffuse leading to a lower surface tension.

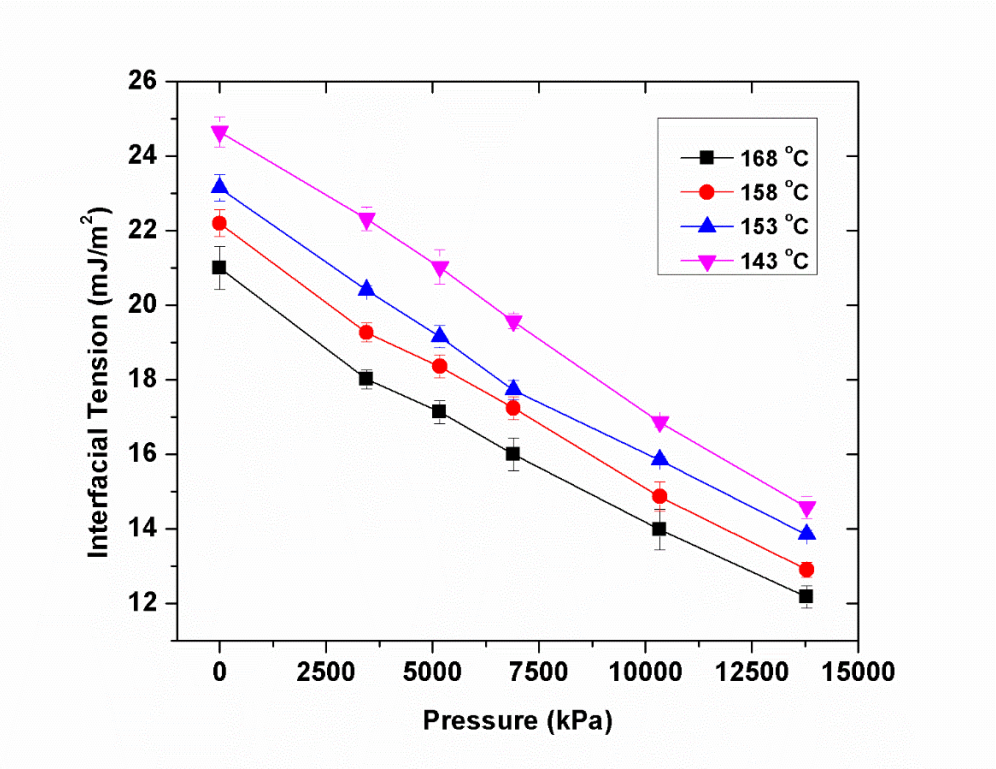

Figure 3-5.Interfacial tension between polymer and supercritical carbon dioxide at different pressures and temperatures

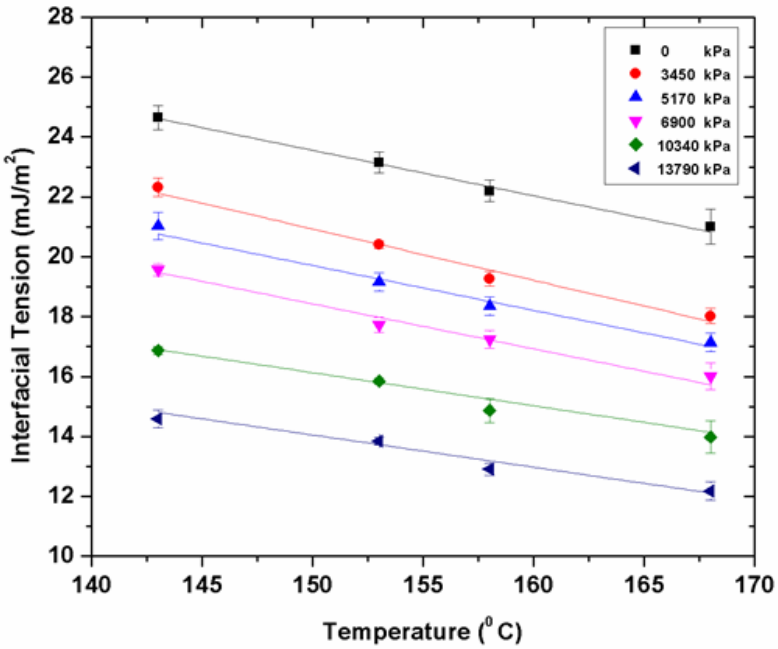

Pressure (kPa)	Slope
0	-0.15
3450	-0.17
5170	-0.15
6900	-0.15
10340	-0.11
13790	-0.10

Figure 3-6. Interfacial tension of PLA and supercritical CO_2 as a function of temperature at different pressures and related slope of linear function at various pressures

In terms of density of the system, for an increase in pressure, the density of the CO_2-rich phase increases. As explained in references [32,33], the surface tension drops when the CO_2 phase increases in density to be more similar to the density on the polymer side of the interface. Thus one can say the drop in surface tension with increasing pressure is due to a reduction of the density difference between two sides of the interface as the reduction in density difference between phases can be seen in Figure 3-7.

Based on Figure 3-6, because of the interaction term between pressure and temperature, the temperature dependency of interfacial tension is different at low and high pressures. It was observed that at low pressures, interfacial tension decreases when temperature increases, while at high pressures, the interfacial tension becomes less dependent on the temperature. This independence occurs because at high temperatures and high pressures two competing effects occur: on the one hand, surface tension is reduced because of an increase in temperature, and on the other hand, the solubility of CO_2 decreases at high temperatures, as can be seen in Figure 3-4. The interaction between the two above-mentioned competing factors leads to a diminishing of the temperature effect on the interfacial tension at high pressures [6,32].

3.4.4 **Density and Surface Tension Relationship**

The trends for density of gas-PLA mixture, density difference between gas-PLA mixture and surrounding (supercritical CO_2), and density of CO_2 at 160 °C are shown in Figure 3-7. From the graph it can be seen that the mixture density does not change significantly with increasing pressure since the increase in drop volume due to CO_2 dissolution is compensated by an increase in mass owing to CO_2 absorption. On the contrary, on the gas side (drop surrounding) the density of CO_2 increases with an increase in pressure, the fact which leads to a decrease in the density difference across the interface.

The generalized Macleod equation is used to find the relationship between the interfacial tension and density of polymer-supercritical CO_2 mixtures:

$$\gamma = C(\rho_p - \rho_f)^n \qquad 3\text{-}8$$

where γ is the interfacial tension between polymer and supercritical CO_2, C is a constant, n is Macleod's exponent, and ρ_p and ρ_f are the density of the polymer and the supercritical fluid, respectively. The relationship between density and surface tension originate from the dependency of surface tension on the distance between the molecules. In other words, the attractive van der Waals forces lessen according to the 4^{th} power of the intramolecular distances: an increase in a fluid's temperature increases the distance between molecules, and consequently, density decreases [120]. Figure 3-8 shows the surface tension of polymer-supercritical CO_2 as a function of density in logarithmic scale for four temperatures. The results for all the temperatures follow the same trend, and the slope is in range of 1.84 to 1.94. This is higher than the surface tension at atmospheric pressure because of the reduction in conformational restriction at the polymer surface due to the presence of CO_2 molecules [32].

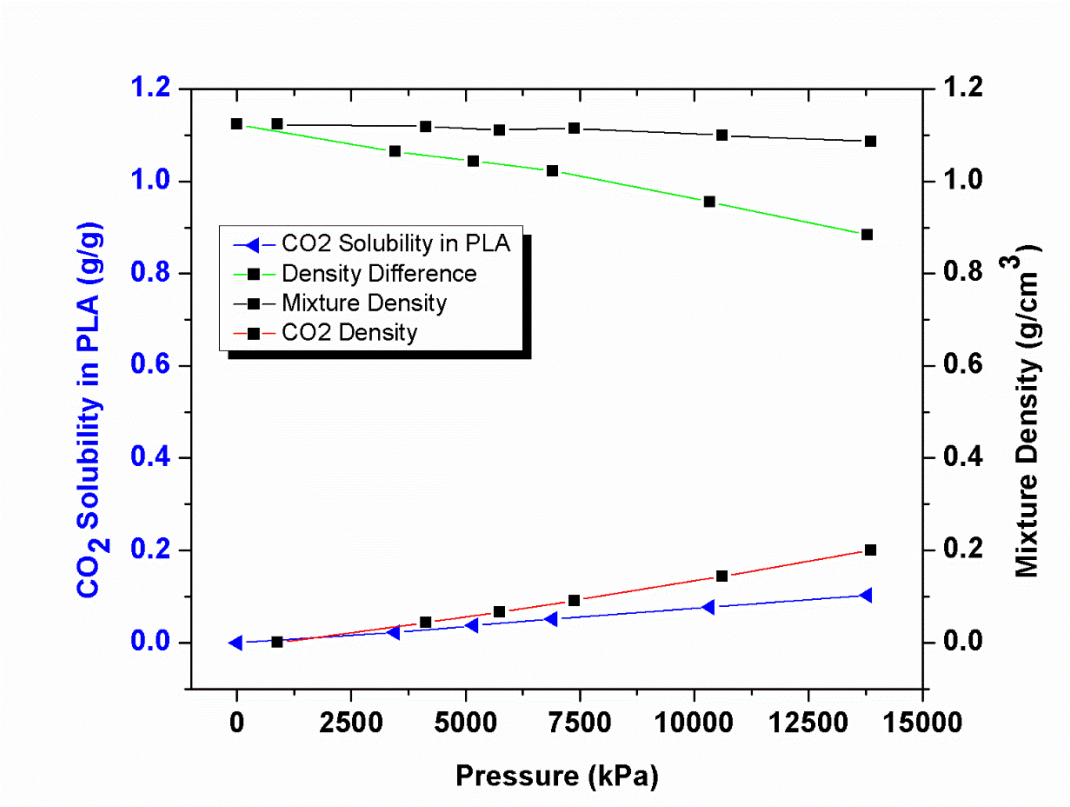

Figure 3-7.Comparison between density, density difference of PLA-CO2 mixture, CO2 density (y-axis on the left side), and CO2 solubility (y-axis on the left side) at different temperatures and 160 °C.

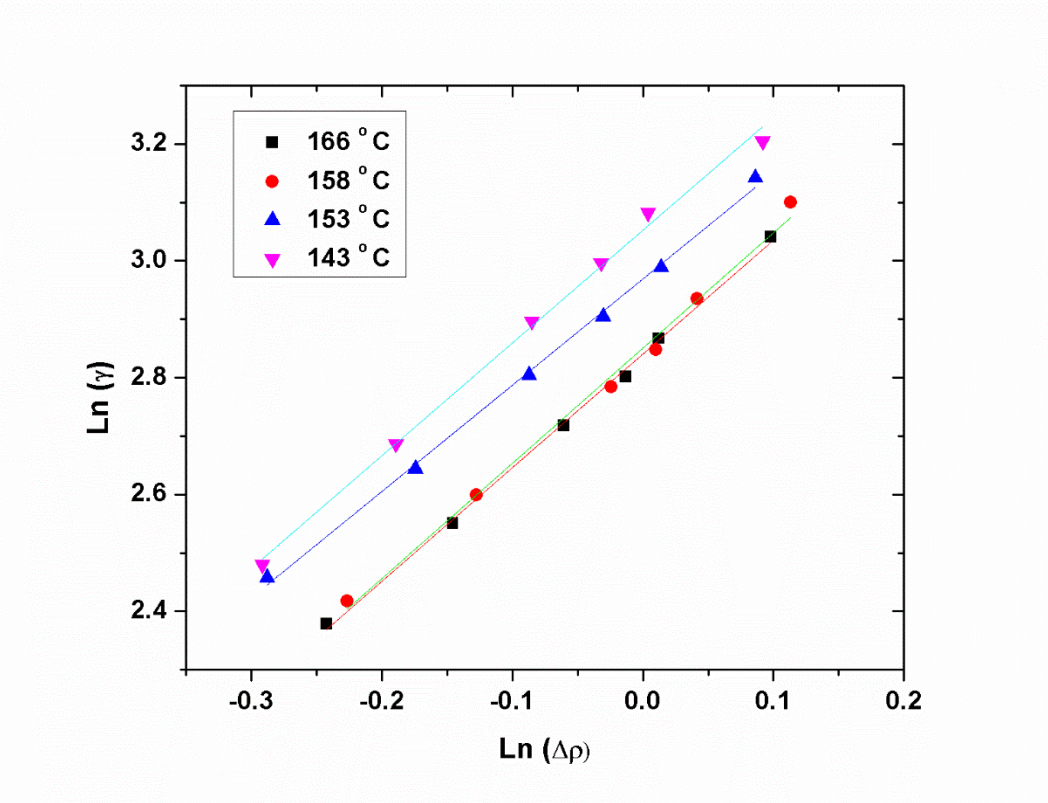

Figure 3-8. Surface tension vs. density difference of polymer-supercritical CO_2 in natural logarithmic scale at different temperatures.

3.5 Conclusions

In this work, we have investigated the dependency of the interfacial tension of poly lactic acid (PLA) in supercritical carbon dioxide on temperature and pressure using the Axisymmetric Drop Shape Analysis Profile (ADSA-P) pendant drop method. The interfacial tension of PLA-supercritical carbon dioxide is measured in the temperature and pressure range of microcellular foaming and blending processes. The results showed a reduction in interfacial tension with increasing temperature and pressure in the ranges of 143°C to 168°C and 3450 to 13790 kPa, respectively. The interfacial tension dependency on temperature at high pressures decreases because of two competing factors: reduction in interfacial tension as a result of an increase in temperature, and the reduction in solubility of CO_2 at high temperatures. The relationship between interfacial tension and the density-difference of polymer-supercritical-CO_2 mixtures showed similar trends in different temperatures with slopes in the range of 1.84 to 1.94. In addition, the stability of melted PLA for pendant drop

measurements was examined by dimensionless Bond number and it turned out that drops in the range of 0.36-0.48 were stable.

4. CHAPTER 4: ADSORPTION OF SURFACE-MODIFIED SILICA NANOPARTICLES TO THE INTERFACE OF MELT POLY (LACTIC ACID) AND SUPERCRITICAL CARBON DIOXIDE

*K. Sarikhani, K. Jeddi, R.B. Thompson, C.B. Park, P. Chen**

Graphical Abstract

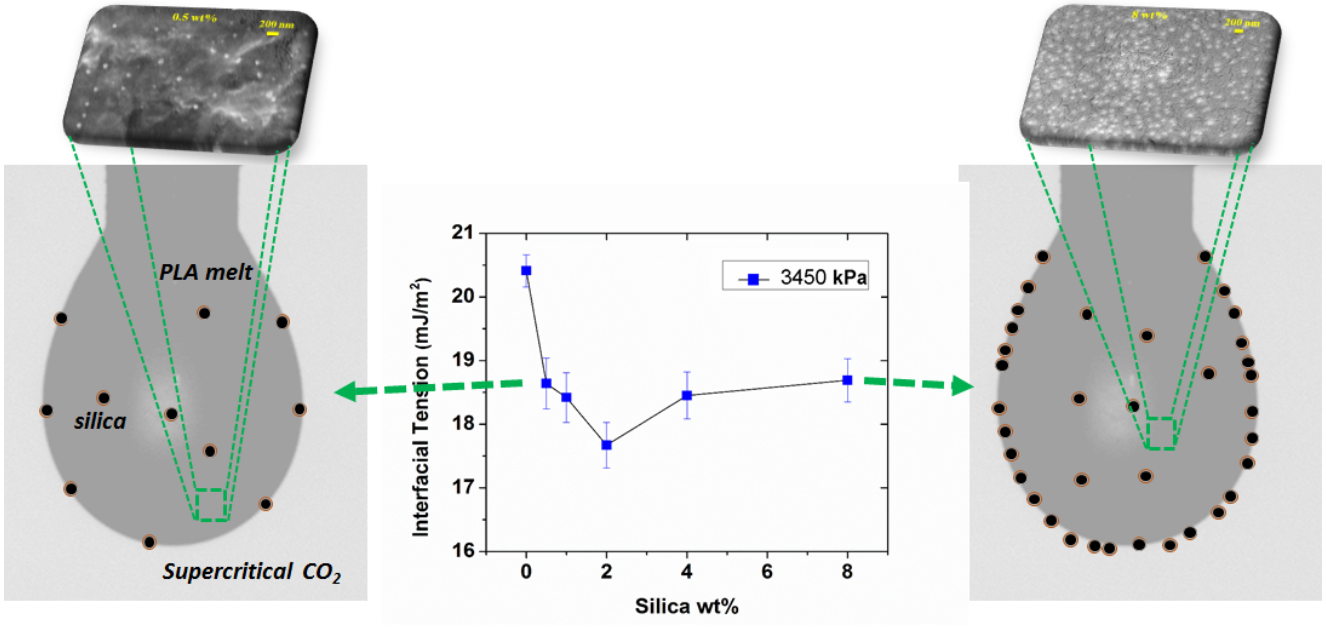

* Published in Langmuir 2015, 31, 5571□ 5579

4.1 Summary

In this chapter the effect of surface-modified nanoparticles on interfacial tension of poly lactic acid (PLA) melt under supercritical carbon dioxide (CO_2) is measured. The nanoparticles can act as nucleating agent in foaming. The interfacial tension between PLA and supercritical CO_2 is observed to decrease as a result of nanoparticles' adsorption to the interface. In some cases to improve the surface rheological properties to prevent coalescence. The results are of practical importance for further development of polymer nanocomposite foams.

The results are published in *Langmuir* (2015). The co-authors include professor Pu Chen as supervisor, professors Chul B. Park and Russell Thompson as co-supervisors, and Kazem Jeddi who assisted me in performing some replica experiments of the interfacial measurements.

4.2 Introduction

Polymer nanocomposites are interesting materials with broad applications and exceptional properties such as better mechanical, thermal, electrical, and electrochemical properties [121–125]. In most cases dispersion of the nanoparticles within the polymer matrix of the nanocomposites is desired, however for some applications, such as colloidosomes, nanoparticle-armed polymer latex, Janus structures, and foams and emulsions stabilized by particles, localization is necessary [42,43,45,126,127].

In polymeric foams made with dissolved supercritical fluids, the cell size and the cell density can be controlled by reducing the interfacial tension between the polymer and the dispersed phase (supercritical fluid). According to classical nucleation theory (CNT), the nucleation rate is inversely related to the exponential cubic power of interfacial tension; [6,22] therefore one can increase the number of nucleating sites by lowering the surface tension. The decrease in surface tension decreases the energy barrier for cell nucleation and consequently increases the number of cells, leading to an exponential increase in cell densities. Moreover, lowering the surface tension results in a smaller cell size, since the critical cell size is directly related to surface tension [1]. It is noteworthy that CNT with its surface tension predictions is expected to break down for nano-cellular foams, although this is beyond the scope of this paper [128,129].

Similar to the role of surfactants in reduction the surface tension of foams, particles can be used to promote foam formation and stabilization. As a general concept, solid nanoparticles, such as silica, can be adsorbed at the interface and decrease the interfacial tension between polymer melts and supercritical fluids. Furthermore, nanoparticles can act as nucleating agents for the foaming of polymers by increasing local stress variations around the particles (directly) [130,131] , and/or by promoting the crystallization of the polymers [89], since the crystals can create local stress variations as the nanoparticles do (indirectly) [88,90].

A large number of recent studies have focused on the incorporation of solid nanoparticles as surfactants in the stabilization of foams and emulsions, provided that they are adsorbed to the fluid-gas or fluid-fluid interface, respectively, and it has been shown that the contact angle of the particles dictates the stability [103,132]. For small particles, for which the effect of gravity is negligible, the energy (E) required to remove the particle from the interface is called binding energy or adsorption energy (the free energy change upon particle adsorption to the interface), and is given by [133]

$$E = -\pi r^2 \ \gamma_{\alpha\beta} (1 \pm \cos\theta)^2 \qquad 4\text{-}1$$

where r is the radius of the particle, $\gamma_{\alpha\beta}$ is the interfacial tension between two phases (polymer-supercritical fluid in our case), and θ is the Young contact angle between the particle and the two phases (particle at the interface). Young contact angle is defined as

$$\cos\theta = (\gamma_{\alpha p} - \gamma_{\beta p})/\gamma_{\alpha\beta} \qquad 4\text{-}2$$

where $\gamma_{\alpha p}$, $\gamma_{\beta p}$ are the interfacial tension of the particle-polymer and particle-supercritical fluid interfaces, respectively. In the binding energy equation, considering the polymer-supercritical fluid interface with colloidal nanoparticles in the polymer phase, the sign inside the bracket is negative for removal into the polymer phase, and positive for removal into the supercritical fluid phase ,or simply the ($\pm$) signs correlate to the cases where the particle center is above (positive) or below (negative) the interfacial plane. The particles will attach to

the interface and the adsorption is irreversible if E >> k_BT, where k_B is the Boltzmann constant and T is temperature in Kelvin [51,133,134].

Although adsorption of solid particles to an interface can decrease interfacial tension, some self-assembled structures at the interface can increase the tension at the interface due to an increase in lateral capillary forces. The interface of the polymer melt can be deformed due to the adsorption of particles at the interface. In general, deformation of a liquid surface can cause a lateral capillary force [135]. Depending on the particles' weight and wetting properties, the force is considered as an immersion force or a floatation force [136,137]. If the force from the weight of the particles is significant and the particles are floating at the interface, the attractive or repulsive force is called a floatation force. On the other hand, for small particles partially immersed in both phases, the force is called an immersion force. The deformation of the liquid surface and magnitude of the immersion capillary force depend on the wetting properties of the particle, the magnitude of the contact angle, and the position of the contact line, and they are independent of particle weight. Equation 4-3 shows the amount of the capillary interaction energy between two immersed particles: [136,138,139]

$$\Delta w = 2\pi\,\gamma\,Q^2 K_0(qL) \qquad 4\text{-}3$$

where γ is the interfacial tension, Q is the capillary charge of the particle, defined as $Q = r\sin\theta$, θ is the contact angle between a particle and the liquid at the interface, r is the radius of the contact line, q is defined as $q^2 = \frac{\Delta\rho\, g}{\gamma}$, g is gravity, Δρ is the density difference, K_0 is the modified Bessel's function of zeroth order, and L is the distance between two particles. Equation 3 is valid when the distance between the particles is much smaller than the capillary length ($L << q^{-1}$ and also when the radii of the two contact lines is much smaller that the particle separation. It can be seen from equation 5-3 that for fairly close particles, the capillary interaction (even for nanoparticles) is significant.

In this work, interfacial behavior of PLA-silica nanocomposites in a CO_2 environment is investigated in detail. Interestingly, a non-linear trend in interfacial tension values with increasing amount of nanoparticles is observed. It is observed that lateral capillary force of the adsorbed aggregates of the nanoparticles to the PLA- CO_2 interface is the reason for the observed increase in interfacial tension at higher contents of the nanoparticles.

4.3 Experimental

4.3.1 Materials

Polylactic acid (PLA), grade 2002D, with M_n= 100 kg/mol and D-content of 4.5% was kindly provided by NatureWorks Inc. Carbon dioxide chromatographic grade with purity of 99.99% was purchased from PRAXAIR, Canada. Tetraethyl orthosilicate (TEOS), ammonium hydroxide (28-30 % aqueous solution), (3-Aminopropyl) triethoxysilane (APTES) 99% were purchased from Sigma-Aldrich. Deionized water (18.2 M□) was obtained from a Millipore Milli-Q system.

4.3.2 Synthesis of silica nanoparticles

Silica nanoparticles were made using the well-known Stöber method [140]. A typical procedure to make an 80 nm silica particle was as follows: at room temperature, 8cc of tetraethylorthosilicate (TEOS; Sigma-Aldrich) was added to 100 cc of ethanol. The pH was adjusted using 16 cc of ammonium hydroxide solution (28wt %). The sol-gel reaction was carried out for four hours. Particle size was monitored using Dynamic Light Scattering (DLS), Scanning Electron Microscopy (SEM), and Transmission Electron Microscopy (TEM). After four hours, the silica was separated by centrifuging at 14000 rpm and washed with ethanol six times. Afterwards, the silica nanoparticles were dried in an oven for 48 hours at 80° C.

4.3.3 Surface modification of silica nanoparticle

Surface modification of silica nanoparticles was carried out through another sol-gel reaction on the surface of re-dispersed silica nanoparticles in toluene or ethanol. The reaction happens between first (3-aminopropyl) trimethoxysilane (APTES) and the hydroxyl functional groups on the surface of silica nanoparticles [141,142]. In order to modify the surface of silica with amine functional groups, 1.6 g of silica nanoparticles were dispersed in 100 ml ethanol containing 5 ml ammonium hydroxide solution (28 %), then 3 ml of APTES was added to the solution and stirred for 24 h at 75 ° C. At the end of the reaction, the particles were collected by centrifuge, washed three times with ethanol, and dried in a vacuum oven at 80 ° C.

4.3.4 Compounding of silica nanoparticles with PLA

A co-rotating miniature twin screw extruder (Haake Mini Lab Rheomex CTW5) was used to disperse the synthesized nanoparticles in PLA matrices at 180 ° C at 150 rpm. The residence time of the polymer in the compounder was set based on thermal analysis and sample testing to make sure there was no polymer degradation during compounding.

4.4 Characterization

4.4.1 Interfacial tension and contact angle measurements

Interfacial tension of PLA composites at various pressures of supercritical CO_2 and at 153° C was measured using axisymmetric drop shape analysis profile (ADSA-P) technique. The technique, instrument, and methodology is explained in detail in section 3.3.3.

Contact angle measurements were also carried out in a similar high pressure high temperature chamber capable of mounting the silicon surface on top of the inversed stainless steel rod.

4.4.2 Characterization of the nanoparticles

Field emission scanning electron microscopy (FE-SEM) (Ultra, Zeiss) with energy-dispersive X-ray (EDX) spectroscopy was used to investigate the morphology of the nanoparticles. The samples were gold-sputtered prior to SEM. SEM images of the solidified PLA-silica APTES nanocomposite melts are also measured through gold-sputtering of solidified sample after the interfacial tension measurement. Sufficient amount of time is provided to assure the equilibrium interfacial tension is provided.The hydrodynamic diameter of silica nanoparticles were determined by dynamic light scattering (DLS) on a Zetasizer Nano ZS (Malvern Instruments, Worcestershire, U.K.) equipped with a 4 mW He□ Ne laser operating at 633 nm. FTIR spectrums were obtained using a Bruker Vertex 70 FTIR spectrometer from 400 to 4000 cm^{-1} on a KBr pellet. A Dimension Icon® AFM (Bruker Nano Surfaces) with a silicon nitride tip (type SCANASYST-AIR, Bruker) with a radius of 2 nm was used for AFM imaging in the PeakForce® QNM mode.

4.5 Results and Discussions

Shape and size of the synthesized silica nanoparticles can be observed in SEM and TEM images Figure 4-1A and B. The uniform spherical particles have an average diameter of around 80 nm as confirmed with DLS results in Figure 4-1 C (number-average diameter ~ 80 nm and z-average diameter ~100 nm).

FTIR spectra in Figure 4-2 prove the presence of modification on silica nanoparticles. In the spectra, the Si-O peaks at 800 and 1100 cm^{-1}, Si-OH at 950 cm^{-1}, and the broad OH peak in range of 3200 to 3700 cm^{-1} can be observed in both silica and silica-APTES. However, after surface modification with APTES, the intensity of OH peak is decreased showing a reduction in the number of surface OH groups. It is noteworthy to mention that the OH peak can be attributed to both surface hydroxyl groups and adsorbed water molecules. There are significant number of hydroxyl groups in terms of isolated silanols, germinals, and vicinals as well as hydrogen bonded hydroxyl groups. The number of hydroxyl groups on surface varies depending on hydroxylation state of silica and can be as high as 4.9 $OH.nm^{-1}$ even after vacuum treatment at high temperatures [143]. On the other hand, there are always water molecules accompanying the OH groups on the surface as the peak at 1630 cm^{-1}. These water molecules only can be removed with high temperature thermal treatment. Once they are removed from the surface, the water molecules will immediately adsorb to the surface from atmosphere and their presence on the surface seems inevitable [144].

For the silica modified with APTES, bending of $-CH_3$ at 1385 cm^{-1} and stretching of C-H at 2933 cm^{-1} for alkanes, and bending of N-H at 694 cm^{-1} are recognizable. The Si-OH peak at 950 cm^{-1} is also decreased significantly.

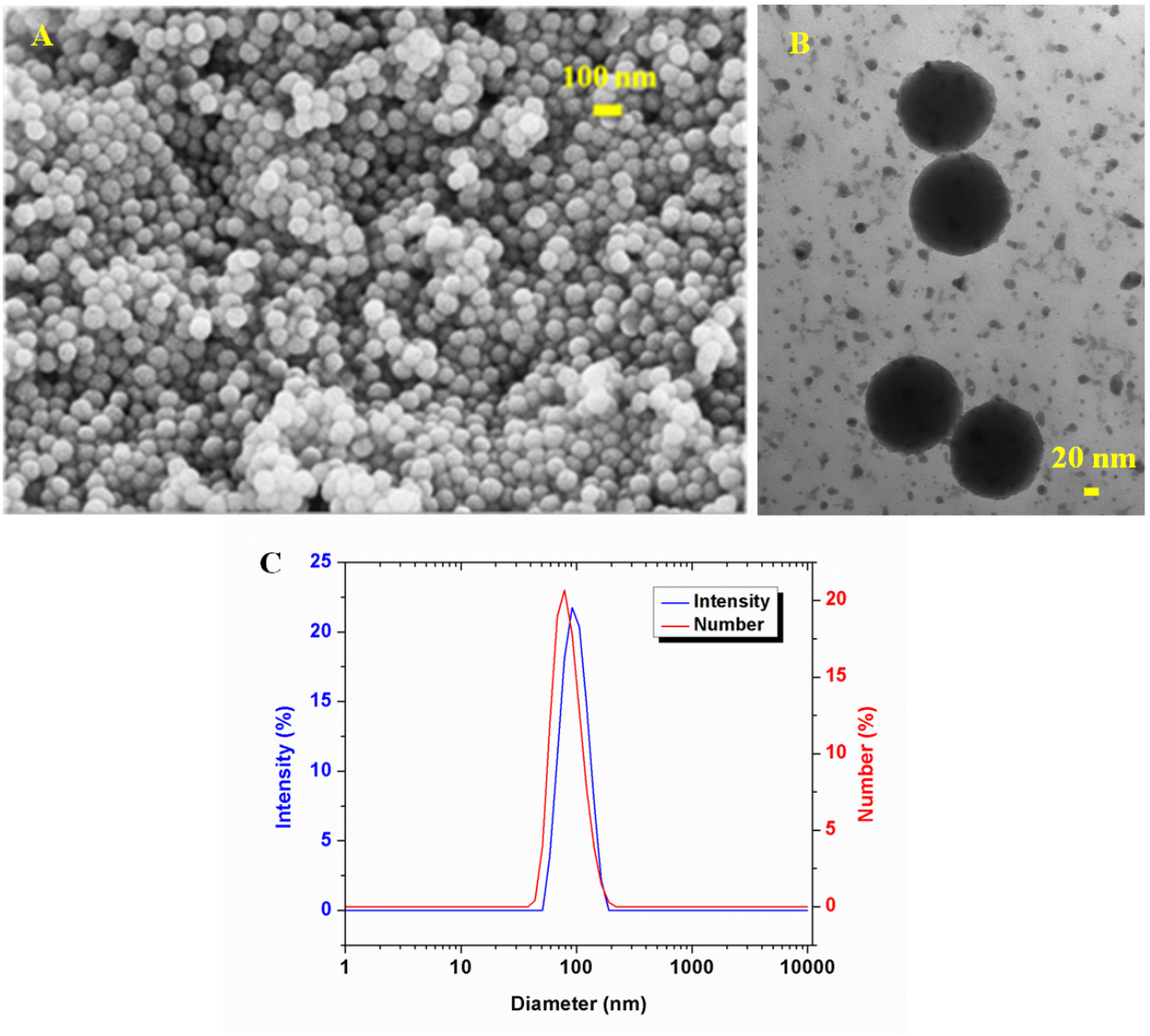

Figure 4-1.Scanning Electron Microscopy (SEM) (A) and Transmission Electron Microscopy (TEM) (B) images of synthesized silica nanoparticles (C) intensity and number diameter distribution results of the silica nanoparticles obtained from DLS.

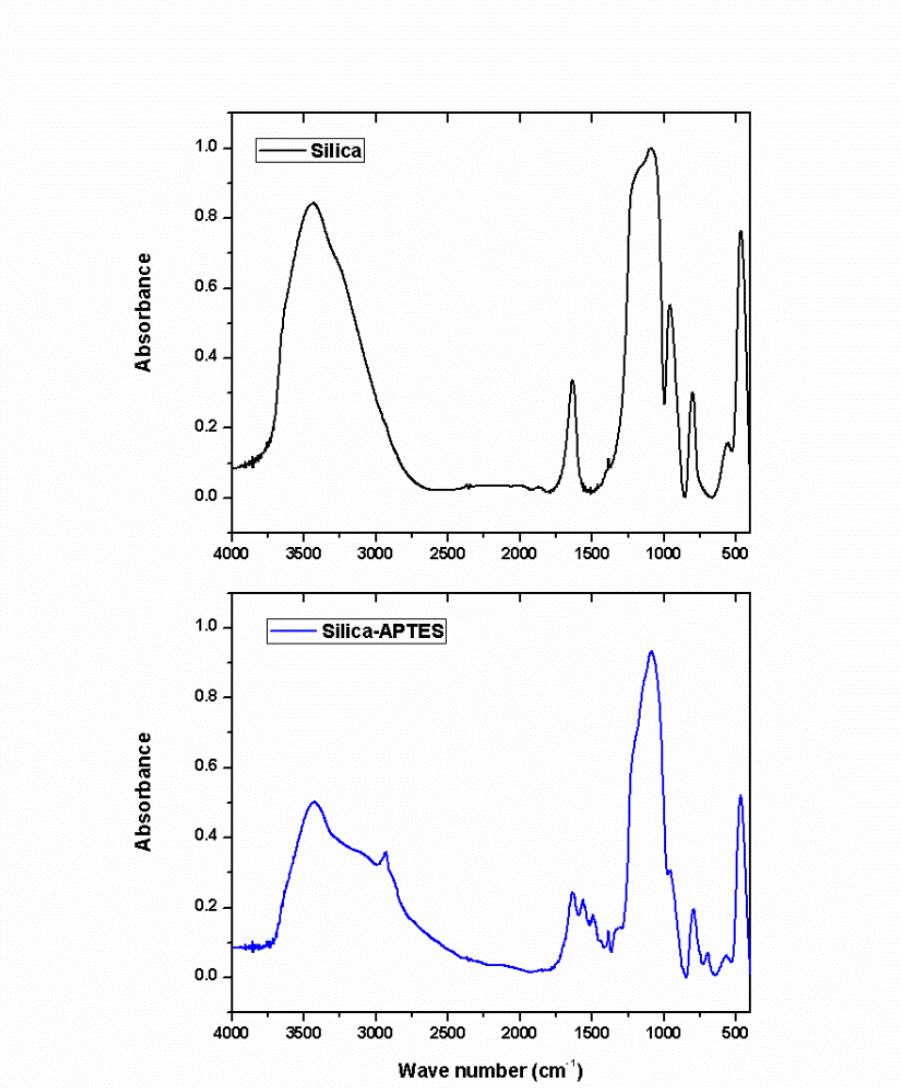

Figure 4-2. FTIR spectrum of silica nanoparticles before (top) and after (bottom) surface modification with APTES.

In Figure 4-3, the surface tension values of PLA-silica composites versus silica content at pressures of CO_2 ranging from 0 to 13790 kPa (gauge pressure) is illustrated. As can be seen, the interfacial tension decreases with an increase in silica content up to 2 wt. % and then an increase and a plateau is observable in all the pressures. The decrease in interfacial tension can be attributed to the adsorption of the silica nanoparticles to the PLA/ CO_2 interface. It has been observed that nanoparticles dispersed in a polymer matrix migrate to a crack generated at the interface between the polymer and a glassy layer. [145] Thompson et al.[36]

showed that the probability of finding a nano-crystal in the vicinity of the polymer surface is higher than the bulk. Nano-crystals form a narrower boundary at an interface with a fluid which lowers the internal energy and thus the interfacial tension. Furthermore, a reduction in surface tension of an air-water interface in a low concentration of nanoparticles as a results of a decrease in internal energy of the interface has been reported. The phenomena has been observed for suspensions of titanium oxides [137], and silica [61] at basic pH values where there is a minimum in interfacial tension versus concentration curve around 5-7 wt.% of the particles. For both cases, eventually the interfacial tension value will be constant after 10-12 wt. %. Notwithstanding the evidences for adsorption of the nanoparticles to the interface, the reduction in interfacial tension is not as significant as silica in oil-water systems [146]. The reason can be explained in the mechanism the nanoparticles act to decrease the interfacial tension; unlike the surfactants, particles are driven to the interfaces to remove contact between the two phases [147] and where the nanoparticles' contact area with the interface is small then the effect on interfacial tension will be less [148].

As a general fact, nanoparticles can be used as a surfactant in stabilizing foams and emulsions [73,126,133]. There are a few reasons for adsorption of nanoparticles to the PLA-CO_2 interface: first of all, for a particle in a two phase system, due to weaker interactions compared with bulk, creating a surface is more favorable at the interface rather than any of the phases (with the same molecules surrounding). Secondly, the adsorption is thermodynamically favorable not only because of a desirable interaction between amine groups on silica surfaces and carbon dioxide, but also because of an increase in entropy of the polymer bulk as a results of increase in free volume and a reduction in entropy-restricting polymer adsorption at the particle interfaces [149].

As can be seen in Figure 4-3 and Figure 4-4, the interfacial tension increases for values higher than 2 wt. % of silica. An increase in interfacial tension after a certain loading of nanoparticles can be related to the lateral capillary force created by a deformation of the PLA melt meniscus as a result of partial immersion of silica nanoparticles in the interface [61,137,150,151].

It is noteworthy that observation of a minimum in interfacial tension-concentration curves should not be mistaken for being the same as the case of aqueous solution of surfactants [152]. In the latter case, the minimum is seen before the critical micelle concentration (CMC) for surface-active impurities in the surfactant system. Due to the

presence of nanoparticles at the interface, the shape of interface surrounding them at the fluid phase boundaries is perturbed and is not flat; this fact causes a significant distant dependent capillary force between the particles [138]. Deformation, and subsequently capillary force is related to the wetting behavior of the particles (contact angle between three phases) and the distance between particles [150]. The immersion force, the force between small particles partially immersed in both phases, can be attractive or repulsive depending on the sign of the meniscus slope angles at the two contact lines of the two particles adjacent to each other: if the product of the sine of the contact angles for the two particles are positive (negative), the capillary force is going to be attractive (repulsive) [150]. For similar silica nanoparticles with similar surface properties, the contact angles are the same and consequently the force is attractive, provided that the particles are close enough to each other. As can be seen in SEM images in Figure 4-5, in higher loadings of silica, the number of the nanoparticles is higher at the interface of solidified PLA nanocomposits, and the chance of finding particles close enough to induce an attractive capillary force towards each other is higher. The high capillary force at the interface resists a deformation or stretching in surface area. Since interfacial tension is defined as the work required against a change in the surface area, an increase in the resistance at the interface leads to an increase in the force required to increase the surface (due to capillary force in our case) which eventually causes an increase in interfacial tension in higher loadings of the particles [137] .

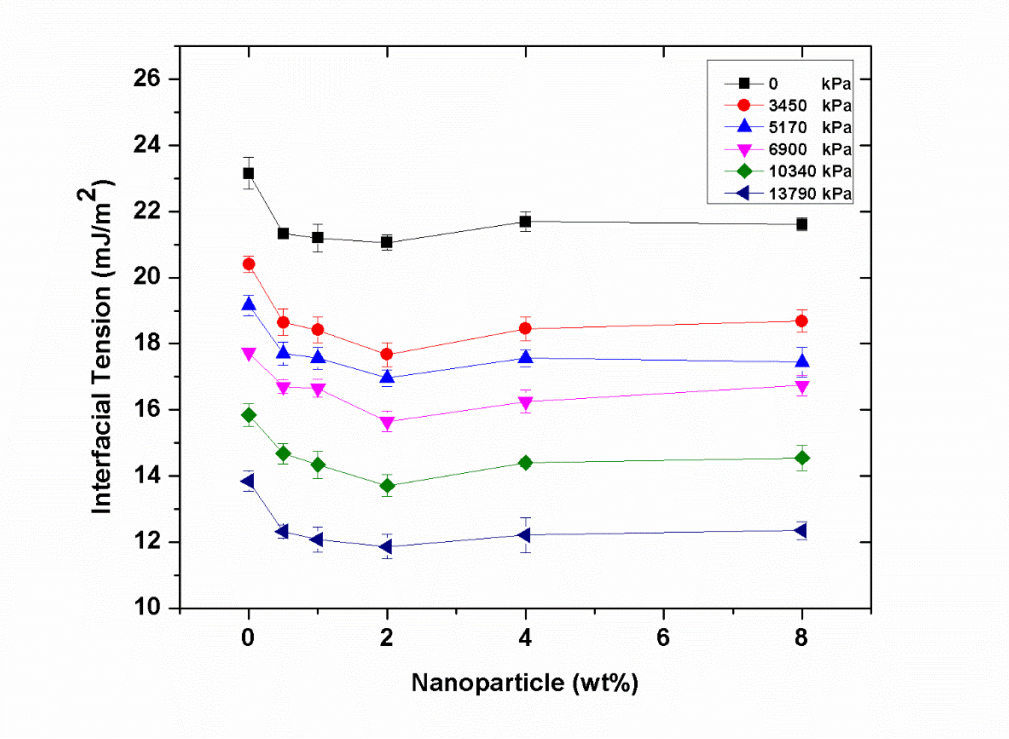

Figure 4-3. Interfacial tension values of PLA-silica APTES composites versus silica content at different pressures of carbon dioxide (gauge pressure) at 153° C

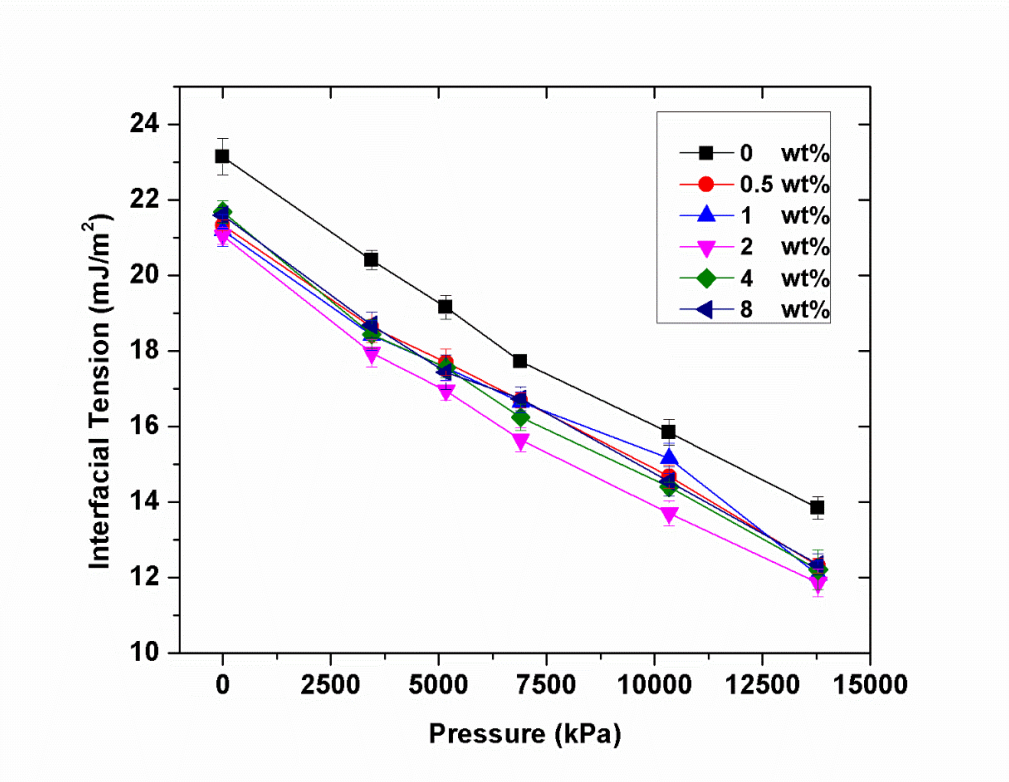

Figure 4-4. Interfacial tension values of PLA-silica APTES composites versus different pressures of carbon dioxide for various loadings of silica nanoparticles at 153° C

In order to prove the presence of the silica nanoparticles at the interface, SEM images of the solidified nanocomposites are obtained after interfacial tension measurements at atmospheric pressure of carbon dioxide environment and consequently solidification of the pendant drop polymer melt. Figure 4-5 shows the SEM results for different loadings of APTES-modified silica-PLA nanocomposites. It is clear in SEM images that in 4 and 8 wt.% of the nanoparticles, the number of the nanoparticles increases significantly which leads to an increase in the chance of finding nanoparticles in vicinity of another particle: particles with distance less than capillary length cause localized lateral capillary forces at higher loadings of the nanoparticles a dominant force. Considering Equation 4-3, at higher loadings of the nanoparticles the two conditions for capillary forces to be effective are available: the distance between the particles in nanoparticle systems are lower than capillary length $L << q^{-1}$ and the particle separation is large enough. It should be noted that even though the surface is more covered at higher loadings of nanoparticles (8 wt.%), the surface coverage is much less than aqueous systems (typically more that 90% coverage) [134], therefore the nanoparticles separation can be considered large. EDX results for a surface of 0.5 wt. % nanocomposite in

Figure 4-6 shows the presence of a silicon peak for bright spots, proving the spots are silica nanoparticles.

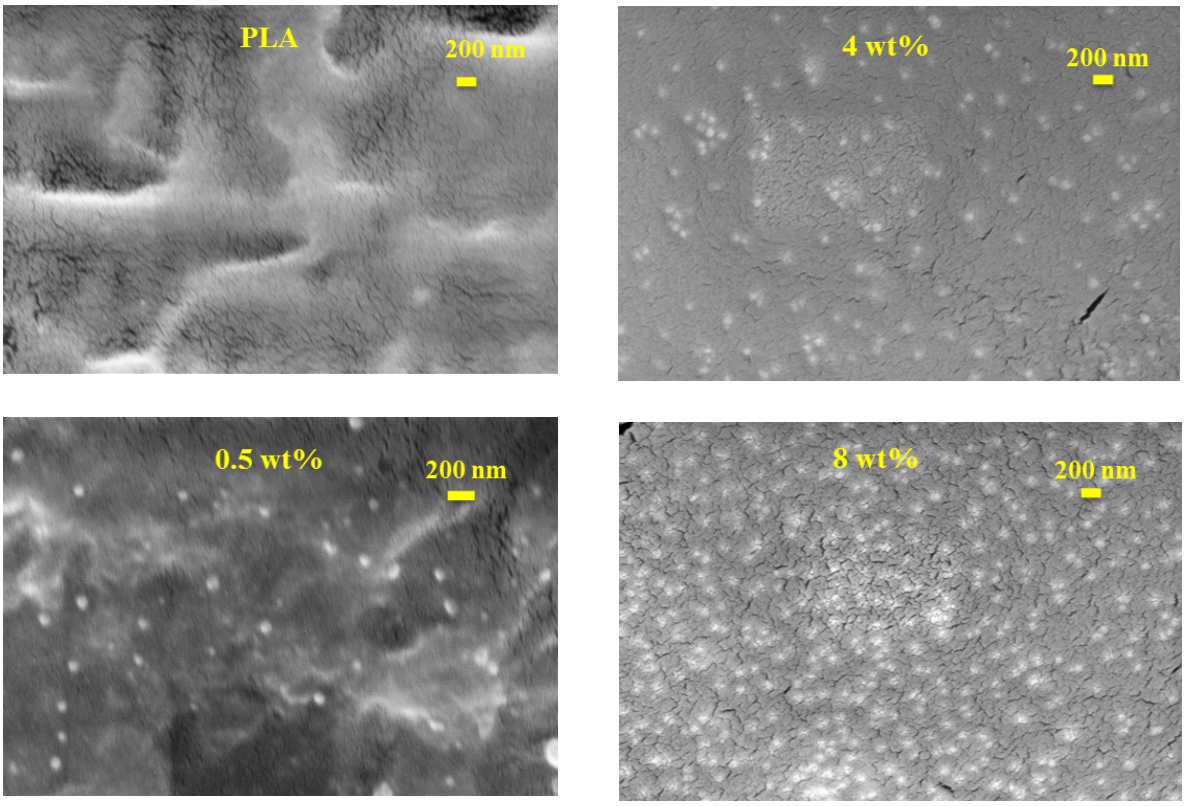

Figure 4-5. SEM images of solidified PLA-silica APTES nanocomposite melts in different loading of silica after interfacial tension measurement

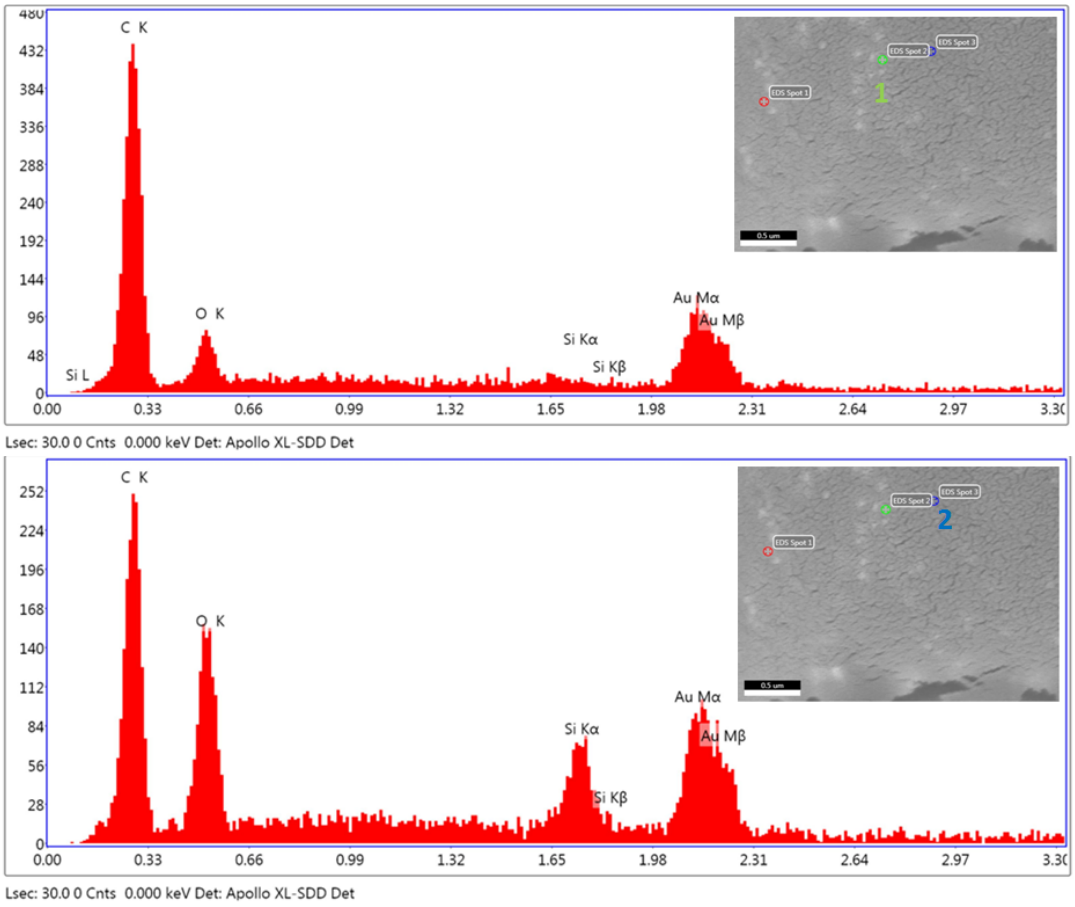

Figure 4-6. EDX spectroscopy of spot 1 (top) and spot 2 (bottom) of PLA nanocomposites after being at 153 ° C for the length of the pendant drop measurement

In addition to direct observation of nanoparticles at the interface, one can show that the adsorption of nanoparticles is thermodynamically favorable and irreversible. It has been shown that if the binding energy of nanoparticles (the energy to detach particles from the interface) is high enough (compared with thermal fluctuations) the adsorption is irreversible [132,133,153].

Equation 5-1 is used to calculate binding energy of the particles at the interface. In addition to SEM, this is another proof showing irreversible adsorption of the nanoparticles to a PLA melt-air or supercritical CO_2 interface. Knowing the interfacial tension between PLA- supercritical CO_2 at the desired temperature and pressure, interfacial tension at 0 wt. % in Figure 4-3 or Figure 4-4, the only unknown is the contact angle between the particles at the PLA melt and supercritical CO_2 interface. In order to measure the contact angle between silica-PLA-CO_2, one can make a pellet out of the particle and perform the contact angle

measurement. However, due to the porosity of the pellet, the liquid or polymer melt on top will diffuse into the pellet making the measurement impossible. To overcome this difficulty, surfaces with the exact surface chemistry of silica and silica modified with APTES can be used for contact angle measurements. Silicon has a natural oxide layer on the surface which after washing with Piranha solution and removing hydrocarbons, has an abundant number of hydroxyl groups on the surface [154,155]. In this work, a silicon wafer with surface modification is used as a homologous surface to modified silica.

AFM images of the silicon wafer before and after surface modification with APTES are shown in Figure 4-7. Both surfaces are uniform and smooth as the root mean square (R_q) and arithmetic average (R_a) roughness values for silicon wafers are 0.3 and 0.2 nm and those of silicon modified with APTES are 9.6 and 7.5, respectively. As shown previously [156,157], contact angle measurements are independent of surface roughness for values less than 150 nm.

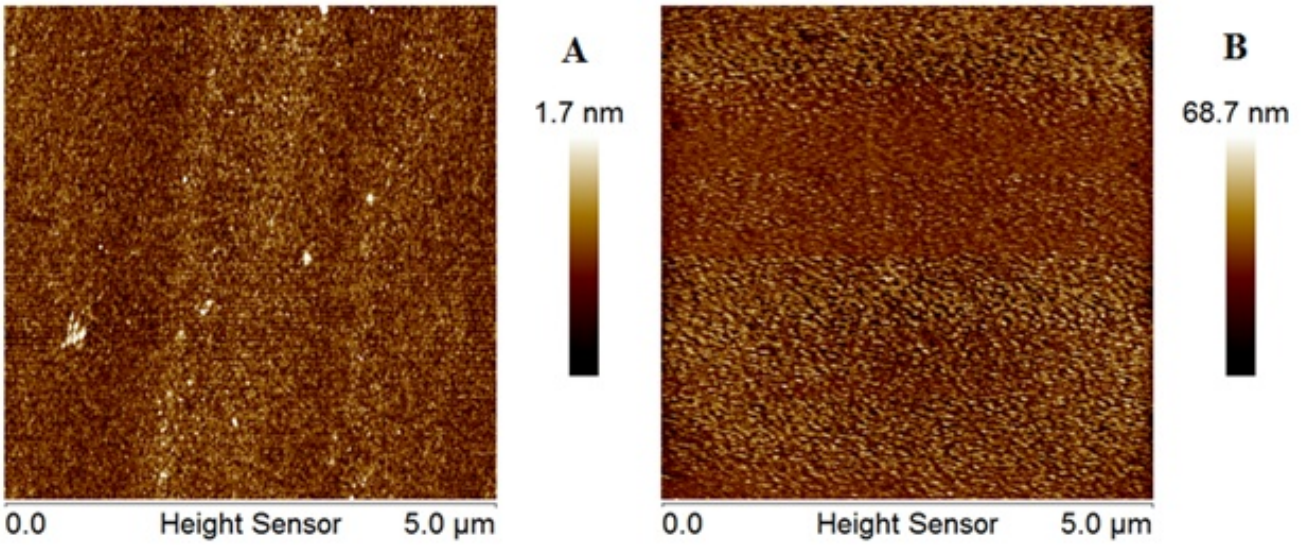

Figure 4-7. AFM images of silicon (A) and silicon-APTES (B)

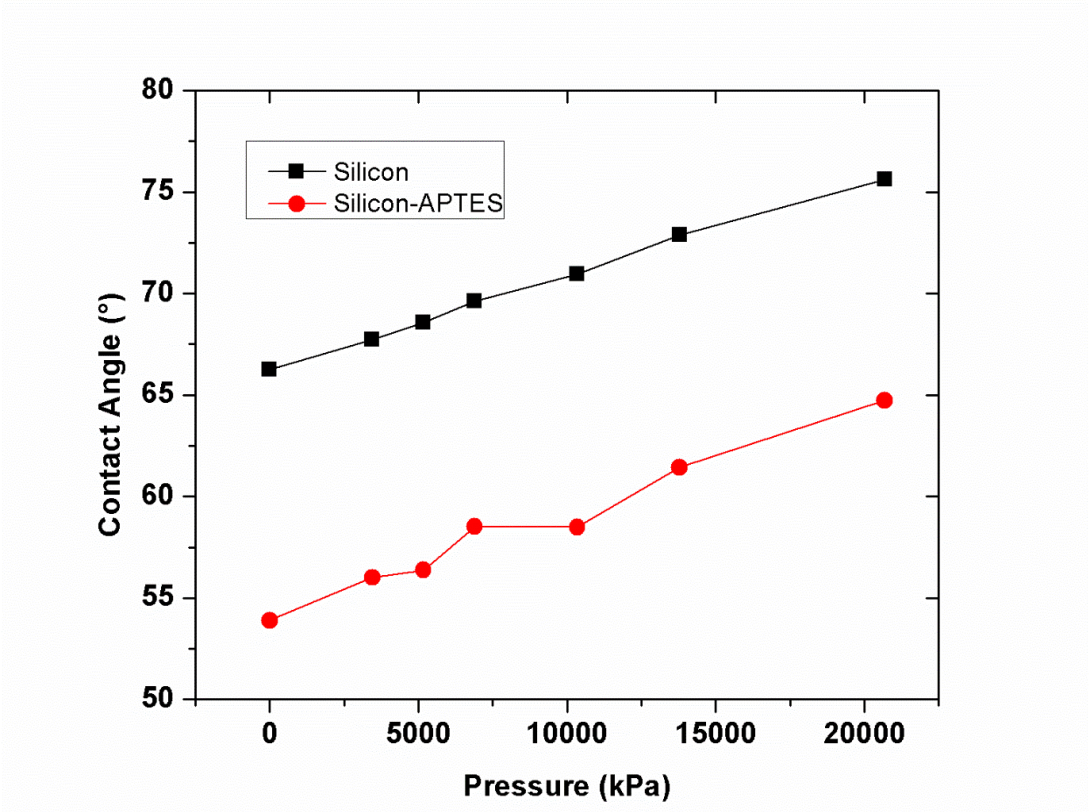

Figure 4-8. Plot of contact angle of PLA on silicon (black squares) and silicon-APTES (red circles) surfaces vs. pressure of surrounding CO_2 at 153° C (the maximum value for error bar is ± 0.2 ° for 95% confidence interval)

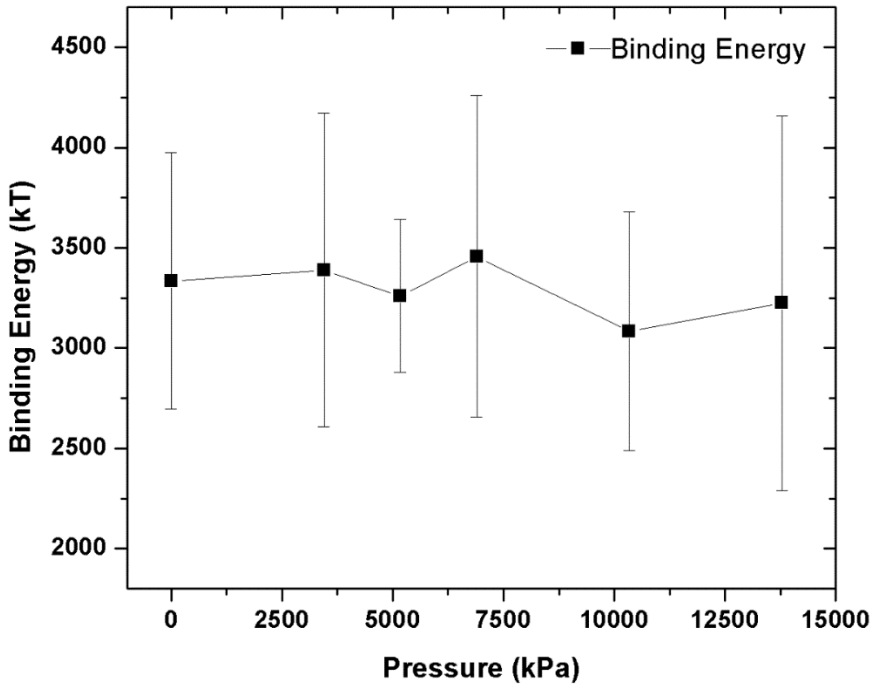

Figure 4-9.Plot of calculated binding energy of silica-APTES nanoparticles at PLA - CO_2 interface using contact angle results as a function of CO_2 pressure at 153º C (426 K)

Figure 4-8 shows the contact angle of PLA on silica-APTES surfaces as a function of the pressure of surrounding CO_2 at 153º C. The silica-APTES contact angle increases with an increase in CO_2 pressure. In the other words, compatibility of nanoparticles with PLA decrease at higher pressures. However, because of a more favorable interaction between the amine group of APTES and PLA, its contact angle is lower. In both cases, the binding energy in Figure 4-9, is significantly higher than the thermal energy (kBT), where kB is the Boltzmann constant and T is temperature in Kelvin, making the adsorption irreversible. Based on contact angle and binding energy results, it can be concluded that as the pressure of CO_2 increases and the contact angle decreases, the work of adhesion will be less, and consequently there is less tendency towards bulk PLA for nanoparticles, the condition which leads to more adsorption of nanoparticles at the interface. The affinity of the nanoparticles towards the interface can be explained in terms of an entropy penalty of polymer chains near the nanoparticles in the presence of CO_2; any constraint on polymer configurations such as stretching in the vicinity of a particle, causes a decrease in the conformational entropy of

polymer chains, a phenomena that leads to the segregation of the nanoparticles at the polymer-gas interface to minimize the entropic penalty [145,158,159]. The "entropy-driven" segregation is more pronounced when the polymer chains are expanded as a result of gas absorption specifically near the critical point of the gas [160,161].

4.6 Conclusions

In summary, the effect of synthesized silica nanoparticles on interfacial tension between PLA and supercritical CO_2 at high temperature and high pressures was studied. In the interfacial tension curve, a minimum in silica loading of 2 wt. % for all the pressures was observed, and for higher amounts of silica the interfacial tension value reached a plateau. Adsorption of the silica nanoparticles decreased the interfacial tension, however for higher amounts (more than 2 wt. %) of nanoparticles, interfacial tension is increased due to attractive lateral capillary forces originating from the perturbation of the PLA- CO_2 interface by particles. Contact angle measurements at high temperatures and pressures showed a decrease in compatibility between the nanoparticles and PLA with increasing CO_2, which facilitated the adsorption phenomena at high pressures. Furthermore, binding energy calculations showed irreversible adsorption due to high values of energy compared with thermal fluctuations.

5. CHAPTER 5: EFFECT OF WELL-DISPERSED SURFACE-MODIFIED SILICA NANOPARTICLES ON CRYSTALLIZATION BEHAVIOR OF POLY (LACTIC ACID) UNDER COMPRESSED CARBON DIOXIDE

K. Sarikhani , R. Nasseri ,V. Lotocki , R.B. Thompson, C.B. Park, P. Chen [3]

Graphical Abstract

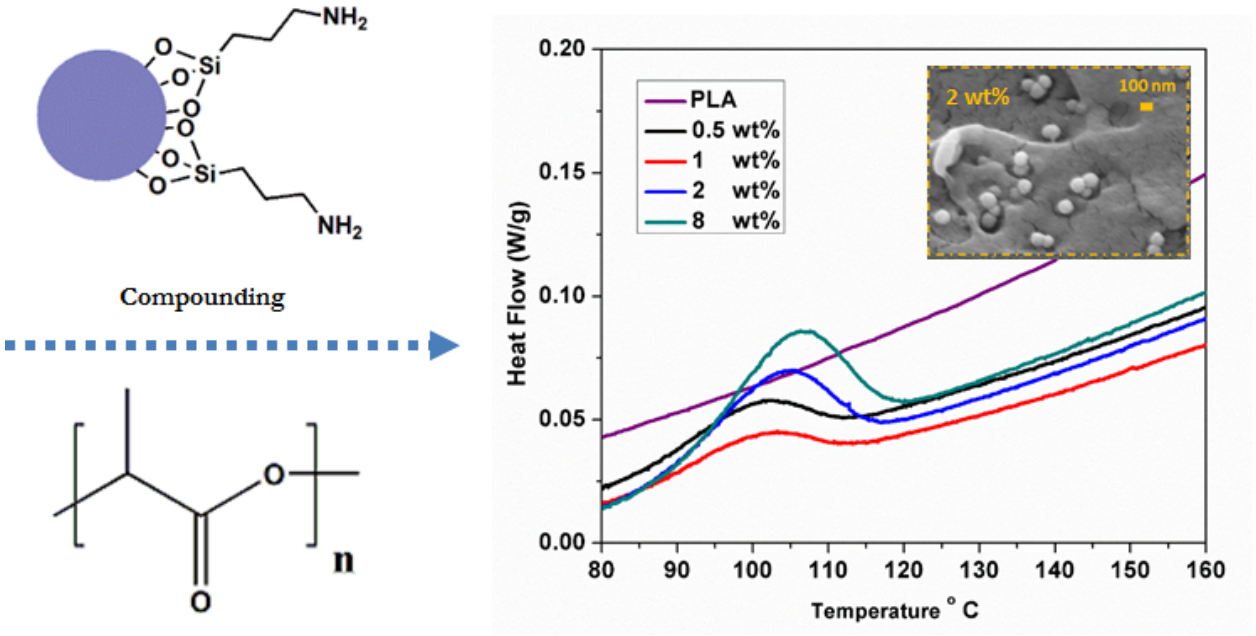

[3] *Submitted to Polymer - POLYMER-16-213*

5.1 Summary

To further investigate the effect of the nanoparticles on fundamental foaming related properties, the crystallization behavior of poly (lactic acid) (PLA)/ amine-modified silica nanocomposites at different loadings of amine-modified silica under isothermal, non-isothermal, and isothermal under compressed CO_2 is studied. Crystallization is an important factor in growth step of foaming, therefore; it is important from practical point of view for further development of polymer nanocomposite foams. Incorporation of the nanoparticles significantly improved the crystallization of PLA in all the conditions.

A manuscript using the data in this chapter is submitted to *Polymer* (2016). The co-authors include professor Pu Chen as supervisor, professors Chul B. Park and Russell Thompson as co-supervisors, Rasool Nasseri who assisted me in developing Hoffman- Lauritzen theory, Victor Lotocki as my co-op student help me in performing some of the DSC experiments.

5.2 Introduction

One promising application for PLA is being used as polymeric foam materials. In addition to the general advantages of foam materials, PLA foams have the biodegradable and biocompatible characteristics which make them an attractive replacement for commodity foam products for solving global waste disposal concerns [16]. Despite numerous valuable advances, production of PLA foams with uniform morphology using physical blowing agents is still challenging [162,163]. One barrier for PLA foam production is its low melt-strength. Various methods, such as introducing chain extenders [164], branching the chains [81,82,88], and compounding with various fillers and additives (micro and nanoparticles) [83–85] have been used to address the low melt strength of PLA. In addition to melt strength, improvement in crystallization behavior and crystallinity can further improve the mechanical properties of PLA [27,165–168].

Nanoparticles can be used to improve PLA foamability through the improvement in crystallization, melt strength, and reduction of interfacial tension of the PLA system. It has been shown that both carbon dioxide (CO_2) dissolution [38,169] and the addition of nanoparticles [170] can reduce the interfacial tension of PLA – CO_2 mixtures. In addition, nanoparticles can serve as nucleating agents in the nucleation step of foaming [130,131]. In heterogeneous nucleation a pre-existing surface causes the reduction in free energy barrier against the primary nucleation. It was shown that in polypropylene composites filled with

hydrophobic fumed silica (modified with dimethyldichlorosilane), the nucleus size for crystallization decreases with incorporation of foreign surfaces as result of less resistance in creation of interface between the crystal and substrate compared with that of free polymer [171,172].This would be an important factor in improvement of PLA crystallization with very slow kinetics.

In this project, the crystallization behavior of PLA/silica nanocomposites at different loadings of silica in both isothermal and non-isothermal conditions is studied. Prior to crystallization analysis, a proper surface modification of the silica nanoparticles is selected to satisfy the need for a well-dispersed nanocomposites, higher-absorption of CO_2, and a faster crystallization rate. Surface energy of the nanoparticles and interfacial energy between polymer/nanoparticle at high temperatures are used in a modified Hoffman-Lauritzen nucleation theory to prove acceleration of the crystallization process in the presence of nanoparticles. In order to consider the crystallization improvement for foaming processes, isothermal crystallization under compressed CO_2 is also investigated. The heterogeneous nucleation provided by nucleation agents such as silica nanoparticles improves the crystallization rate at high temperatures when there is less driving force for homogeneous nucleation. In addition to the role as a blowing agent in foaming, the effect of carbon dioxide as a plasticizer on crystallization is more dominant at lower temperatures where higher chain mobility is required for crystallization. That is the reason why the effect of CO_2 has been studied at a low and narrow crystallization temperature window. Combining nucleation (through heterogeneous nucleation of surface-modified silica nanoparticles) and plasticization (via dissolution of carbon dioxide in polymer matrices) is expected to increase the crystallization rate and broaden the crystallization temperature window in the foaming process of PLA.

5.3 Experimental

5.3.1 **Materials**

Three different grades of polylactic acid (PLA) under trade names of 2002D, 3001D, and 4032D were kindly provided by NatureWorks Inc. The molecular weight and D-content of the PLA grades are listed in Table 5.1. Chromatographic grade carbon dioxide with a purity of 99.98% was purchased from Linde Gas for high-pressure DSC measurements. Tetraethyl

orthosilicate (TEOS- Sigma-Aldrich) and ammonium hydroxide (28-30% solution - Sigma-Aldrich), were used for synthesis and (3-Aminopropyl) triethoxysilane (APTES) (99% - Sigma-Aldrich) was used for surface modification of the silica nanoparticles. The deionized water was from a Millipore Milli-Q system with 18.2 MΩ resistivity.

Table 5.1.Molecular weight and D-content of PLA materials in the current work

PLA Trade Name	*Number Average Molecular Weight (kg/mol)*	*D-content (%)*
PLA 2002D	**100**	**4.5**
PLA 3001D	**72**	**1.4**
PLA 4032D	**58**	**1.8**

5.3.2 Synthesis, surface modification, and compounding of silica nanoparticles

The synthesis, surface modification, characterization of silica nanoparticles as well as compounding of the silica nanoparticles with PLA can be found in detail in sections 4.3.2 to 4.3.3.

Morphology and dispersion of the nanoparticles in PLA was obtained using field emission scanning electron microscopy (FE-SEM) (Ultra, Zeiss). Thermal analysis was performed using a DSC2000 (TA Instruments) at atmospheric pressure and a DSC 204 HP (NETZSCH, Germany) at high pressures of CO_2. The crystal structure of PLA was characterized using X-ray diffraction (XRD) techniques (Bruker) with Cu-Kα radiation with wavelength of 1.5406 Å operating at 40 kV and 30 mA.

5.3.3 Isothermal analysis and kinetics of crystallization

Calorimetry was used to study the kinetics of crystallization. The samples were heated from room temperature to 200 °C at the rate of 10 °C/min then equilibrated at that temperature for 5 min to remove all previous thermal and stress histories. The samples were cooled to the isothermal temperature at the rate of 30 °C/min and then were equilibrated at the isothermal temperature, and heat flow was measured as a function of time for 60 min or until crystallization was completed. The heat flow data was converted to a fraction relative to the final crystallinity level, and the results were plotted as a function of time to obtain

Avrami plots. The Avrami equation (6-1) was used to analyze the crystallization kinetics of the samples [173,174]:

$$x(t) = 1 - e^{(-kt)^n} \qquad 5\text{-}1$$

where *x(t)* is the relative crystallinity at time *t*, *k* is a kinetic rate constant and *n* is the Avrami exponent. The double-log Avrami plots of $\ln(-\ln(1-x(t)))$ versus $\ln(t)$ were plotted to obtain the Avrami exponent, n, and the crystallization kinetic constant, k.

The Avrami exponent normally has a value, which lies between 2 and 4 for polymer crystallization, and it determines the mechanism of nucleation (homogeneous or heterogeneous and simultaneous or sporadic), the dimensionality of crystal growth (two or three dimensional) and growth mechanism (linear or diffusion controlled) of the system. The higher Avrami exponents are attributed to sporadic (or combination of sporadic and simultaneous) nucleation with three-dimensional spherulitic growth. On the other hand, the lower exponent values represent instantaneous (accompanied with some sporadic) nucleation with two-dimensional growth [87,175]. Another important piece of information obtained from isothermal crystallization is the crystallization half-time ($t_{1/2}$) which is defined as the time it takes to reach 50% of crystallization. The reciprocal of $t_{1/2}$ is a measure of crystallization kinetics and is defined as the crystallization rate (G).

5.4 Results and Discussion

5.4.1 Calculation of surface energy calculations and its effect on dispersion of nanoparticles and crystallization of PLA

The size, uniformity, and surface modification of silica nanoparticles has been already examined with SEM, TEM, DLS, and FTIR, and the results were presented in our previous work [170]. The silica nanoparticles were spherical and monodispersed with a z-average size of 100 nm. Figure 5-1 shows the SEM image of the cryogenically fractured surface of PLA 2 wt.% nanocomposite at two different magnifications. The surface modified silica nanoparticles show excellent distribution and good dispersion inside the polymeric matrices, and the individual spherical particles and small aggregates of two to three particles are uniformly distributed inside the PLA matrices.

The surfaces of silica nanoparticles are modified with amine containing silanes for the following reasons: first of all, it provide a surface with lower energy. The surface–modified silica contributes to better dispersion of the particles in the matrices and the work of adhesion will be higher in the case of a proper selection of surface modification. Secondly, the amine group can improve the adsorption of CO_2 on the surface of the silica particles [176] via induced interaction between the basic amines functional groups on the surface of modified particles and the acidic CO_2 molecules to form ammonium carbamates in anhydrous conditions [177]. Thirdly, the amphiphilic characteristic of the surface–modified nanoparticles, and their affinity towards CO_2, promotes their irreversible adsorption to the polymer/ CO_2 interface [170]. On the other hand, the three–phase contact angle between nanoparticle/ polymer/ CO_2 is a determining factor in the free energy barrier for heterogeneous nucleation (W_{het}) in polymer foams [178,179]:

$$W_{het} = \frac{16\,\pi\,\gamma_l^3\,F}{3\,(P_{bubble} - P_{system})^2} = W_{homo}\,F \qquad 5\text{-}2$$

where F is the energy reduction factor for heterogeneous nucleation and γ_1 is the liquid (melt) surface tension. The factor depends on the geometry of the nucleating site and it can be a function of θ [180]:

$$F(\theta) = \frac{2 + 3\cos\theta - \cos^3\theta}{4} \qquad 5\text{-}3$$

where θ is the three – phase contact angle between nanoparticle (solid)/ polymer (liquid)/ CO_2 (gas) from Young's equation:

$$\gamma_l \cos\theta = \gamma_s - \gamma_{sl} \qquad 5\text{-}4$$

where γ_l is the liquid-vapor surface tension, γ_s is the solid-vapor surface tension, and γ_{sl} is the solid-liquid interfacial tension.

Equation 5-3 shows that an increase in θ leads to a decrease in F and consequently W_{het}. Considering Young's equation, in order to have a larger θ one can either decreases γ_s or

increases γ_{sl}. On the other hand, due to low surface energy of polymer melts, a low-energy solid-gas interface is required to minimize the interfacial tension between the dispersed particles and the polymer matrix for improvement of particles wettability, better dispersion of particles and a uniform composite. Moreover, in foams stabilized with nanoparticles it is required for the particles to have the ability to adsorb to the interface of the two phases. Partial wetting of the solid particles by the two phases is one of the key requirements for their adsorption at the interface [181]. In polymer foams, surface modification of silica with CO_2–philic functional groups is shown to promote nanoparticles' adsorption to the polymer-carbon dioxide interface with high binding energies to the interface [170]. As a result of all this, surface modification of silica nanoparticles in the current study is a key step to both reduce the energy barrier for nucleation in foaming and to provide a low surface energy particle for better dispersion.

Contact angle measurements of silicon wafers and silicon modified with APTES at room and high temperatures are used to determine the surface energy of the nanoparticles (Table I.1). The surface of silicon has a natural oxide layer that makes it chemically identical to silica. The same surface can be modified with different silanes or polymers to study the contact angle and wetting properties of the corresponding particles [170,182].

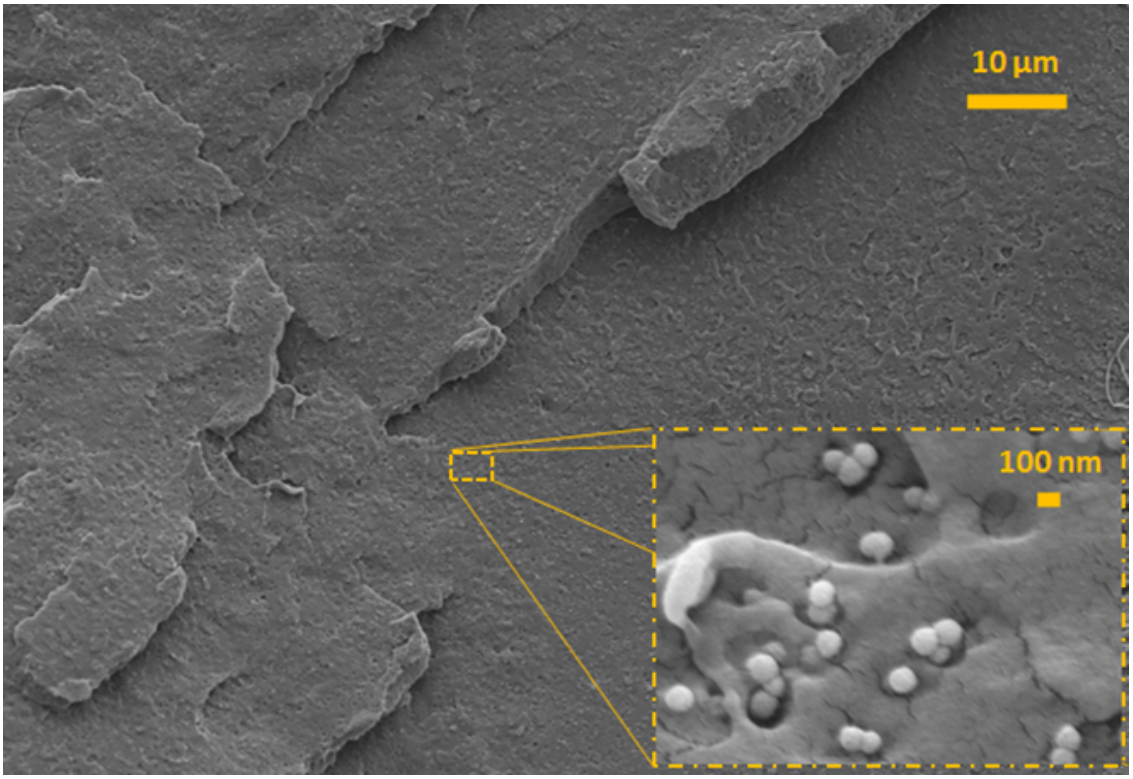

Figure 5-1.SEM image of 2 wt% PLA nanocomposite fractured in liquid nitrogen. The large image is at 1k and the inset is at 50k magnification

Contact angle and pendant drop measurements at high temperature were carried as described previously [32,169,183]. As shown in Table 5.2, at high temperatures, the silicon-APTES contact angle is lower than the unmodified one, showing more compatibility and affinity between nanoparticles and PLA. Both modified and unmodified silicon samples show a slight increase in contact angle with an increase in temperature possibly due to different thermal coefficients for surface tension and surface energy (Figure I-2 Appendix I). Based on surface tension measurement of the PLA melt at high temperatures presented in Figure I-1 (Appendix I) and the contact angle measurement in Figure I-2 (Appendix I), one can measure the work of adhesion via Young-Dupre's equation. The adhesion energy or work of adhesion per unit area of the two interface is defined as the energy change of bringing unit area of one part (or surface) into contact with unit area of another part in a vacuum [62]. The calculated work of adhesion (Figure 5-2) for surface modified nanoparticles is higher than the unmodified one, showing better interaction between the APTES-modified silica and PLA. Nanoparticles with lower surface energy and higher work of adhesion result in higher levels of dispersion. Acquiring higher dispersion is a key step to

practically achieve the desired properties of the composite. In the case of nanoparticles as nucleating agents in crystallization, a better dispersion means more individual nucleating sites across matrices [184].

Table 5.2. Surface energy calculation of silicon and silicon-APTES and corresponding interfacial tension with PLA obtained by contact angle and surface tension values of PLA at high temperature

	PLA		***Silicon***		***Silicon APTES***		
Temperature	*Surface tension*	*Contact Angle*	*Surface energy (Neumann)*	*Interfacial tension*	*Contact Angle*	*Surface energy (Neumann)*	*Interfacial tension*
°C	(mJ/m^2)	(°)	(mJ/m^2)	(mJ/m^2)	(°)	(mJ/m^2)	(mJ/m^2)
153	23.2	65.8	11.8	2.4	53.9	14.9	1.2
170	21.0	67.3	10.3	2.3	55.1	13.1	1.2
180	19.0	68.6	9.1	2.1	56.7	11.5	1.1

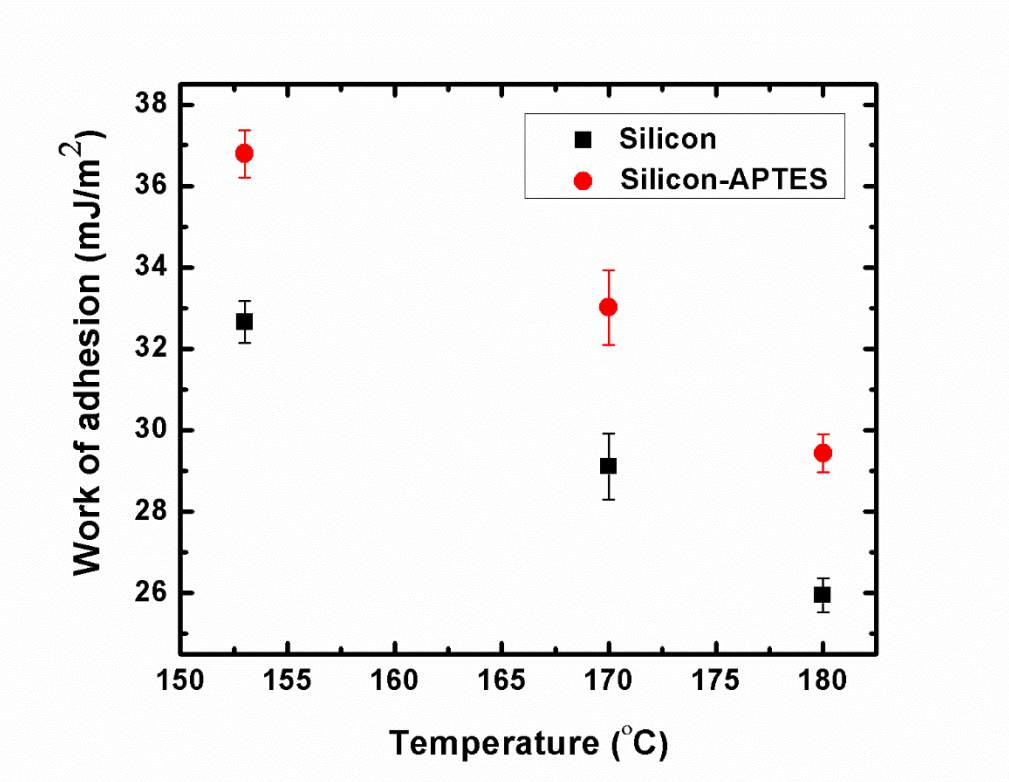

Figure 5-2.Work of adhesion between PLA and silicon and silicon-APTES surfaces as representatives of silica and silica-APTES nanoparticle surfaces

5.4.2 Isothermal and non-isothermal melt crystallization of nanocomposites

The non-isothermal thermal plots of PLA and PLA silica nanocomposites are shown in Figure 5-3. Cooling graphs were obtained at a 2 °C/min cooling rate at atmospheric pressure. The corresponding thermal properties are also shown in Table 5.3. Although it underwent cold-crystallization and the subsequently formed crystals were melted, there is no detectable peak for virgin PLA during the cooling section The slow crystallization kinetics of the 2002D PLA samples are a result of their high D-content and high molecular weight [185,186]. Even at low cooling rates, the time necessary for polymer chain rearrangement and reorientation is longer than the time required for measurement. In other words, stable nuclei cannot be formed at fast cooling rates and at higher temperatures [187]. This problem also arises when there is a large amount of co-monomers that possess different stereochemistry [186]. Only after rearrangement during cooling and the availability of more activation energy during heating does the material show cold-crystallization, and consequently, a melting peak. At higher cooling and heating rates (10 °C/min), both cold-crystallization and melting peaks are barely detectable for PLA 2002D. However, after the incorporation of only a small amount of surface modified silica nanoparticles (0.5 wt.%), a significant change in crystallization behavior of PLA can be observed; exothermic crystallization peaks appear at temperatures between 100 and 107 °C for different loadings of silica. An increase in the amount of silica nanoparticles leads to an increase in both crystallization temperature and heat of crystallization up to 107 °C and 23 J/g, respectively. The shifts to higher crystallization temperatures by the presence of surface modified silica indicate an acceleration in the overall PLA crystallization [188]. Figure 5-4 shows the wide-angle XRD patterns of PLA and PLA silica nanocomposites. For the virgin PLA, there is no distinct peak, and only a wide peak can be seen while all the nanocomposites show □ type crystal structure with orthorhombic unit cells with diffraction peaks at 2θ = 16.8, 19.2, and 22.3° corresponding to (110), (203) and (205) crystal planes [87,189,190]. The intensity of □ peaks is nearly constant with an increase in the amount of silica nanoparticles.

Isothermal analysis has been performed at temperatures in the range of non-isothermal crystallization peaks. Two temperatures, 102 and 110 °C, were selected based on the

crystallization peaks of the non-isothermal curves. As expected, there was no peak for PLA. However, from Figure 5-5 one can observe that after the incorporation of 0.5 wt.% surface-modified silica nanoparticles, the isothermal peak appears with crystallization half-times of 12.5 and 9.2 min for 102 and 110 °C, respectively. As a general trend for the isothermal curves at both temperatures, the half-time decreases with an increase in the amount of surface modified silica nanoparticles [87,89].

6.4.2.1 Comparison of nucleation rate in pure matrix and nanocomposite based on Hoffman-Lauritzen nucleation theory

The Hoffman-Lauritzen nucleation theory is used to show the effect of the nanoparticles and their surface modification on crystallization nucleation, Investigation on the steady-state nucleation rate in crystallization of a condensed system was firstly proposed by Turnbull and Fischer [191]:

$$I = I_o \, exp(-\frac{\Delta H^*}{kT}) \, exp(-\frac{\Delta \phi^*}{kT}) \qquad 5\text{-}5$$

where I_o is the pre-exponential factor, T is the absolute temperature, ΔH^* is the heat of activation of the jump rate process, $\Delta \phi^*$ is the free energy of formation of a nucleus of critical size, and k is the Boltzmann constant. The first exponential term of this equation is a transport term which is the probability of a chain segment of critical length reaching to the surface of the crystal. Hoffman *et al.* [192] developed the equation 5-5 and replaced the local motion jump rate for the first exponential term:

$$I = I_o \, exp(-\frac{U^*}{k(T-T_\infty)}) \, exp(-\frac{\Delta \phi^*}{kT}) \qquad 5\text{-}6$$

where U* is the activation energy for reptational diffusion. And $\Delta \phi^*$ is defined as follows:

$$\Delta \phi = 2\nu ab\sigma_e + 2\nu al\sigma + 2bl\sigma - \nu abl(\Delta f) \qquad 5\text{-}7$$

where a, b, and l are width, thickness and length of a stem and a nucleus is composed of ν stems. σ and σ_e are lateral and fold surface free energies of nucleus, respectively. Should

the heat of fusion be independent of temperature, the quantity of Δf (bulk free energy of fusion) near the melting point (T_m^o) can be approximated by [193]:

$$\Delta f = \Delta h_f - T\Delta S_f = \Delta h_f - T\left(\frac{\Delta h_f}{T_m^o}\right) = \Delta h_f \left(\frac{\Delta T}{T_m^o}\right) \qquad 5\text{-}8$$

and Δh_f is the heat of fusion with $\Delta T = T_m^o - T$ the undercooling.

As it can be observed in equation 7, only the polymer bulk properties define the free energy of nucleus formation. As illustrated in Scheme 5-1, the free energy of formation of a nucleus starting from the surface of a nanoparticle is different from a nucleus starting inside the matrix of a polymer [194]. The free energy of formation of a nucleus in presence of a nanoparticle can be written as:

$$\Delta\phi^*_{nano} = 2vab\sigma_e + val(\sigma + \sigma_i - \sigma_s) + 2bl\sigma - vabl(\Delta f) \qquad 5\text{-}9$$

where σ_s is the surface energy of nanoparticle and σ_i is the interfacial energy between the nucleus and nanoparticle surfaces.

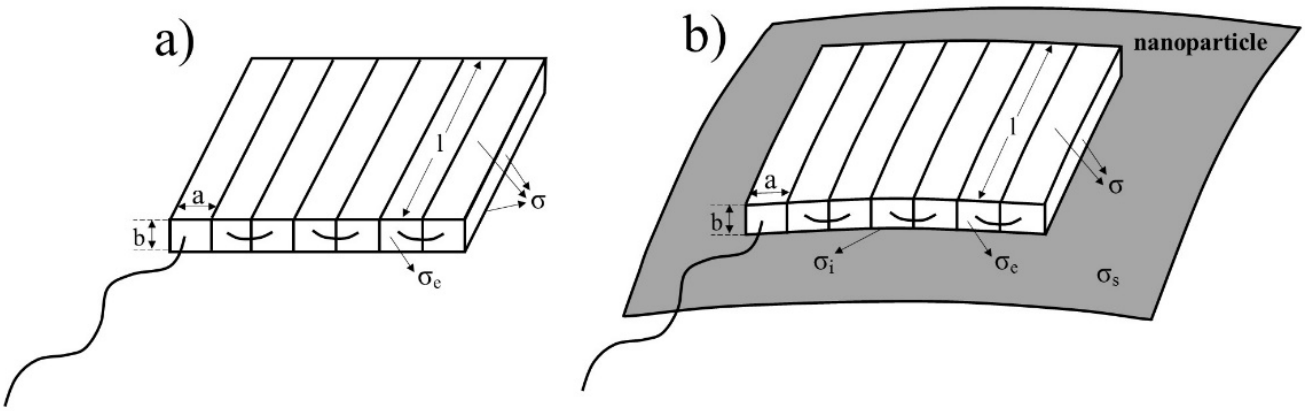

Scheme 5-1. Schematic representation of a nucleus: a) inside the matrix of a nanocomposite or in pure polymer; b) on the surface of a nanoparticle

Derivation of the free energy of nucleation in respect to the nucleus dimensions results to a set of equations for each scenario (with or without nanoparticles). Solving the equations leads to obtaining the critical dimensions of the nucleus:

$$\begin{cases} \frac{\partial \Delta\phi}{\partial a}|_{b,l} = 0 \\ \frac{\partial \Delta\phi}{\partial b}|_{a,l} = 0 \\ \frac{\partial \Delta\phi}{\partial l}|_{a,b} = 0 \end{cases} \quad 5\text{-}10$$

The values of a^*,b^*, and l^* (critical dimensions of nucleus) obtained by solving the set of equation, are substituted into equations 5-7 and 5-8. The $\Delta\phi^*$ for both cases are developed and used to find the nucleation rate of both nuclei starting from the surface of nanoparticles and starting inside the matrix of pure polymer as follows:

$$I = I_o \, exp(-\frac{U^*}{k(T-T_\infty)}) \, exp[-\frac{16\sigma_e\sigma}{kT\Delta f^2}(2\sigma)] \quad 5\text{-}11$$

$$I_{nano} = I_o \, exp(-\frac{U^*}{k(T-T_\infty)}) \, exp[-\frac{16\sigma_e\sigma}{kT\Delta f^2}(\sigma + \sigma_i - \sigma_s)] \quad 5\text{-}12$$

The obtained nucleation rate in presence of a nanoparticle is similar to the case of non-coherent surface nucleation formulated by Hoffman and Lauritzen [193] where non-coherent surface nucleation term was used for molecules with different orientation on the nucleus surface from that of substrate polymer crystal.

In the case of APTES modified silica, based on surface/interfacial energy results of Table 5.2, the lateral surface free energy is much higher than the difference of surface energy of nanoparticle and interfacial energy of the nucleus and nanoparticle surfaces ($\sigma \gg (\sigma_i - \sigma_s)$). Therefore, the second exponential of equation 5-12 is much larger than the same term in equation 5-11 leading to the conclusion that the nucleation in the presence of nanoparticle surfaces is much faster and more facile to occur than the pure polymer state (in this specific grade of PLA).

Following the nucleation rate, the rate of crystallization can also be expressed as [192]

$$G = G_o \, exp(-\frac{U^*}{k(T-T_\infty)}) \, exp[-\frac{4b\sigma_e\sigma}{kT\Delta f}] \quad 5\text{-}13$$

where G_0 is the pre-exponential factor. If the nucleation step is much slower than the growth step, nucleation will be the determining step in crystallization rate. In the other

words, one can say that if the energy barrier for nucleation is significantly high, the polymer chains cannot be in crystal structure and consequently no growth happens. Figure 5-3 shows that on the time scale of the experiment there is no crystallization occurring in pure polymer while occurrence of crystallization is obvious in all nanocomposite samples. Since there is no difference between the growth rate of pure polymer and nanocomposites (first exponential term), it can be concluded that nucleation is the determining step in crystallization of PLA 2002 and lack of nucleation prevent the crystallization in the time scale of calorimetry experiment. Modified Hoffman-Lauritzen nucleation theory for the nanocomposites justifies the facilitation of the nucleation and consequently the occurrence of crystallization.

It is noteworthy that in all the above equations, the lateral surface energy is approximated with that of the bulk surface tension of polymer.

6.4.2.2 Investigation of the crystallization mechanism by Avrami equation

Isothermal analysis based on the Avrami equation [173,174] was performed to investigate the kinetics of crystallization. Although the Avrami equation represents the initial section of polymer crystallization correctly, its exponent can provide valuable information about the crystallization behavior of polymers [195]. The relative crystallinity curves of the nanocomposites in two different temperatures are shown in Figure 5-5. The crystallization half-times obtained from the relative crystallinity curves are summarized in Table 5.4. The Avrami double-log plots of the nanocomposites in both temperatures are also shown in Figure 5-6. As it can be seen, all nanocomposites have an n value (Avrami exponent value) in the range of 3-4 and 2-3 at 102 and 110 °C, respectively. The low n values correspond to two dimensional (disc shaped) spherulite growth with predetermined and sporadic mechanisms at the beginning of crystallization respectively, while higher n values are correlated to three dimensional spherulitic growth with a sporadic or a combination of sporadic and simultaneous nucleation types [195,196]. The results show that in the presence of silica nanoparticles, an increase in temperature pushes the crystallization mechanism for PLA from three-dimensional to two-dimensional spherulitic nucleation and growth. Similar effects were observed due to the plasticizing effect CO_2 has on the reorientation of polymer chains to less close-packed planar crystals [197]. The crystallization rates (G) (reciprocal of $t_{1/2}$) of the nanocomposites are also summarized in Table 5.4. The crystallization rate

increases with an increase in the loading of silica. Furthermore, the nanocomposites show higher crystallization rates at higher temperatures.

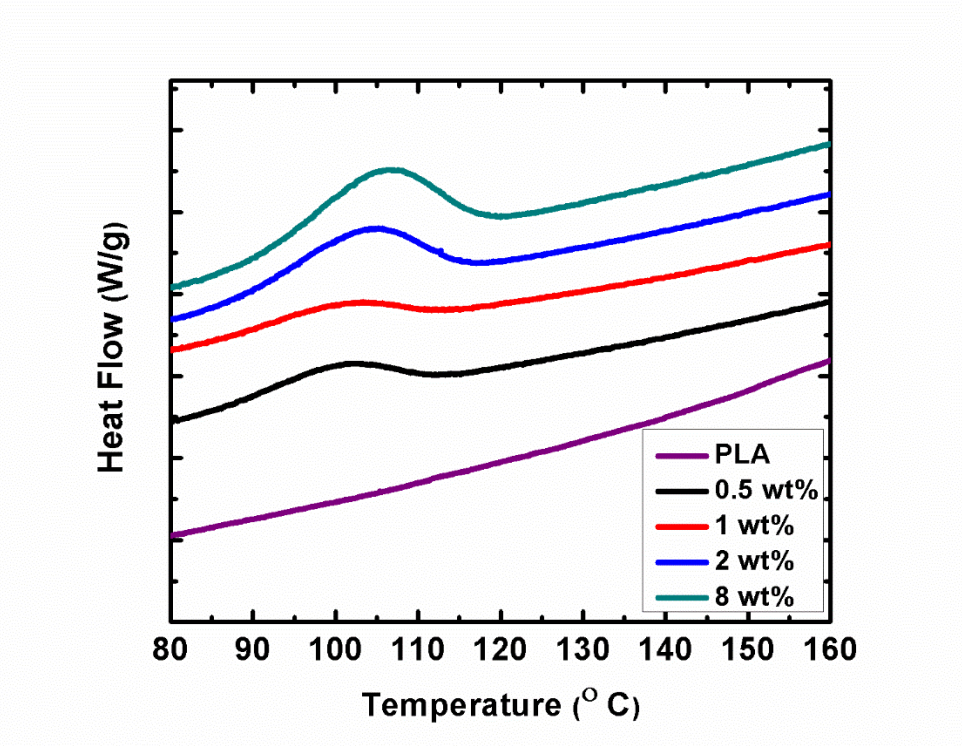

Figure 5-3.Cooling segment of non-isothermal thermal analysis of PLA and its silica nanocomposites obtained at atmospheric pressure with 2 °C/min cooling rate (peaks are exothermic)

Table 5.3. Summary of non-isothermal analysis of PLA and PLA-silica nanocomposites

Samples	*T_c (° C)*	*ΔH_c (J/g)*	*Crystallinity %*
PLA 2002D	**-**	**-**	**-**
0.5 wt%	**101**	**9**	**10**
1 wt%	**101**	**8**	**9**
2 wt%	**104**	**18**	**19**
8 wt%	**107**	**23**	**25**

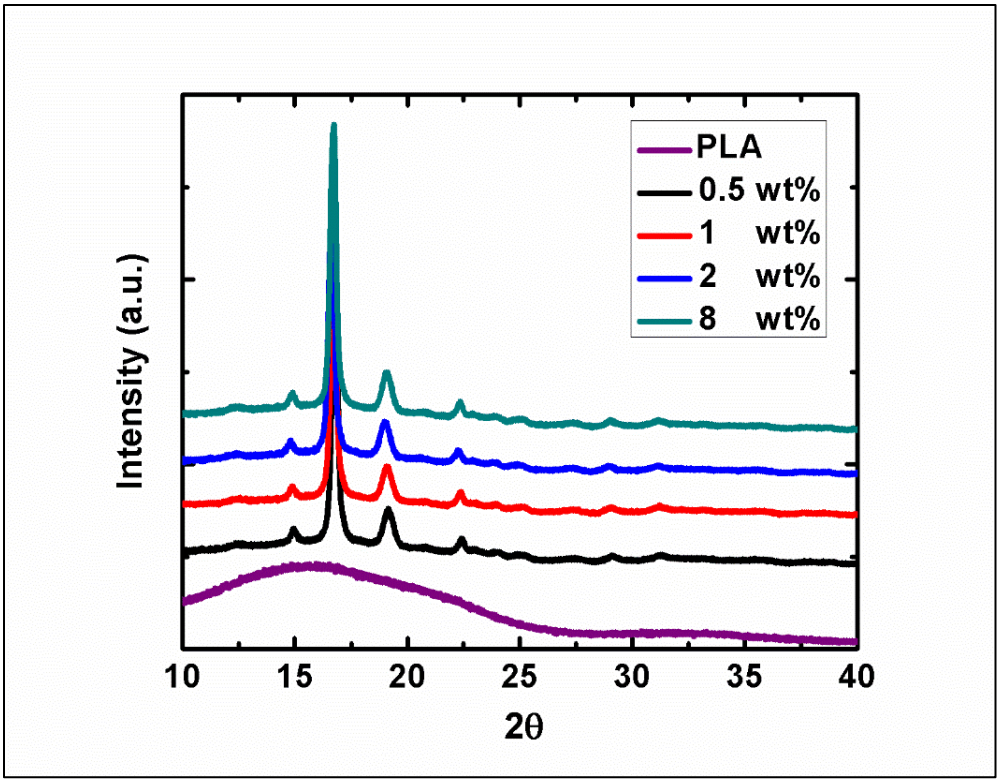

Figure 5-4.Wide-angle X-ray diffraction patterns of PLA and its corresponding silica nanocomposites

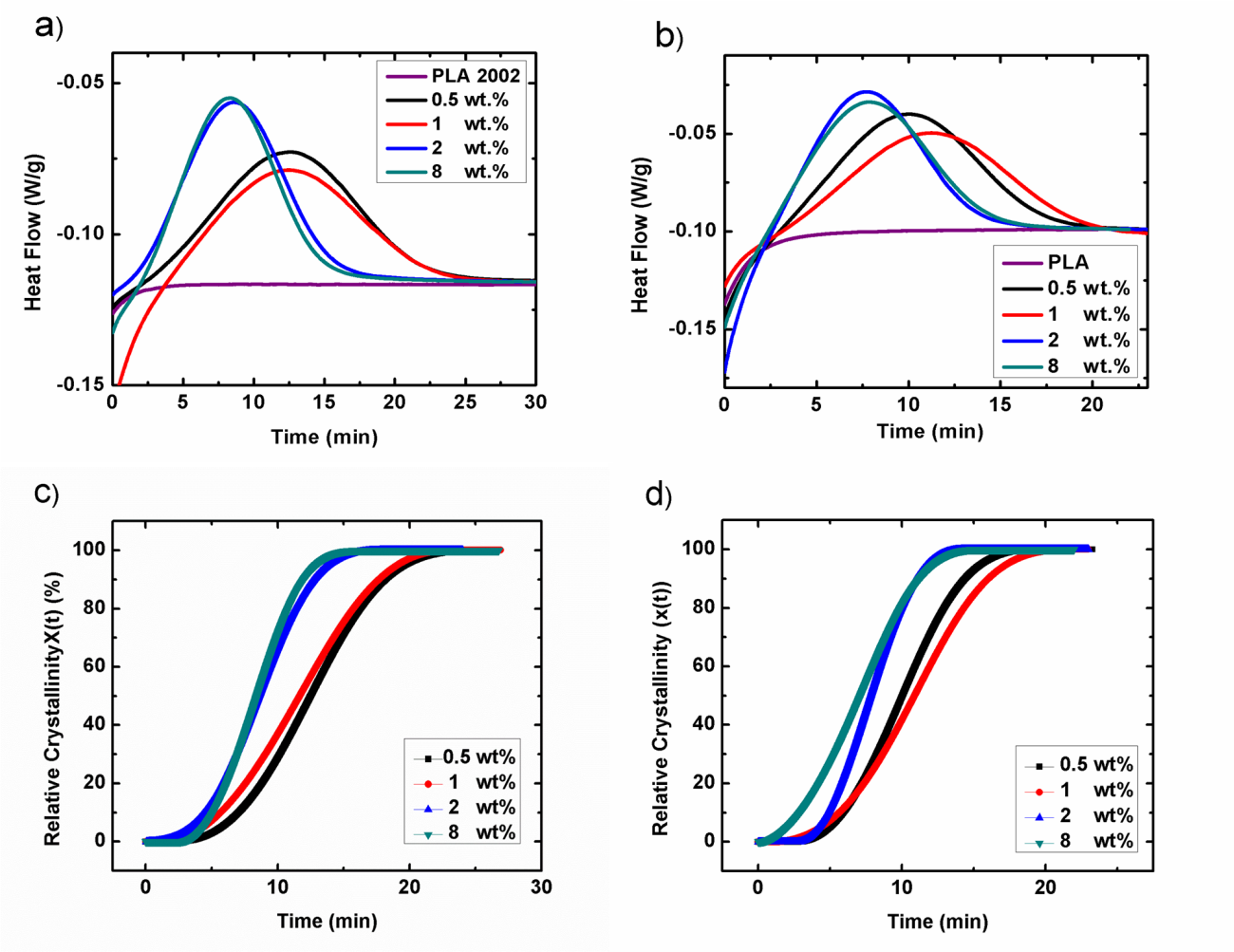

Figure 5-5.Isothermal DSC plots of PLA 2002D and its silica nanocomposites at a) 102 °C and b) 110 °C (peaks are exothermic) and Relative crystallinity plots of PLA 2002D silica nanocomposites at c) 102 °C and d) 110 °C

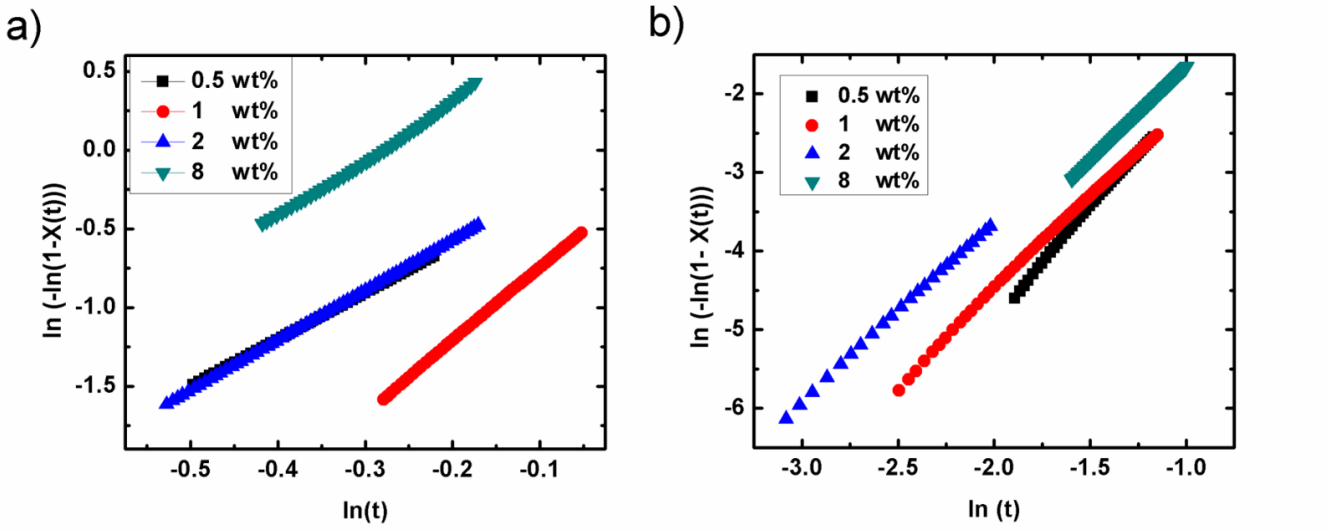

Figure 5-6.Avrami double-log plots of PLA2002D silica nanocomposites at a) 102 °C and b) 110 °C

Table 5.4. Avrami exponent, kinetic constant, half-time, and crystallization rate of the PLA2002D silica nanocomposites at 102 and 110 °C

Sample	*Temperature (°C)*	*n*	*k*	*t ½ (min)*	*G (min^{-1})*
0.5 wt%	**102**	**3.15**	**1.04**	**12.5**	**0.080**
1 wt%		**4.64**	**0.75**	**10.8**	**0.092**
2 wt%		**3.17**	**1.06**	**9.4**	**0.106**
8 wt%		**3.63**	**2.77**	**8.4**	**0.119**
0.5 wt%	**110**	**2.57**	**1.52**	**9.2**	**0.108**
1 wt%		**2.36**	**1.27**	**10.2**	**0.098**
2 wt%		**2.29**	**2.60**	**7.2**	**0.138**
8 wt%		**2.62**	**2.50**	**6.6**	**0.151**

5.4.3 **Effect of carbon dioxide on melt crystallization of nanocomposites**

The isothermal high pressure DSC plots of PLA silica nanocomposites under 15 and 21 bar carbon dioxide are presented in Figure 5-7. The crystallization half-time results from high-pressure DSC measurements were also compared with atmospheric pressure in Table 5.5. As can be observed, the crystallization half-time decreases significantly due to the plasticization effect of CO_2 molecules, which in turn causes an increase in the mobility of the polymer chains and a decrease in the energy barrier for crystallization [197]. Based on the Hoffman-Lauritzen nucleation theory, the solubilized CO_2 plasticizes the matrix and facilitates the molecular movement that leads to the decrease of energy barrier for reptational diffusion of polymer chain (U^*). On the other hand, application of high pressure increases the melting point and undercooling (ΔT) according to the Clausius-Clapeyron equation and, consequently, based on equation 9 an increase in Δf increases the second exponential term in equation 13 and further accelerates the crystallization rate.

In the other words, the activation energy barrier for crystallization comes from the chain energy dissipation which comes as a result of chain retraction and folding [198]. The retraction and folding phenomenon depends on not only the viscosity, but also CO_2, which, as a solvent is capable of diluting and plasticizing it [29,199,200]. On the other hand, for a

polymer chain to retract and fold, it is required to create a new surface while interfacial tension resists against this phenomenon. It has been shown that under compressed CO_2, the interfacial tension of polymer melts decreases, and by this same effect, compressed CO_2 can increase the rate of crystallization by lowering the activation energy associated with it [6,104,169]. As the results show, by further increasing CO_2 pressure, the crystallization half-time remains constant or slightly increases. Other studies [197,201] showed an increase in both the total crystallinity and the crystallization rate at pressures of CO_2 up to 20 bar.

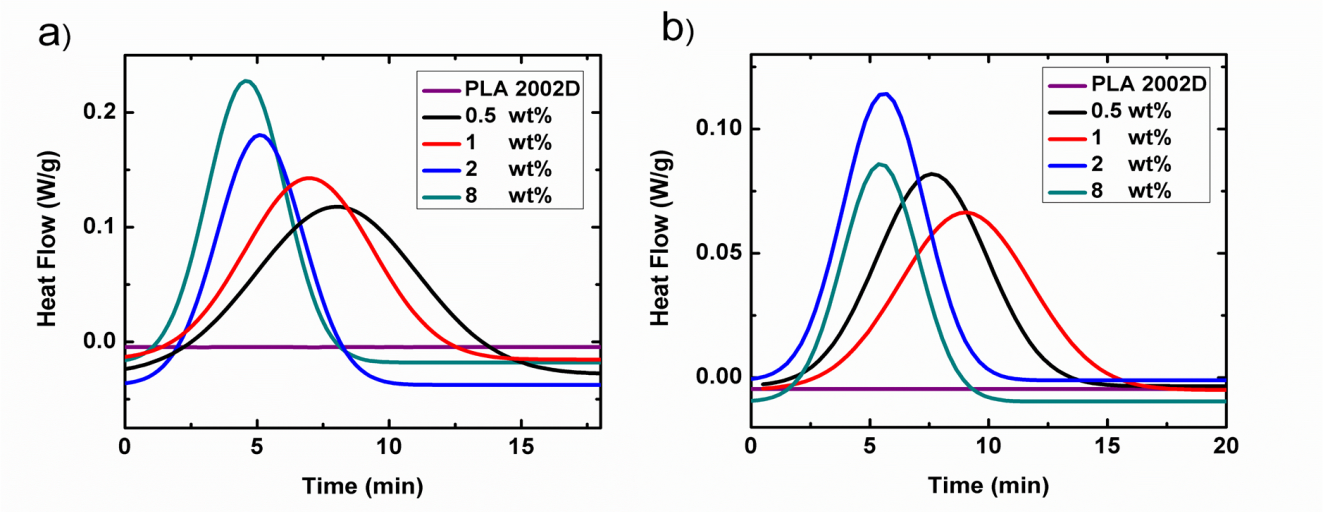

Figure 5-7.Isothermal high pressure DSC plots of PLA 2002D and its silica nanocomposites at 102 °C and a) 15 bar and b) 21 bar (peaks are exothermic)

Table 5.5. Comparison between crystallization half-time of silica nanocomposites at three different pressures of carbon dioxide

	$t_{1/2}$ (min)		
Sample	***Atmospheric***	***15 bar***	***21 bar***
0.5 wt%	**12.5**	**6.5**	**7.0**
1 wt%	**11.7**	**7.8**	**8.5**
2 wt%	**8.5**	**4.8**	**5.1**
8 wt%	**8.1**	**4.5**	**5.0**

5.4.4 **Nanocomposites of different molecular weights and D-contents of PLA**

The effect of nanoparticles on PLA crystallization can be observed more clearly in the 4032D and 3001D grades which have a lower molecular weight and less D-content compared to 2002D. As shown in Figure 5-8 and Figure 5-9, the 3001D and 4032D grades have a very wide peak in the range of 35-40 min at both 102 and 110 °C. It can be further observed that surface-modified silica nanoparticles accelerate the crystallization process by decreasing the half-time by up to a factor of 10 at both 102 and 110 °C. Analysis of the Avrami curves shows that the n value after incorporation of silica nanoparticles has not changed significantly In other words, PLA undergoes three-dimensional bulk crystallization before and after the incorporation of nanoparticles [89,202]. It has also been shown that the Avrami exponent is usually higher than 3 for linear PLA which corresponds to heterogeneous three-dimensional nucleation and growth [197]. In other words, the lack of entanglement in PLA's linear chain structure promotes the three-dimensional growth mechanism. However, for PLA 2002D nanocomposite samples with higher molecular weight, as long as the conditions for both nucleation (presence of silica nanoparticles) and higher mobility and dynamics of polymer chains (crystallization at higher temperature) are provided, the Avrami exponent tends to be lower and corresponds to the two-dimensional mechanism.

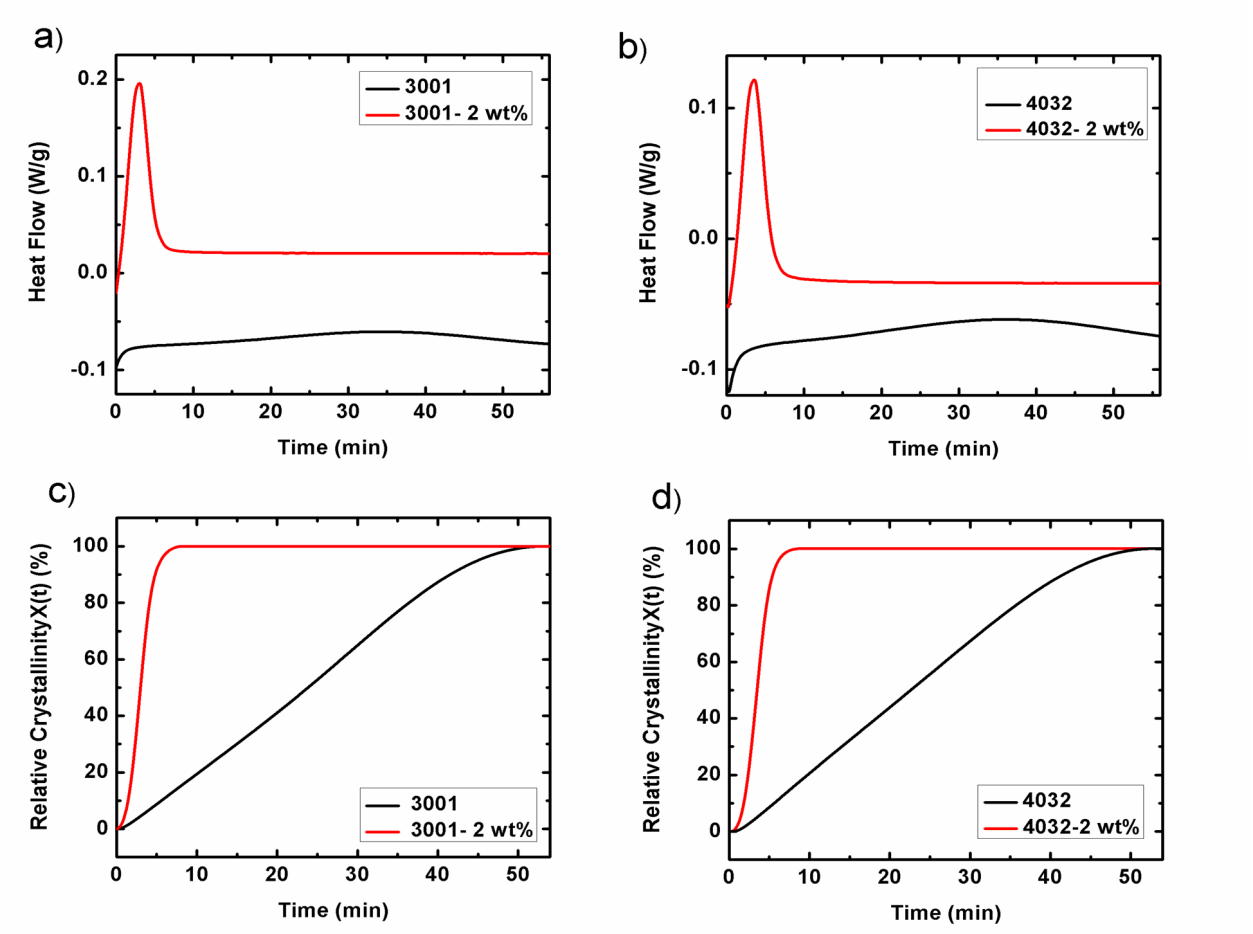

Figure 5-8.Isothermal DSC and relative crystallinity plots of PLA 3001D (a and c) and PLA 4032D (b and d) and their silica nanocomposites at 102 °C (peaks are exothermic)

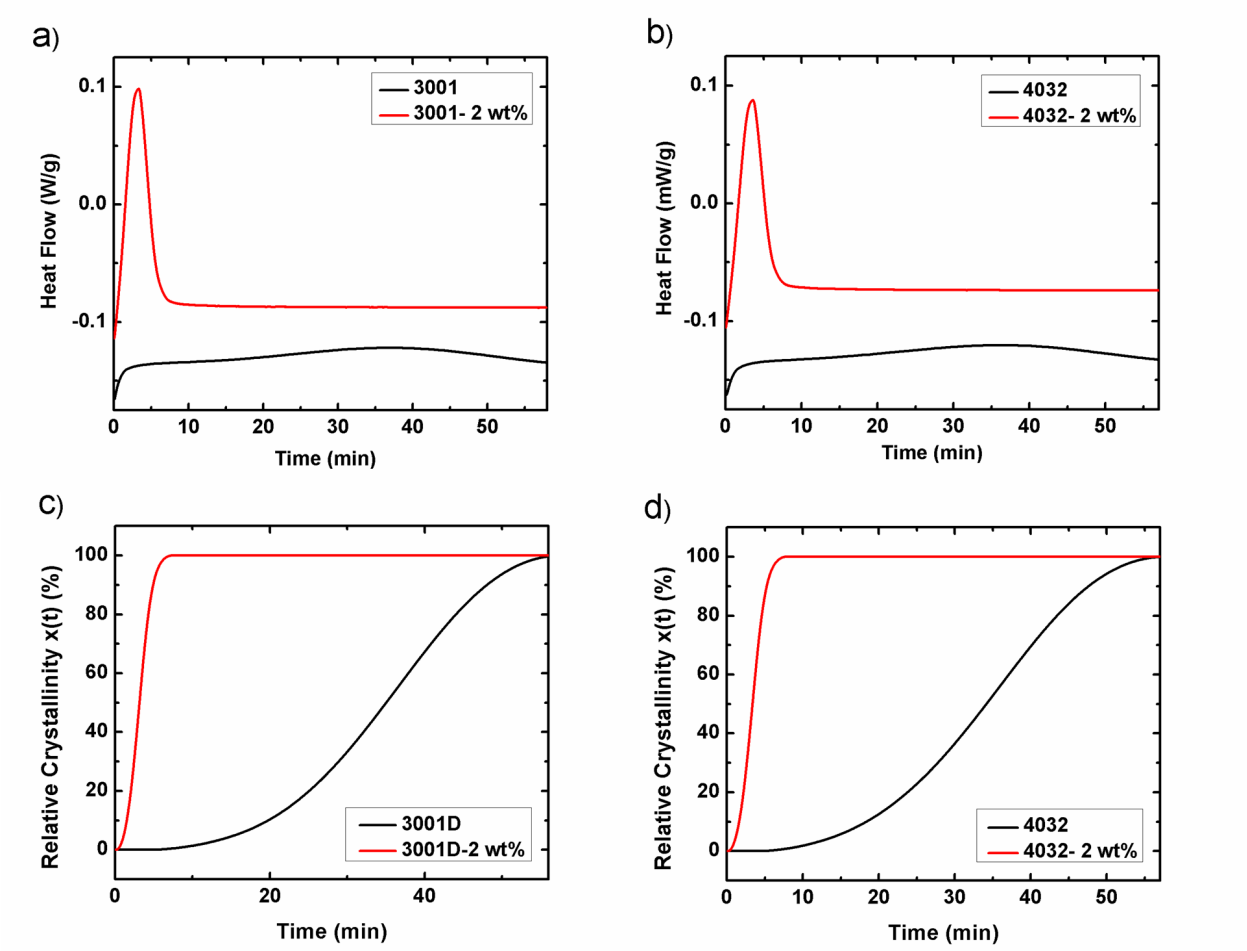

Figure 5-9.Isothermal DSC and relative crystallinity plots of PLA 3001D (a and c) and PLA 4032D (b and d) and their silica nanocomposites at 110 °C (peaks are exothermic)

Table 5.6.Avrami exponent, kinetic constant, half-time, and crystallization rate of the PLA 3001D, 4032D and their silica nanocomposites at 102 and 110 °C

Sample	*Temperature (°C)*	*n*	*k*	*t ½ (min)*	*G (min^{-1})*
3001D	**102**	**4.2**	**0.41**	**28**	**0.035**
3001D-2 wt%		**4.09**	**11.04**	**3.5**	**0.285**
4032D		**4.6**	**0.31**	**32**	**0.031**
4032D-2 wt%		**4.44**	**5.56**	**3.2**	**0.312**
3001D	**110**	**4.1**	**0.84**	**31**	**0.032**
3001D-2 wt%		**3.29**	**11.58**	**3.2**	**0.312**
4032D		**3.27**	**1.08**	**32**	**0.031**
4032D-2 wt%		**3.5**	**11.16**	**3.5**	**0.285**

5.5 Conclusions

The present study was designed to determine the effect of surface-modified silica nanoparticles on PLA crystallization. Both isothermal and non- isothermal crystallization for various loadings of silica nanoparticles were explored. The results showed a remarkable improvement in crystallization rate and crystallinity for PLA with high molecular weight and D-content. The WAXD patterns of the samples showed the appearance of α type crystal structures with orthorhombic unit cells after the incorporation of surface-modified silica nanoparticles. A modified Hoffman-Lauritzen nucleation theory justified the acceleration of crystallization by introduction of the surface energy of nanoparticles, interfacial energy between nanoparticle and lateral surface of crystals into the rate equation. Analysis of the Avrami equation showed a three-dimensional spherulitic structure which, at higher temperatures, proceeds towards a two-dimensional structure with less packed crystals. It was shown that the presence of carbon dioxide increases the crystallization rate at 15 bar, but at the higher pressure of 21 bar, the crystallization rate became nearly constant. The crystallization rate of PLA grades with lower molecular weights and lower D-content increased by up to a factor of 10 with no change in crystallization mechanism after the incorporation of surface-modified silica nanoparticles.

6. CHAPTER 6: CONCLUSIONS AND RECOMMENDATIONS

6.1 Conclusions

In this dissertation, a fundamental study is reported on the effect of the surface-modified silica nanoparticles on foam processing related properties of the poly (lactic acid) (PLA). The effect of synthesized amine-modified silica nanoparticles on interfacial tension and crystallization of PLA has been studied. In the foaming process, the nucleation and foaming of polymers was strongly influenced by surface/interfacial tension. As nucleation rate is inversely related to the exponential cubic power of surface/interfacial tension, one can lower the surface tension to decrease the energy barrier for cell nucleation and exponentially increases the number of cells. On the other hand, enough molecules of gas should be available and the size of the bubbles should reach a critical bubble radius to have a stable growing bubble in system. For bubbles smaller than the critical radius, the surface tension force is high and causes the gas clusters to collapse.

Similar to their role in systems in food science, cosmetics, oil production and renewable energies, particles can adsorb to the fluid interfaces. Adsorption of particles at fluid interfaces is not only a new rout to produce new self-assembled materials, but also their presence at the interface can stabilize fluid-fluid interface. One of the key characteristics of particles at the interface is their wettability at the three-phase interface and it mainly depends on the surface chemistry of the particle and on the chemical nature of the two phases at the interface. Silica nanoparticles are inexpensive and easy to manufacture nanoparticles that can adsorb to the interface and decrease the interfacial tension between polymer melts and supercritical fluids. The nanoparticles can act as nucleating agents for the foaming of polymers by decreasing the energy barrier for nucleation, increasing local stress variations around the particles, or indirectly affect the nucleation via crystallization induction of the polymers. On the hand, in PLA foams cell coalescence and cell rupture happens during in cell growth step because of its low melt strength. Improvement in PLA's crystallization kinetics during processing and foaming is considered as an effective way to improve the melt strength through formation of the network of nucleated crystals. Moreover, promoting the crystallization of the polymers can lead to heterogeneous cell nucleation around the crystals

as the presence of an interface reduces the free energy for nucleation and consequently increases the nucleation rate.

Surface modification of silica nanoparticles and alteration of its wettability was an important step in this project. The surface-modified nanoparticles provide a surface with lower energy which contribute in both better dispersion of the particles in the matrix and higher work of adhesion. For the amine modification, the interaction and adsorption of CO_2 on the surface of the silica particles can be increased via interaction between basic amine groups on the surface and acidic CO_2 molecules. Furthermore, the surface-modified nanoparticles are surface-active and their affinity towards CO_2 promotes their irreversible adsorption to the polymer/ CO_2 interface. On the hand, the free energy barrier for heterogeneous nucleation of polymer foams depends on the three–phase contact angle between the nanoparticle/ polymer/ CO_2. An increase in three-phase contact angle leads to a decrease in nucleation barrier.

As the first step of this study, we have used Axisymmetric Drop Shape Analysis Profile (ADSA-P) pendant drop method to investigate the interfacial tension of PLA in supercritical carbon dioxide at high temperatures and pressures. The temperature and pressure range of the measurement is in those of microcellular foaming and blending processes, i.e. 143°C to 168°C and 3450 to 13790 kPa. The results showed a reduction in interfacial tension with increasing temperature and pressure and a decrease in its dependency on temperature at high pressures. At high pressures interfacial tension decreases as a result of an increase in temperature, but at the same time solubility of CO_2 decreases at high temperatures. The relationship between interfacial tension and the density-difference of polymer-supercritical-CO_2 mixtures using generalized Macleod equation showed a decrease in values of interfacial tension with an increase in temperature. The slopes were in the range of 1.84 to 1.94. The dimensionless Bond number was used to study the stability of melted PLA for pendant drop measurements and the results showed that the drops with values in range of 0.36-0.48 were stable.

In the next step, the effect of synthesized silica nanoparticles with CO_2 – philic (amine) surface modification on interfacial tension between PLA and supercritical CO_2 was studied. The interfacial tension of silica-containing PLA and supercritical CO_2 is measured using pendant drop method at high pressures and high temperatures. Although the interfacial tension decreases as a result of the nanoparticles' adsorption to the interface, a minimum in

silica loading of 2 wt. % for all the pressures was observed. At higher loadings of the silica nanoparticles, interfacial tension increased to a final plateau value due to attractive lateral capillary forces originating from the perturbation of the PLA- CO_2 interface by particles. Although the capillary force at the interface resists a deformation or stretching in surface area and slightly increase the surface tension, it can increase the surface elasticity of the interface. Contact angle measurements at high temperatures and pressures showed a decrease in compatibility between the nanoparticles and PLA with increasing CO_2, but in general the adsorption of nanoparticles was thermodynamically favorable and irreversible. The binding energy calculations showed irreversible adsorption due to high values of energy compared with thermal fluctuations.

The other step was to study the effect of surface-modified silica nanoparticles on PLA crystallization. Both isothermal and non- isothermal crystallization for various loadings of silica nanoparticles were investigated. Ahead of nanocomposite preparation, a proper surface modification of the silica nanoparticles was selected to satisfy the need for a well-dispersed nanocomposites, higher-absorption of CO_2, and faster crystallization rate. Surface energy and interfacial energy between polymer/nanoparticle calculations at high temperatures are used to calculate work of adhesion and also explanation of acceleration of the crystallization process in presence of the nanoparticles. For PLA with high molecular weight and D-content, the crystallization rate and crystallinity increased significantly. The incorporation of surface-modified silica nanoparticles developed alfa type crystal structure with orthorhombic unit cells. A modified Hoffman-Lauritzen nucleation theory was developed considering the surface energy of nanoparticles, interfacial energy between nanoparticle and lateral surface of crystals into rate equation. The model confirmed the acceleration and occurrence of crystallization for nanocomposite samples. Isothermal analysis based on the Avrami equation was performed to investigate the kinetics of crystallization. The results revealed a sporadically formed three-dimensional spherulitic structure. The Avrami exponent analysis at higher temperatures moved towards a two-dimensional structure with less packed crystals. In order to consider the crystallization improvement for foaming processes, isothermal crystallization under compressed CO_2 is also investigated. The heterogeneous nucleation provided by nucleation agents such as silica nanoparticles improves the crystallization rate at high temperatures when there is less driving force for homogeneous nucleation. In addition to the role as a blowing agent in foaming, the effect of carbon dioxide as a plasticizer on

crystallization is more dominant at lower temperatures where higher chain mobility is required for crystallization. That is the reason why the effect of CO_2 has been studied at a low and narrow crystallization temperature window. Therefore, combining nucleation and plasticization is expected to increase the crystallization rate and broaden the crystallization temperature window in the foaming process of PLA. It was shown that the presence of carbon dioxide increases the crystallization rate at 15 bar, but at the higher pressure of 21 bar, the crystallization rate became nearly constant. The crystallization rate of PLA grades with lower molecular weights and lower D-content increased by up to a factor of 10 with no change in crystallization mechanism after the incorporation of surface-modified silica nanoparticles.

6.2 Original Contributions

Long after their discovery in early 20th century by Pickering and Ramsden, solid stabilized foams and emulsion came to the centre of attention less than a decade ago. There has been numerous work done on aqueous Pickering foams and emulsions, however; to the best of our knowledge, there is no study been performed on the solid stabilization of polymer foams, study on adsorption of nanoparticles to polymer interface in a supercritical environment, and the effect amine-modified silica nanoparticles on crystallization in atmospheric and compressed CO_2. In this thesis, nanoparticles are used to observe their effect on foaming of poly lactic acid from fundamental point of views. As it was discussed in chapter 1 and 2, interfacial tension and crystallization are two fundamental and key characteristics that determine foaming behavior of polymers.

The three main chapters, including Chapter 4, 5, and 6, are focusing on the effect of carbon dioxide on PLA interfacial tension, effect of silica nanoparticles and their adsorption behavior in PLA/CO_2 system, and effect of the nanoparticles and CO_2 on PLA crystallization, respectively. The dependency of PLA/ CO_2 interfacial tension to processing conditions is the first step to find the processing window and demonstration of nucleation and growth phenomena. Interfacial tension of PLA in presence of CO_2 was studied in details in Chapter 4 and the results were published journal of Thermochimica Acta in 2015.

According to our results, the surface-modified silica nanoparticles can irreversibly adsorb to see PLA/ CO_2 interface. The effectiveness of the nanoparticles in interfacial tension reduction was studied thoroughly in the previously optimized processing conditions. The

presence of nanoparticles at the interface can stabilize the bubbles and prevent the growing bubbles from coalescence phenomena due to repulsion between nanoparticles in adjacent interface. Furthermore, the interfacial tension increased after a certain percentage of the nanoparticles due to capillary interaction between the particles at the interface. Higher interfacial modulus is the critical in foam stabilization as Ostwald-ripening and draining destabilization mechanisms are coupled to the interfacial viscoelasticity. This part of study was discussed in details in Chapter 5 and the results were published in journal of Langmuir in 2015.

Crystallization improvement using nanoparticles as another step in improvement of PLA foaming was also studied thoroughly in Chapter 6. PLA's low melt strength leads to cell coalescence and cell rupture during growth step. Heterogeneous nucleation effect of surface-modified silica nanoparticles and plasticization effect of carbon dioxide was shown to increase the crystallization rate, induce the crystallization, and broaden the crystallization temperature window in the foaming process of PLA. This part of the research is submitted to Polymer.

6.3 Recommendations

We propose the following suggestions and recommendations as future work to further delve into the different steps of this research:

In this work the two important parameter controlling the foaming process of polymeric foams have been studied. The results of chapters 4 and 5 show that interfacial tension and crystallization of PLA have been changed because of the silica nanoparticles in the system. It is beneficial from practical point of view to do batch foaming of the nanocomposites to correlate the change in interfacial and crystallization properties to the final foam properties.

As discussed in chapter 2 and chapter 5, the contact angle and wettability of the nanoparticles is a key factor to reduce the energy barrier for nucleation in foaming and to provide a low surface energy particle for better dispersion, as well as better crystal nucleation. It is suggested to study the effect of various surface modifications of silica on interfacial behavior, crystallization, and stabilization of polymeric systems. Furthermore, the effect of these nanoparticles and surface modification can also be studied in aqueous foams as a more simple system for investigation.

In order to increase the amount of absorbed CO_2 and prevent the undesired effect of vitrified polymer layer around the nanoparticles, it is interesting to study the effect of porous nanoparticles with CO_2 – philic modification on CO_2 solubility and melt strength of the nanocomposites. The porous structure can also be effective in creation of nano-sized cell structure in foaming of the nanocomposites.

The rheological properties of the interface Interfacial modulus is a critical characteristics in foam stability. An interfacial layer with a high surface elastic modulus and a resistance to compression reduces the coarsening process in foams. It is important from practical point of view to study the interfacial rheology of the solid-stabilized foams

The effect of nanoparticles aspect ratio and shape on adsorption to the interface and the stability of Pickering foams is also important as different shapes have different dynamics of adsorption and surface coverage at the interface.

Appendix I. Supporting Information (SI) for Chapter 6

I1. Interfacial tension and contact angle measurements

Surface tension of PLA at various temperatures was measured using axisymmetric drop shape analysis profile (ADSA-P) technique. The interfacial tension of the polymer samples was measured by fitting the shape and dimensions of their menisci to the theoretical drop profile based on the Laplace equation of capillarity:

$$\Delta P = \gamma(\frac{1}{R1} + \frac{1}{R2}) \quad \text{I-1}$$

where γ is surface tension, ΔP is the pressure difference across the interface, and R1 and R2 are two principal radii of curvature. If gravity is the only external force, ΔP can be expressed as a linear function of height:

$$\Delta P = \Delta P_0 + (\Delta\rho)gz \quad \text{I-2}$$

where ΔP_0 is the pressure difference at a reference plane, and z is the vertical height of the drop measured from a reference plane [203]. A high-temperature chamber was designed for both pendant drop and sessile drop measurement [32,35,169]. For the contact angle measurements the silicon surfaces were mounted on top of the inversed stainless steel rod. Prior to the surface tension measurement, the accuracy was tested using a pendant drop measurement of water. The value of 72.12 ± 0.11 $mJ.m^{-2}$ was consistent for water at room temperature.

I2. Contact Angle Measurements and Surface Energy Calculations at Room Temperature

The contact angle measurement and surface energy calculations based on Equations 8-4 and 8-7 are summarized in Table I.1. The results were obtained using two different equations of state; one using the Neumann approach and the other one based on a surface energy component approach using the Van Oss equation of state [203,204]. The contact

angles of three liquids are used in the calculation of Van Oss components. For the results obtained through the Neumann approach (Equations 8-3 and 8-4), the contact angle of only one liquid suffices to calculate the surface energy:

$$\gamma_{sl} = \gamma_l + \gamma_s - 2\sqrt{\gamma_l \gamma_s}\, e^{-\beta(\gamma_l - \gamma_s)^2} \quad \text{I-3}$$

where $\beta = 0.0001247(\text{m}^2/\text{mJ})^2$ .Combining the equation 7 with Young's equation:

$$\cos\theta = -1 + 2\sqrt{\frac{\gamma_s}{\gamma_l}}\, e^{-\beta(\gamma_l - \gamma_s)^2} \quad \text{I-4}$$

And for the Van Oss equation of state, the surface tension components are introduced as:

$$\gamma = \gamma^{LW} + 2\sqrt{\gamma^+ \gamma^-} \quad \text{I-5}$$

which lead to the equation for solid – liquid interfacial tension:

$$\gamma_{sl} = (\sqrt{\gamma_l^{LW}} - \sqrt{\gamma_s^{LW}})^2 + 2\left(\sqrt{\gamma_l^+} - \sqrt{\gamma_s^+}\right)(\sqrt{\gamma_l^-} - \sqrt{\gamma_s^-}) \quad \text{I-6}$$

Combining with Young's equation:

$$\gamma_l(1 + \cos\theta) = 2\sqrt{\gamma_l^{LW}\gamma_s^{LW}} + 2\sqrt{\gamma_l^+\gamma_s^-} + 2\sqrt{\gamma_l^-\gamma_s^+} \quad \text{I-7}$$

Table I.1. Room – temperature water contact angle and surface energy results for silica and silica-APTES obtained via Van Oss and Neumann equations of state

			Van Oss components (mJ/m²)				***Neumann (mJ/m²)***	
Samples	*Water Contact Angle (°)*	*95 % CI*	*LW*	*acid*	*base*	*total*	*total (water)*	*total (Glycerol)*
Silica	18.8	±1.4	38.1	46.2	2.3	58.8	68.4	58.6
Silica-APTES	32.8	±1.9	37.3	42.1	1.2	51.8	62.4	52.4

I3. Surface Tension and Contact Angle at High Temperatures

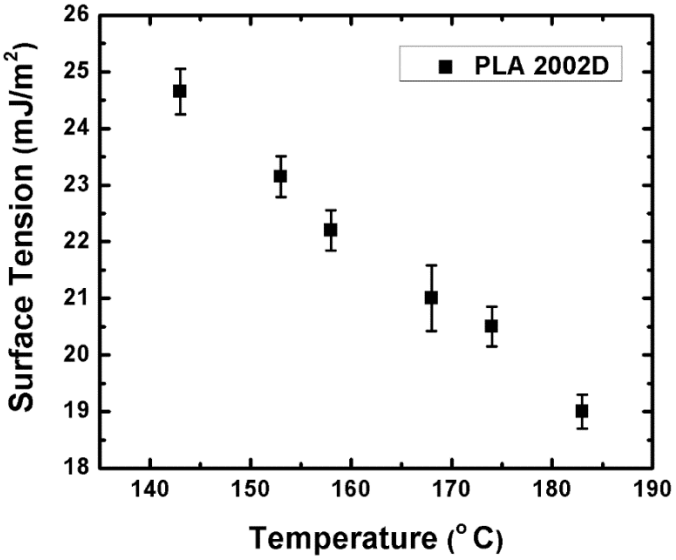

Figure I-1.Surface tension of PLA 2002D obtained from pendant drop measurement at high temperatures

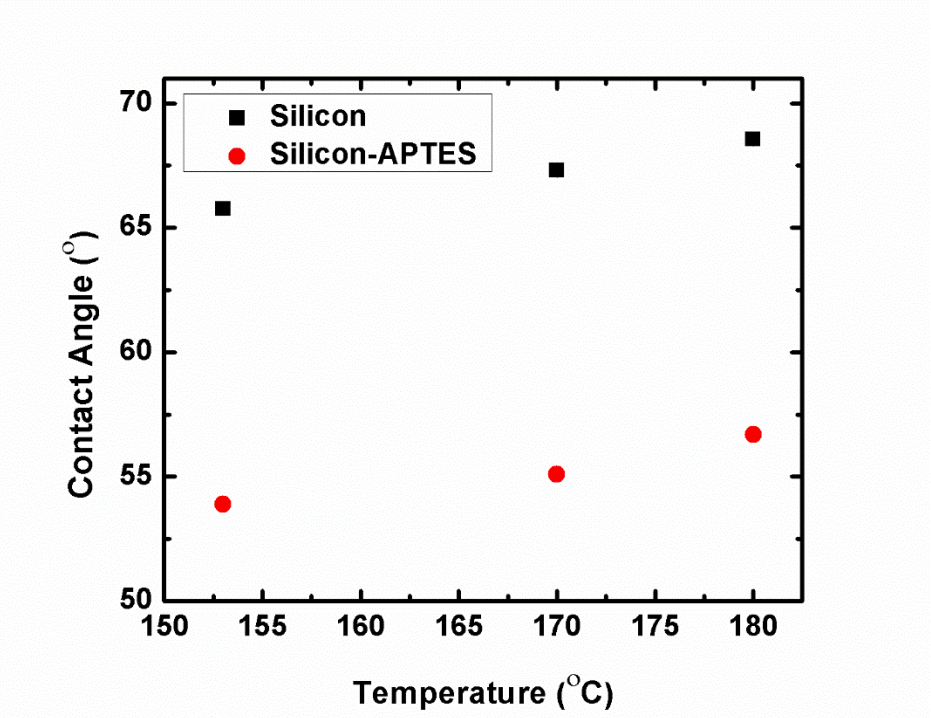

Figure I-2.Contact angle of PLA polymer melt on silicon (black square) and silicon-APTES (red circle) surfaces at high temperatures (the maximum value for error bar is ± 0.2 ° for 95% confidence interval)

References

[1] R.N.S. Lee S, Park C. B., Polymeric Foams: Science and Technology, Taylor and Francis Group, LLC, 2007.

[2] D. Eaves, Handbook of polymer foams, Rapra Technology Limited, 2004.

[3] K.P. Johnston, S.R.P. Da Rocha, Colloids in supercritical fluids over the last 20 years and future directions, J. Supercrit. Fluids. 47 (2009) 523–530. doi:10.1016/j.supflu.2008.10.024.

[4] C. Wang, S.N. Leung, M. Bussmann, W.T. Zhai, C.B. Park, Numerical Investigation of Nucleating-Agent-Enhanced Heterogeneous Nucleation, Ind. Eng. Chem. Res. 49 (2010) 12783–12792. doi:10.1021/ie1017207.

[5] S.N. Leung, A. Wong, C.B. Park, J.H. Zong, Ideal Surface Geometries of Nucleating Agents to Enhance Cell Nucleation in Polymeric Foaming Processes, 108 (2008) 3997–4003. doi:10.1002/app.

[6] X. Liao, Y.G. Li, C.B. Park, P. Chen, Interfacial tension of linear and branched PP in supercritical carbon dioxide, J. Supercrit. Fluids. 55 (2010) 386–394. doi:10.1016/j.supflu.2010.06.011.

[7] J. Faraudo, F. Bresme, Stability of particles adsorbed at liquid/fluid interfaces: Shape effects induced by line tension, J. Chem. Phys. 118 (2003) 6518. doi:10.1063/1.1559728.

[8] T.M. Ruhland, A.H. Gröschel, N. Ballard, T.S. Skelhon, A. Walther, A.H.E. Müller, et al., Influence of Janus particle shape on their interfacial behavior at liquid-liquid interfaces., Langmuir ACS J. Surfaces Colloids. 29 (2013) 1388–94. http://www.ncbi.nlm.nih.gov/pubmed/23311383.

[9] E. Girard, T. Tassaing, S. Camy, J.-S. Condoret, J.-D. Marty, M. Destarac, Enhancement of poly(vinyl ester) solubility in supercritical CO2 by partial fluorination: the key role of polymer-polymer interactions., J. Am. Chem. Soc. 134 (2012) 11920–3. doi:10.1021/ja304585d.

[10] S.T. Lee, L. Kareko, J. Jun, Study of Thermoplastic PLA Foam Extrusion, J. Cell. Plast. 44 (2008) 293–305. doi:10.1177/0021955X08088859.

[11] B.S. Murray, Stabilization of bubbles and foams, Curr. Opin. Colloid Interface Sci. 12 (2007) 232–241. doi:10.1016/j.cocis.2007.07.009.

[12] V. Garbin, J.C. Crocker, K.J. Stebe, Nanoparticles at fluid interfaces: Exploiting capping ligands to control adsorption, stability and dynamics, J. Colloid Interface Sci. 387 (2012) 1–11. doi:10.1016/j.jcis.2012.07.047.

[13] T. Saigal, H. Dong, K. Matyjaszewski, R.D. Tilton, Pickering emulsions stabilized by nanoparticles with thermally responsive grafted polymer brushes., Langmuir. 26 (2010) 15200–9. doi:10.1021/la1027898.

[14] J.W.O. Salari, F. a M. Leermakers, B. Klumperman, Pickering emulsions: wetting and colloidal stability of hairy particles--a self-consistent field theory., Langmuir Acs J. Surfaces Colloids. 27 (2011) 6574–6583. http://www.ncbi.nlm.nih.gov/pubmed/21539302.

[15] K. Larson-Smith, D.C. Pozzo, Pickering emulsions stabilized by nanoparticle surfactants, Langmuir. 28 (2012) 11725–11732. doi:10.1021/la301896c.

[16] M. Nofar, C.B. Park, Poly (lactic acid) foaming, Prog. Polym. Sci. 39 (2014) 1–21. doi:10.1016/j.progpolymsci.2014.04.001.

[17] B. Gupta, N. Revagade, J. Hilborn, Poly(lactic acid) fiber: An overview, Prog. Polym. Sci. 32 (2007) 455–482. doi:10.1016/j.progpolymsci.2007.01.005.

[18] M. Savioli Lopes, a. L. Jardini, R. Maciel Filho, Poly (lactic acid) production for tissue engineering applications, Procedia Eng. 42 (2012) 1402–1413. doi:10.1016/j.proeng.2012.07.534.

[19] J.K. Oh, Polylactide (PLA)-based amphiphilic block copolymers: synthesis, self-assembly, and biomedical applications, Soft Matter. 7 (2011) 5096–5108. doi:10.1039/C0SM01539C.
[20] R. Gendron, Thermoplastic Foam Processing: Principles and Development, CRC Press, 2004.
[21] J.S. Colton, N.P. Suh, Nucleation of Microcellular Foam: Theory and Practice, Polym. Eng. Sci. 27 (1987) 500–503. doi:10.1002/pen.760270704.
[22] H. Li, L.J. Lee, D.L. Tomasko, Effect of Carbon Dioxide on the Interfacial Tension of Polymer Melts, Ind. Eng. Chem. Res. 43 (2004) 509–514. doi:10.1021/ie034092n.
[23] R. Auras, B. Harte, S. Selke, An overview of polylactides as packaging materials, Macromol. Biosci. 4 (2004) 835–864. doi:10.1002/mabi.200400043.
[24] M. Nofar, A. Ameli, C.B. Park, A novel technology to manufacture biodegradable polylactide bead foam products, Mater. Des. 83 (2015) 413–421. doi:10.1016/j.matdes.2015.06.052.
[25] M. Keshtkar, M. Nofar, C.B. Park, P.J. Carreau, Extruded PLA/clay nanocomposite foams blown with supercritical CO 2, Polym. (United Kingdom). 55 (2014) 4077–4090. doi:10.1016/j.polymer.2014.06.059.
[26] A. Ameli, M. Nofar, D. Jahani, G. Rizvi, C.B. Park, Development of high void fraction polylactide composite foams using injection molding: Crystallization and foaming behaviors, Chem. Eng. J. 262 (2015) 78–87. doi:10.1016/j.cej.2014.09.087.
[27] A. Ameli, D. Jahani, M. Nofar, P.U. Jung, C.B. Park, Processing and characterization of solid and foamed injection-molded polylactide with talc, J. Cell. Plast. Online ver (2013) 1–24. doi:10.1177/0021955X13481993.
[28] J.A. Darr, M. Poliakoff, New Directions in Inorganic and Metal-Organic Coordination Chemistry in Supercritical Fluids, Chem. Rev. 99 (1999) 495–541. doi:10.1021/CR970036I.
[29] R. Auras, B. Harte, S. Selke, An overview of polylactides as packaging materials., Macromol. Biosci. 4 (2004) 835–864. doi:10.1002/mabi.200400043.
[30] A.I. Cooper, Polymer synthesis and processing using supercritical carbon dioxide, J. Mater. Chem. 10 (2000) 207–234. doi:10.1039/a906486i.
[31] D.Y. Kwok, L.K. Cheung, C.B. Park, a W. Neumann, Study on the surface tensions of polymer melts using axisymmetric drop shape analysis, Polym. Eng. Sci. 38 (1998) 757–764. doi:10.1002/pen.10241.
[32] H. Park, C.B. Park, C. Tzoganakis, K.H. Tan, P. Chen, Surface Tension Measurement of Polystyrene Melts in Supercritical Carbon Dioxide, Ind. Eng. Chem. Res. 45 (2006) 1650–1658.
[33] H. Park, R.B. Thompson, N. Lanson, C. Tzoganakis, C.B. Park, P. Chen, Effect of temperature and pressure on surface tension of polystyrene in supercritical carbon dioxide., J. Phys. Chem. B. 111 (2007) 3859–68. doi:10.1021/jp065851t.
[34] H. Park, C.B. Park, C. Tzoganakis, P. Chen, Effect of Molecular Weight on the Surface Tension of Polystyrene Melt in Supercritical Nitrogen, Ind. Eng. Chem. Res. 46 (2007) 3849–3851. doi:10.1021/ie070311j.
[35] H. Wei, R.B. Thompson, C.B. Park, P. Chen, Surface tension of high density polyethylene (HDPE) in supercritical nitrogen: Effect of polymer crystallization, Colloids Surfaces A Physicochem. Eng. Asp. 354 (2010) 347–352. doi:10.1016/j.colsurfa.2009.06.005.
[36] R.B. Thompson, C.B. Park, P. Chen, Reduction of polymer surface tension by crystallized polymer nanoparticles., J. Chem. Phys. 133 (2010) 144913. doi:10.1063/1.3493334.
[37] S.H. Mahmood, M. Keshtkar, C.B. Park, Determination of carbon dioxide solubility in polylactide acid with accurate {PVT} properties, J. Chem. Thermodyn. 70 (2014) 13–23. doi:http://dx.doi.org/10.1016/j.jct.2013.10.019.
[38] S.H. Mahmood, A. Ameli, N. Hossieny, C.B. Park, The interfacial tension of molten

polylactide in supercritical carbon dioxide, J. Chem. Thermodyn. 75 (2014) 69–76. doi:http://dx.doi.org/10.1016/j.jct.2014.02.017.
[39] B.P. Binks, T.S. Horozov, Colloidal Particles at Liquid Interfaces: An Introduction, in: B.P. Binks, T.S. Horozov (Eds.), Colloid. Part. Liq. Interfaces, Cambridge University Press, 2006: pp. 1–74. http://dx.doi.org/10.1017/CBO9780511536670.002.
[40] S. Pickering, Cxcvi. emulsions, J. Chem. Soc. Trans. (1907) 2001–2021. doi:10.1039/ct9079102001.
[41] W. Ramsden, Separation of Solids in the Surface-Layers of Solutions and "Suspensions" (Observations on Surface-Membranes, Bubbles, Emulsions, and Mechanical Coagulation). -- Preliminary Account, Proc. R. Soc. London . 72 (1903) 156–164. doi:10.1098/rspl.1903.0034.
[42] Z. Niu, J. He, T.P. Russell, Q. Wang, Synthesis of nano/microstructures at fluid interfaces, Angew. Chemie - Int. Ed. 49 (2010) 10052–10066. doi:10.1002/anie.201001623.
[43] R. Aveyard, B.P. Binks, J.H. Clint, Emulsions stabilised solely by colloidal particles, Adv. Colloid Interface Sci. 100-102 (2003) 503–546. doi:10.1016/S0001-8686(02)00069-6.
[44] B.P. Binks, Particles as surfactants—similarities and differences, Curr. Opin. Colloid Interface Sci. 7 (2002) 21–41. doi:10.1016/S1359-0294(02)00008-0.
[45] A.D. Dinsmore, M.F. Hsu, M.G. Nikolaides, M. Marquez, A.R. Bausch, D.A. Weitz, Colloidosomes: selectively permeable capsules composed of colloidal particles., Science. 298 (2002) 1006–1009. doi:10.1126/science.1074868.
[46] O.D. Velev, S. Gupta, Materials fabricated by micro- and nanoparticle assembly - The challenging path from science to engineering, Adv. Mater. 21 (2009) 1897–1905. doi:10.1002/adma.200801837.
[47] F. Ravera, M. Ferrari, L. Liggieri, R. Miller, A. Passerone, Measurement of the Partition Coefficient of Surfactants in Water/Oil Systems, Langmuir. 13 (1997) 4817–4820. doi:10.1021/la962096+.
[48] a Maestro, L.J. Bonales, H. Ritacco, R.G. Rubio, F. Ortega, Effect of the spreading solvent on the three-phase contact angle of microparticles attached at fluid interfaces., Phys. Chem. Chem. Phys. 12 (2010) 14115–14120. doi:10.1039/c0cp00570c.
[49] A. Maestro, E. Guzmán, E. Santini, F. Ravera, L. Liggieri, F. Ortega, et al., Wettability of silica nanoparticle-surfactant nanocomposite interfacial layers, Soft Matter. 8 (2012) 837–843. doi:10.1039/C1SM06421E.
[50] D. Zang, A. Stocco, D. Langevin, B. Wei, B.P. Binks, An ellipsometry study of silica nanoparticle layers at the water surface, Phys. Chem. Chem. Phys. 11 (2009) 9522–9529. doi:10.1039/B907903C.
[51] A. Maestro, E. Guzmán, F. Ortega, R.G. Rubio, Contact angle of micro- and nanoparticles at fluid interfaces, Curr. Opin. Colloid Interface Sci. 19 (2014) 355–367. doi:10.1016/j.cocis.2014.04.008.
[52] T. Okubo, Surface Tension of Structured Colloidal Suspensions of Polystyrene and Silica Spheres at the Air-Water Interface, J. Colloid Interface Sci. 171 (1995) 55–62. doi:http://dx.doi.org/10.1006/jcis.1995.1150.
[53] I. Blute, R.J. Pugh, J. van de Pas, I. Callaghan, Industrial manufactured silica nanoparticle sols. 2: Surface tension, particle concentration, foam generation and stability, Colloids Surfaces A Physicochem. Eng. Asp. 337 (2009) 127–135. doi:10.1016/j.colsurfa.2008.12.009.
[54] N. Saleh, T. Sarbu, K. Sirk, G. V Lowry, K. Matyjaszewski, R.D. Tilton, Oil-in-water emulsions stabilized by highly charged polyelectrolyte-grafted silica nanoparticles, Langmuir. 21 (2005) 9873–9878. http://www.scopus.com/inward/record.url?eid=2-s2.0-27544440122&partnerID=40&md5=f9155a54128e2071c468aedd97d02b50.
[55] N.J. Alvarez, S.L. Anna, T. Saigal, R.D. Tilton, L.M. Walker, Interfacial dynamics and

rheology of polymer-grafted nanoparticles at air-water and xylene-water interfaces, Langmuir. 28 (2012) 8052–8063. doi:10.1021/la300737p.
[56] L.N. Arnaudov, O.J. Cayre, M.A.C. Stuart, S.D. Stoyanov, V.N. Paunov, Measuring the three-phase contact angle of nanoparticles at fluid interfaces, Phys. Chem. Chem. Phys. 12 (2010) 328–331. doi:10.1039/b917353f.
[57] L. Isa, D.C.E. Calzolari, D. Pontoni, T. Gillich, A. Nelson, R. Zirbs, et al., Core–shell nanoparticle monolayers at planar liquid–liquid interfaces: effects of polymer architecture on the interface microstructure, Soft Matter. 9 (2013) 3789. doi:10.1039/c3sm27367a.
[58] S. Ferdous, M. a. Ioannidis, D.E. Henneke, Effects of temperature, pH, and ionic strength on the adsorption of nanoparticles at liquid–liquid interfaces, J. Nanoparticle Res. 14 (2012) 850. doi:10.1007/s11051-012-0850-4.
[59] R.B. Thompson, V. V Ginzburg, M.W. Matsen, a C. Balazs, Predicting the mesophases of copolymer-nanoparticle composites, Science (80-.). 292 (2001) 2469–2472. doi:10.1126/science.1060585.
[60] J.J. Chiu, B.J. Kim, E.J. Kramer, D.J. Pine, Control of nanoparticle location in block copolymers, J. Am. Chem. Soc. 127 (2005) 5036–5037. doi:10.1021/ja050376i.
[61] L. Dong, D.T. Johnson, The Study of the Surface Tension of Charge-Stabilized Colloidal Dispersions, J. Dispers. Sci. Technol. 25 (2005) 575–583. doi:10.1081/DIS-200027307.
[62] J.N. Israelachvili, Intermolecular and Surface Forces Third Edition, Intermol. Surf. Forces. (2010) 710. doi:10.1016/B978-0-12-375182-9.10025-9.
[63] R. Aveyard, J.H. Clint, Particle wettability and line tension, J. Chem. Soc. Faraday Trans. 92 (1996) 85. doi:10.1039/ft9969200085.
[64] F. Bresme, N. Quirke, Nanoparticulates at liquid/liquid interfaces, Phys. Chem. Chem. Phys. 1 (1999) 2149–2155. doi:10.1039/a901006h.
[65] J. Faraudo, F. Bresme, Stability of particles adsorbed at liquid/fluid interfaces: Shape effects induced by line tension, J. Chem. Phys. 118 (2003) 6518–6528. doi:10.1063/1.1559728.
[66] G. Bournival, S. Ata, E.J. Wanless, The roles of particles in multiphase processes: Particles on bubble surfaces., Adv. Colloid Interface Sci. 225 (2015) 114–33. doi:10.1016/j.cis.2015.08.008.
[67] E. Dickinson, Interfacial Particles in Food Emulsions and Foams, in: B.P. Binks, T.S. Horozov (Eds.), Colloid. Part. Liq. Interfaces, Cambridge University Press, 2006: pp. 298–327. http://dx.doi.org/10.1017/CBO9780511536670.009.
[68] B.P. Binks, T.S. Horozov, Aqueous foams stabilized solely by silica nanoparticles, Angew. Chemie - Int. Ed. 44 (2005) 3722–3725. doi:10.1002/anie.200462470.
[69] R.J.G. Lopetinsky, J.H. Masliyah, Z. Xu, Solids-Stabilized Emulsions: A Review, in: B.P. Binks, T.S. Horozov (Eds.), Colloid. Part. Liq. Interfaces, Cambridge University Press, 2006: pp. 186–224. http://dx.doi.org/10.1017/CBO9780511536670.007.
[70] A.J. Worthen, P.S. Parikh, Y. Chen, S.L. Bryant, C. Huh, K.P. Johnston, Carbon Dioxide-in-Water Foams Stabilized with a Mixture of Nanoparticles and Surfactant for CO2 Storage and Utilization Applications, Energy Procedia. 63 (2014) 7929–7938. doi:10.1016/j.egypro.2014.11.827.
[71] J.S. Guevara, A.F. Mejia, M. Shuai, Y.-W. Chang, M.S. Mannan, Z. Cheng, Stabilization of Pickering foams by high-aspect-ratio nano-sheets, Soft Matter. 9 (2013) 1327–1336. doi:10.1039/C2SM27061G.
[72] S. Lam, E. Blanco, S.K. Smoukov, K.P. Velikov, O.D. Velev, Magnetically responsive pickering foams., J. Am. Chem. Soc. 133 (2011) 13856–9. doi:10.1021/ja205065w.
[73] U.T. Gonzenbach, A.R. Studart, E. Tervoort, L.J. Gauckler, Ultrastable particle-stabilized

foams, Angew. Chemie - Int. Ed. 45 (2006) 3526–3530. doi:10.1002/anie.200503676.
[74] T.N. Hunter, E.J. Wanless, G.J. Jameson, Effect of esterically bonded agents on the monolayer structure and foamability of nano-silica, Colloids Surfaces A Physicochem. Eng. Asp. 334 (2009) 181–190. doi:10.1016/j.colsurfa.2008.10.039.
[75] S. Fujii, P.D. Iddon, a. J. Ryan, S.P. Armes, Aqueous particulate foams stabilized solely with polymer latex particles, Langmuir. 22 (2006) 7512–7520. doi:10.1021/la060812u.
[76] H. a. Wege, S. Kim, V.N. Paunov, Q. Zhong, O.D. Velev, Long-term stabilization of foams and emulsions with in-situ formed microparticles from hydrophobic cellulose, Langmuir. 24 (2008) 9245–9253. doi:10.1021/la801634j.
[77] D.N. Tran, C.P. Whitby, D. Fornasiero, J. Ralston, Foamability of aqueous suspensions of fine graphite and quartz particles with a triblock copolymer, J Colloid Interface Sci. 348 (2010) 460–468. doi:10.1016/j.jcis.2010.04.073.
[78] R.G. Alargova, D.S. Warhadpande, V.N. Paunov, O.D. Velev, Foam superstabilization by polymer microrods, Langmuir. 20 (2004) 10371–10374. doi:10.1021/la048647a.
[79] B. Madivala, S. Vandebril, J. Fransaer, J. Vermant, Exploiting particle shape in solid stabilized emulsions, Soft Matter. 5 (2009) 1717. doi:10.1039/b816680c.
[80] B.P. Binks, T. Sekine, A.T. Tyowua, Dry oil powders and oil foams stabilised by fluorinated clay platelet particles., Soft Matter. 10 (2014) 578–89. doi:10.1039/c3sm52748d.
[81] L.-T. Lim, R. Auras, M. Rubino, Processing technologies for poly(lactic acid), Prog. Polym. Sci. 33 (2008) 820–852. doi:10.1016/j.progpolymsci.2008.05.004.
[82] L.-I. Palade, H.J. Lehermeier, J.R. Dorgan, Melt Rheology of High l-Content Poly(lactic acid), Macromolecules. 34 (2001) 1384–1390. doi:10.1021/ma001173b.
[83] S.-Y. Gu, J. Ren, B. Dong, Melt rheology of polylactide/montmorillonite nanocomposites, J. Polym. Sci. Part B Polym. Phys. 45 (2007) 3189–3196. doi:10.1002/polb.21317.
[84] Y. Di, S. Iannace, E. Di Maio, L. Nicolais, Poly(lactic acid)/organoclay nanocomposites: Thermal, rheological properties and foam processing, J. Polym. Sci. Part B Polym. Phys. 43 (2005) 689–698. doi:10.1002/polb.20366.
[85] M. Nofar, A. Tabatabaei, C.B. Park, Effects of nano-/micro-sized additives on the crystallization behaviors of PLA and PLA/CO2 mixtures, Polym. (United Kingdom). 54 (2013) 2382–2391. doi:10.1016/j.polymer.2013.02.049.
[86] M. Mihai, M.A. Huneault, B.D. Favis, Crystallinity Development in Cellular Poly(lactic acid) in the Presence of Supercritical Carbon Dioxide, J. Appl. Polym. Sci. 113 (2009) 2920–2932. doi:10.1002/app.30338.
[87] S. Saeidlou, M. a. Huneault, H. Li, C.B. Park, Poly(lactic acid) crystallization, Prog. Polym. Sci. 37 (2012) 1657–1677. doi:10.1016/j.progpolymsci.2012.07.005.
[88] J. Wang, W. Zhu, H. Zhang, C.B. Park, Continuous processing of low-density, microcellular poly(lactic acid) foams with controlled cell morphology and crystallinity, Chem. Eng. Sci. 75 (2012) 390–399. doi:10.1016/j.ces.2012.02.051.
[89] M. Nofar, A. Tabatabaei, C.B. Park, Effects of nano-/micro-sized additives on the crystallization behaviors of PLA and PLA/CO2 mixtures, Polym. (United Kingdom). 54 (2013) 2382–2391. doi:10.1016/j.polymer.2013.02.049.
[90] A. Wong, Y. Guo, C.B. Parka, Fundamental mechanisms of cell nucleation in polypropylene foaming with supercritical carbon dioxide - Effects of extensional stresses and crystals, J. Supercrit. Fluids. 79 (2013) 142–151. doi:10.1016/j.supflu.2013.02.013.
[91] K. Taki, D. Kitano, M. Ohshima, Effect of growing crystalline phase on bubble nucleation in poly(L -lactide)/CO2 batch foaming, Ind. Eng. Chem. Res. 50 (2011) 3247–3252. doi:10.1021/ie101637f.
[92] C. Marrazzo, E. Di Maio, S. Iannace, Conventional and nanometric nucleating agents in

poly(epsilon-caprolactone) foaming: Crystals vs. bubbles nucleation, Polym Eng Sci. 48 (2008) 336–344. doi:10.1002/pen.20937.
[93] G. Li, C.B. Park, A new crystallization kinetics study of polycarbonate under high-pressure carbon dioxide and various crystallinization temperatures by using magnetic suspension balance, J. Appl. Polym. Sci. 118 (2010) 2898–2903. doi:10.1002/app.32697.
[94] S. Saeidlou, M.A. Huneault, H. Li, C.B. Park, Poly(lactic acid) crystallization, Prog. Polym. Sci. 37 (2012) 1657–1677. doi:10.1016/j.progpolymsci.2012.07.005.
[95] Y. Zhang, B. Deng, Q. Liu, G. Chang, Nonisothermal Crystallization Kinetics of Poly(lactic acid)/Nanosilica Composites, J. Macromol. Sci. Part B. 52 (2013) 334–343. doi:10.1080/00222348.2012.701551.
[96] L. Basilissi, G. Di Silvestro, H. Farina, M.A. Ortenzi, Synthesis and characterization of PLA nanocomposites containing nanosilica modified with different organosilanes II: Effect of the organosilanes on the properties of nanocomposites: Thermal characterization, J. Appl. Polym. Sci. 128 (2013) 3057–3063. doi:10.1002/app.38504.
[97] N. Virgilio, P. Desjardins, G. L'Esperance, B.D. Favis, In Situ Measure of Interfacial Tensions in Ternary and Quaternary Immiscible Polymer Blends Demonstrating Partial Wetting, Macromolecules. 42 (2009) 7518–7529. doi:10.1021/ma9005507.
[98] S. Sugiura, M. Nakajima, T. Oda, M. Satake, M. Seki, Effect of interfacial tension on the dynamic behavior of droplet formation during microchannel emulsification., J. Colloid Interface Sci. 269 (2004) 178–185. doi:10.1016/j.jcis.2003.07.031.
[99] V. Khoshkava, M.R. Kamal, Effect of Surface Energy on Dispersion and Mechanical Properties of Polymer/Nanocrystalline Cellulose Nanocomposites., Biomacromolecules. (2013). doi:10.1021/bm400784j.
[100] M. Hoorfar, M. a. Kurz, a. W. Neumann, Evaluation of the surface tension measurement of axisymmetric drop shape analysis (ADSA) using a shape parameter, Colloids Surfaces A Physicochem. Eng. Asp. 260 (2005) 277–285. doi:10.1016/j.colsurfa.2004.08.080.
[101] O. Río, A. Neumann, Axisymmetric Drop Shape Analysis: Computational Methods for the Measurement of Interfacial Properties from the Shape and Dimensions of Pendant and Sessile Drops., J. Colloid Interface Sci. 196 (1997) 136–147. doi:10.1006/jcis.1997.5214.
[102] J.R. Dorgan, H.J. Lehermeier, L.-I. Palade, J. Cicero, Polylactides/PP : properties and prospects of an environmentally benign plastic from renewable resources, Macromol. Symp. 175 (2001) 55–66. doi:10.1002/1521-3900(200110)175:1<55::aid-masy55>3.0.co;2-k.
[103] K.P. Johnston, S.R.P. Da Rocha, Colloids in supercritical fluids over the last 20 years and future directions, J. Supercrit. Fluids. 47 (2009) 523–530. doi:10.1016/j.supflu.2008.10.024.
[104] S.H. Mahmood, A. Ameli, N. Hossieny, C.B. Park, The interfacial tension of molten polylactide in supercritical carbon dioxide, J. Chem. Thermodyn. (2014). doi:10.1016/j.jct.2014.02.017.
[105] Y. Sato, T. Takikawa, A. Sorakubo, S. Takishima, H. Masuoka, M. Imaizumi, Solubility and Diffusion Coefficient of Carbon Dioxide in Biodegradable Polymers, Ind. Eng. Chem. Res. 39 (2000) 4813–4819. doi:10.1021/ie0001220.
[106] S. Areerat, E. Funami, Y. Hayata, D. Nakagawa, M. Ohshima, Measurement and prediction of diffusion coefficients of supercritical CO2 in molten polymers, Polym. Eng. Sci. 44 (2004) 1915–1924. doi:10.1002/pen.20194.
[107] S.H. Mahmood, M. Keshtkar, C.B. Park, Determination of carbon dioxide solubility in polylactide acid with accurate {PVT} properties, J. Chem. Thermodyn. 70 (2014) 13–23. doi:http://dx.doi.org/10.1016/j.jct.2013.10.019.
[108] Y. Sato, T. Takikawa, A. Sorakubo, S. Takishima, H. Masuoka, M. Imaizumi, Solubility and

Diffusion Coefficient of Carbon Dioxide in Biodegradable Polymers, Ind. Eng. Chem. Res. 39 (2000) 4813–4819. doi:10.1021/ie0001220.
[109] G. Li, J. Wang, C.B. Park, R. Simha, Measurement of Gas Solubility in Linear / Branched PP Melts, (2007) 2497–2508. doi:10.1002/polb.
[110] Y.G. Li, C.B. Park, H.B. Li, J. Wang, Measurement of the PVT property of PP/CO2 solution, Fluid Phase Equilib. 270 (2008) 15–22. doi:10.1016/j.fluid.2008.05.007.
[111] N.R. Pallas, Y. Harrison, An automated drop shape apparatus and the surface tension of pure water, Colloids and Surfaces. 43 (1990) 169–194. doi:10.1016/0166-6622(90)80287-E.
[112] H. Park, C.B. Park, C. Tzoganakis, K.-H. Tan, P. Chen, Simultaneous Determination of the Surface Tension and Density of Polystyrene in Supercritical Nitrogen, Ind. Eng. Chem. Res. 47 (2008) 4369–4373. doi:10.1021/ie071472q.
[113] D. Sage, M. Müller, A.F. Stalder, T. Melchior, T. Blu, M. Unser, Low-bond axisymmetric drop shape analysis for surface tension and contact angle measurements of sessile drops, Colloids Surfaces A Physicochem. Eng. Asp. 364 (2010) 72–81. doi:10.1016/j.colsurfa.2010.04.040.
[114] M. Wulf, S. Michel, K. Grundke, del Rio OI, D. Kwok, A. Neumann, Simultaneous Determination of Surface Tension and Density of Polymer Melts Using Axisymmetric Drop Shape Analysis., J. Colloid Interface Sci. 210 (1999) 172–181. doi:10.1006/jcis.1998.5942.
[115] S.M.I. Saad, Z. Policova, E.J. Acosta, a W. Neumann, Range of validity of drop shape techniques for surface tension measurement., Langmuir. 26 (2010) 14004–13. doi:10.1021/la1020675.
[116] S.M.I. Saad, Z. Policova, a. W. Neumann, Design and accuracy of pendant drop methods for surface tension measurement, Colloids Surfaces A Physicochem. Eng. Asp. 384 (2011) 442–452. doi:10.1016/j.colsurfa.2011.05.002.
[117] Y. Sato, M. Yurugi, K. Fujiwara, S. Takishima, H. Masuoka, Solubilities of carbon dioxide and nitrogen in polystyrene under high temperature and pressure, Fluid Phase Equilib. 125 (1996) 129–138. doi:10.1016/S0378-3812(96)03094-4.
[118] M.M. Hasan, Y.G. Li, G. Li, C.B. Park, P. Chen, Determination of Solubilities of CO 2 in Linear and Branched Polypropylene Using a Magnetic Suspension Balance and a PVT Apparatus, J. Chem. Eng. Data. 55 (2010) 4885–4895. doi:10.1021/je100488v.
[119] J.R. and K.S. Françoise Rouquerol, Adsorption by Powders and Porous Solids Principles, Methodology and Applications, Academic Press, 1998.
[120] D. B. Macleod, On a relation between surface tension and density, Trans. Faraday Soc. 19 (1923) 38–41. doi:10.1039/TF9231900038.
[121] S. Sinha Ray, M. Okamoto, Polymer/layered silicate nanocomposites: A review from preparation to processing, Prog. Polym. Sci. 28 (2003) 1539–1641. doi:10.1016/j.progpolymsci.2003.08.002.
[122] M. Moniruzzaman, K.I. Winey, Polymer nanocomposites containing carbon nanotubes, Macromolecules. 39 (2006) 5194–5205. doi:10.1021/ma060733p.
[123] K. Sarikhani, S. Abdollahi, H. Garmabi, Preparation of PE nanocomposites using pristine nano clay via alkyl ammonium solution injection in a twin-screw extruder, J. Appl. Polym. Sci. 124 (2012) 1344–1351. doi:10.1002/app.35124.
[124] K. Jeddi, K. Sarikhani, N.T. Qazvini, P. Chen, Stabilizing lithium/sulfur batteries by a composite polymer electrolyte containing mesoporous silica particles, J. Power Sources. 245 (2014) 656–662. doi:10.1016/j.jpowsour.2013.06.147.
[125] R. Nasseri, N. Mohammadi, Starch-based nanocomposites: A comparative performance study of cellulose whiskers and starch nanoparticles, Carbohydr. Polym. (2014). doi:10.1016/j.carbpol.2014.01.029.

[126] E. Dickinson, Food emulsions and foams: Stabilization by particles, Curr. Opin. Colloid Interface Sci. 15 (2010) 40–49. doi:10.1016/j.cocis.2009.11.001.
[127] U.T. Gonzenbach, A.R. Studart, E. Tervoort, L.J. Gauckler, Stabilization of foams with inorganic colloidal particles, Langmuir. 22 (2006) 10983–10988. doi:10.1021/la061825a.
[128] Y. Kim, C.B. Park, P. Chen, R.B. Thompson, Maximal cell density predictions for compressible polymer foams, Polymer (Guildf). 54 (2013) 841–845. doi:10.1016/j.polymer.2012.11.067.
[129] Y. Kim, C.B. Park, P. Chen, R.B. Thompson, Towards maximal cell density predictions for polymeric foams, Polymer (Guildf). 52 (2011) 5622–5629. doi:10.1016/j.polymer.2011.09.046.
[130] A. Wong, S.F.L. Wijnands, T. Kuboki, C.B. Park, Mechanisms of nanoclay-enhanced plastic foaming processes: Effects of nanoclay intercalation and exfoliation, J. Nanoparticle Res. 15 (2013). doi:10.1007/s11051-013-1815-y.
[131] S.N. Leung, A. Wong, L.C. Wang, C.B. Park, Mechanism of extensional stress-induced cell formation in polymeric foaming processes with the presence of nucleating agents, J. Supercrit. Fluids. 63 (2012) 187–198. doi:10.1016/j.supflu.2011.12.018.
[132] B.P. Binks, R. Murakami, Phase inversion of particle-stabilized materials from foams to dry water., Nat. Mater. 5 (2006) 865–869. doi:10.1038/nmat1757.
[133] B.P. Binks, Particles as surfactants - Similarities and differences, Curr. Opin. Colloid Interface Sci. 7 (2002) 21–41. doi:10.1016/S1359-0294(02)00008-0.
[134] K. Du, E. Glogowski, T. Emrick, T.P. Russell, A.D. Dinsmore, Adsorption energy of nano- and microparticles at liquid-liquid interfaces., Langmuir. 26 (2010) 12518–22. doi:10.1021/la100497h.
[135] K.D. Danov, P.A. Kralchevsky, Capillary forces between particles at a liquid interface: General theoretical approach and interactions between capillary multipoles, Adv. Colloid Interface Sci. 154 (2010) 91–103. doi:10.1016/j.cis.2010.01.010.
[136] K. Casson, D. Johnson, Surface-Tension-Driven Flow Due to the Adsorption and Desorption of Colloidal Particles, J. Colloid Interface Sci. 242 (2001) 279.
[137] L. Dong, D. Johnson, Surface Tension of Charge-Stabilized Colloidal Suspensions at the Water-Air Interface, Langmuir. 19 (2003) 10205–10209. doi:10.1021/la035128j.
[138] P.A. Kralchevsky, K. Nagayama, Capillary interactions between particles bound to interfaces, liquid films and biomembranes, Adv. Colloid Interface Sci. 85 (2000) 145–192. doi:10.1016/S0001-8686(99)00016-0.
[139] F. Bresme, M. Oettel, Nanoparticles at fluid interfaces, J. Phys. Condens. Matter. 19 (2007) 413101. doi:10.1088/0953-8984/19/41/413101.
[140] W. Stober, Controlled growth of monodisperse silica spheres in the micron size range*1, J. Colloid Interface Sci. 26 (1968) 62–69. doi:10.1016/0021-9797(68)90272-5.
[141] D. Nystrӧm, P. Antoni, E. Malmstrӧm, M. Johansson, M. Whittaker, A. Hult, Highly-Ordered Hybrid Organic-Inorganic Isoporous Membranes from Polymer Modified Nanoparticles, Macromol. Rapid Commun. 26 (2005) 524–528. doi:10.1002/marc.200400617.
[142] E.T. Vandenberg, L. Bertilsson, B. Liedberg, K. Uvdal, R. Erlandsson, H. Elwing, et al., Structure of 3-aminopropyl triethoxy silane on silicon oxide, J. Colloid Interface Sci. 147 (1991) 103–118. doi:10.1016/0021-9797(91)90139-Y.
[143] L.T. Zhuravlev, Concentration of hydroxyl groups on the surface of amorphous silicas, Langmuir. 3 (1987) 316–318. doi:10.1021/la00075a004.
[144] M.L. Hair, Hydroxyl groups on silica surface, J. Non. Cryst. Solids. 19 (1975) 299–309. doi:10.1016/0022-3093(75)90095-2.

[145] S. Gupta, Q. Zhang, T. Emrick, A.C. Balazs, T.P. Russell, Entropy-driven segregation of nanoparticles to cracks in multilayered composite polymer structures, Nat. Mater. 5 (2006) 229–233. doi:10.1038/nmat1582.
[146] C.P. Whitby, D. Fornasiero, J. Ralston, L. Liggieri, F. Ravera, Properties of Fatty Amine–Silica Nanoparticle Interfacial Layers at the Hexane–Water Interface, J. Phys. Chem. C. 116 (2012) 3050–3058. doi:10.1021/jp210870v.
[147] R.J.K.U. Ranatunga, C.T. Nguyen, B.A. Wilson, W. Shinoda, S.O. Nielsen, Molecular dynamics study of nanoparticles and non-ionic surfactant at an oil–water interface, Soft Matter. 7 (2011) 6942. doi:10.1039/c1sm05145h.
[148] M. Luo, L.L. Dai, Molecular dynamics simulations of surfactant and nanoparticle self-assembly at liquid–liquid interfaces, J. Phys. Condens. Matter. 19 (2007) 375109. doi:10.1088/0953-8984/19/37/375109.
[149] R.B. Thompson, V. V Ginzburg, M.W. Matsen, A.C. Balazs, Predicting the mesophases of copolymer-nanoparticle composites., Science. 292 (2001) 2469–2472. doi:10.1126/science.1060585.
[150] P. a Kralchevsky, K. Nagayama, Capillary forces between colloidal particles, Langmuir. 10 (1994) 23–36. http://pubs.acs.org/doi/abs/10.1021/la00013a004.
[151] L. Dong, D. Johnson, Interfacial tension measurements of colloidal suspensions: An explanation of colloidal particle-driven interfacial flows, Adv. Sp. Res. 32 (2003) 149–153. doi:10.1016/S0273-1177(03)90245-6.
[152] S.-Y. Lin, Y.-Y. Lin, E.-M. Chen, C.-T. Hsu, C.-C. Kwan, A Study of the Equilibrium Surface Tension and the Critical Micelle Concentration of Mixed Surfactant Solutions, Langmuir. 15 (1999) 4370–4376. doi:10.1021/la981149f.
[153] V. Garbin, J.C. Crocker, K.J. Stebe, Nanoparticles at fluid interfaces: exploiting capping ligands to control adsorption, stability and dynamics., J Colloid Interf Sci. 387 (2012) 1. doi:10.1016/j.jcis.2012.07.047.
[154] E. Turan, S. Demirci, T. Caykara, Synthesis of thermoresponsive poly(N-isopropylacrylamide) brush on silicon wafer surface via atom transfer radical polymerization, Thin Solid Films. 518 (2010) 5950–5954. doi:10.1016/j.tsf.2010.05.103.
[155] K. Matyjaszewski, H. Dong, W. Jakubowski, J. Pietrasik, A. Kusumo, Grafting from surfaces for "everyone": ARGET ATRP in the presence of air., Langmuir. 23 (2007) 4528–31. doi:10.1021/la063402e.
[156] V. Khoshkava, M.R. Kamal, Effect of surface energy on dispersion and mechanical properties of polymer/nanocrystalline cellulose nanocomposites., Biomacromolecules. 14 (2013) 3155–63. doi:10.1021/bm400784j.
[157] Hideo Nakae, Ryuichi Inui, Yosuke Hirata, Hiroyuki Saito, Effects of surface roughness on wettability, Acta Mater. 46 (1998) 2313–2318. doi:10.1016/S1359-6454(98)80012-8.
[158] J.-Y. Lee, Q. Zhang, T. Emrick, A.J. Crosby, Nanoparticle Alignment and Repulsion during Failure of Glassy Polymer Nanocomposites, Macromolecules. 39 (2006) 7392–7396. doi:10.1021/ma061210k.
[159] S. Tyagi, J.Y. Lee, G.A. Buxton, A.C. Balazs, Using nanocomposite coatings to heal surface defects, Macromolecules. 37 (2004) 9160–9168. doi:10.1021/ma048773l.
[160] M. Asada, P. Gin, M.K. Endoh, S.K. Satija, T. Taniguchi, T. Koga, Directed self-assembly of nanoparticles at the polymer surface by highly compressible supercritical carbon dioxide, Soft Matter. 7 (2011) 9231. doi:10.1039/c1sm05693j.
[161] T. Koga, P. Gin, H. Yamaguchi, M.K. Endoh, M. Asada, L. Sendogdular, et al., Generality of anomalous expansion of polymer chains in supercritical fluids, Polym. (United Kingdom). 52 (2011) 4331–4336. doi:10.1016/j.polymer.2011.07.039.

[162] A. Ameli, M. Nofar, D. Jahani, G. Rizvi, C.B. Park, Development of high void fraction polylactide composite foams using injection molding: Crystallization and foaming behaviors, Chem. Eng. J. 262 (2015) 78–87. doi:10.1016/j.cej.2014.09.087.
[163] A. Ameli, D. Jahani, M. Nofar, P.U. Jung, C.B. Park, Development of high void fraction polylactide composite foams using injection molding: Mechanical and thermal insulation properties, Compos. Sci. Technol. 90 (2014) 88–95. doi:10.1016/j.compscitech.2013.10.019.
[164] C.-Y. Hung, C.-C. Wang, C.-Y. Chen, Enhanced the thermal stability and crystallinity of polylactic acid (PLA) by incorporated reactive PS-b-PMMA-b-PGMA and PS-b-PGMA block copolymers as chain extenders, Polymer (Guildf). 54 (2013) 1860–1866. doi:10.1016/j.polymer.2013.01.045.
[165] H. Tsuji, M. Sawada, L. Bouapao, Biodegradable polyesters as crystallization-accelerating agents of poly(l-lactide)., ACS Appl. Mater. Interfaces. 1 (2009) 1719–1730. doi:10.1021/am9002759.
[166] V. Nagarajan, K. Zhang, M. Misra, A.K. Mohanty, Overcoming the Fundamental Challenges in Improving the Impact Strength and Crystallinity of PLA Biocomposites: Influence of Nucleating Agent and Mold Temperature, ACS Appl. Mater. Interfaces. 7 (2015) 11203–11214. doi:10.1021/acsami.5b01145.
[167] H. Li, M.A. Huneault, Effect of nucleation and plasticization on the crystallization of poly(lactic acid), Polymer (Guildf). 48 (2007) 6855–6866. doi:10.1016/j.polymer.2007.09.020.
[168] R. Androsch, H.M.N. Iqbal, C. Schick, Non-isothermal crystal nucleation of poly (l-lactic acid), Polymer (Guildf). 81 (2015) 151–158. doi:10.1016/j.polymer.2015.11.006.
[169] K. Sarikhani, K. Jeddi, R.B. Thompson, C.B. Park, P. Chen, Effect of pressure and temperature on interfacial tension of poly lactic acid melt in supercritical carbon dioxide, Thermochim. Acta. 609 (2015) 1–6. doi:10.1016/j.tca.2015.04.005.
[170] K. Sarikhani, K. Jeddi, R.B. Thompson, C.B. Park, P. Chen, Adsorption of Surface-Modified Silica Nanoparticles to the Interface of Melt Poly(lactic acid) and Supercritical Carbon Dioxide, Langmuir. 31 (2015) 5571–5579. doi:10.1021/acs.langmuir.5b00306.
[171] G.Z. Papageorgiou, D.S. Achilias, D.N. Bikiaris, G.P. Karayannidis, Crystallization kinetics and nucleation activity of filler in polypropylene/surface-treated SiO2 nanocomposites, Thermochim. Acta. 427 (2005) 117–128. doi:10.1016/j.tca.2004.09.001.
[172] O.C. Wokadala, S.S. Ray, J. Bandyopadhyay, J. Wesley-Smith, N.M. Emmambux, Morphology, thermal properties and crystallization kinetics of ternary blends of the polylactide and starch biopolymers and nanoclay: The role of nanoclay hydrophobicity, Polymer (Guildf). 71 (2015) 82–92. doi:10.1016/j.polymer.2015.06.058.
[173] M. Avrami, Kinetics of Phase Change. I General Theory, J. Chem. Phys. 7 (1939) 1103. doi:10.1063/1.1750380.
[174] M. Avrami, Kinetics of Phase Change. II - Transformation-Time Relations for Random Distribution of Nuclei, J. Chem. Phys. 8 (1940) 212–224. doi:10.1063/1.1750631.
[175] L.H. Sperling, Introduction to Physical Polymer Science, 2006. doi:10.1021/ed078p1469.1.
[176] K.S. Kim, H.M. Lee, I.S. Youn, M. Saleh, J.W. Lee, Interactions of CO2 with various functional molecules, Phys. Chem. Chem. Phys. 17 (2015) 10925–10933. doi:10.1039/C5CP00673B.
[177] G.P. Knowles, J. V. Graham, S.W. Delaney, A.L. Chaffee, Aminopropyl-functionalized mesoporous silicas as CO2 adsorbents, Fuel Process. Technol. 86 (2005) 1435–1448. doi:10.1016/j.fuproc.2005.01.014.
[178] S.N. Leung, C.B. Park, H. Li, Numerical simulation of polymeric foaming processes using modified nucleation theory, Plast. Rubber Compos. 35 (2006) 93–100. doi:10.1179/174328906X103079.

[179] P.. Wilt, Nucleation rates and bubble stability in water-carbon dioxide solutions, J. Colloid Interface Sci. 112 (1986) 530–538. doi:10.1016/0021-9797(86)90122-0.
[180] J.C. Fisher, The fracture of liquids, J. Appl. Phys. 19 (1948) 1062–1067. doi:10.1063/1.1698012.
[181] Y. Chevalier, M.A. Bolzinger, Emulsions stabilized with solid nanoparticles: Pickering emulsions, Colloids Surfaces A Physicochem. Eng. Asp. 439 (2013) 23–34. doi:10.1016/j.colsurfa.2013.02.054.
[182] K. Matyjaszewski, D. Hongchen, W. Jakubowski, J. Pietrasik, A. Kusumo, Grafting from surfaces for "everyone": ARGET ATRP in the presence of air, Langmuir. 23 (2007) 4528–4531. doi:10.1021/la063402e.
[183] S.H. Mahmood, A. Ameli, N. Hossieny, C.B. Park, The interfacial tension of molten polylactide in supercritical carbon dioxide, J. Chem. Thermodyn. 75 (2014) 69–76. doi:10.1016/j.jct.2014.02.017.
[184] B. Nagendra, K. Mohan, E.B. Gowd, Polypropylene/Layered Double Hydroxide (LDH) Nanocomposites: Influence of LDH Particle Size on the Crystallization Behavior of Polypropylene, ACS Appl. Mater. Interfaces. 7 (2015) 12399–12410. doi:10.1021/am5075826.
[185] J. Huang, M.S. Lisowski, J. Runt, E.S. Hall, R.T. Kean, N. Buehler, et al., Crystallization and Microstructure of Poly(L-lactide-co-meso-lactide) Copolymers, Macromolecules. 31 (1998) 2593–2599. doi:10.1021/ma9714629.
[186] S. Baratian, E.S. Hall, J.S. Lin, R. Xu, J. Runt, Crystallization and solid-state structure of random polylactide copolymers: Poly(L-lactide-co-D-lactide)s, Macromolecules. 34 (2001) 4857–4864. doi:10.1021/ma001125r.
[187] L.C. López, G.L. Wilkes, Crystallization kinetics of poly(p-phenylene sulphide): effect of molecular weight, Polymer (Guildf). 29 (1988) 106–113. doi:10.1016/0032-3861(88)90207-8.
[188] H. Tsuji, H. Takai, N. Fukuda, H. Takikawa, Non-Isothermal Crystallization Behavior of Poly(L-lactic acid) in the Presence of Various Additives, Macromol. Mater. Eng. 291 (2006) 325–335. doi:10.1002/mame.200500371.
[189] P. De Santis, A.J. Kovacs, Molecular conformation of poly(S-lactic acid), Biopolymers. 6 (1968) 299–306. doi:10.1002/bip.1968.360060305.
[190] C.W. Z.Su, Y.Liu, W.Guo, Q. Li, Crystallization Behavior of Poly(Lactic Acid) Filled with Modified Carbon Black, J. Macromol. Sci. Part B Phys. 48 (n.d.) 670–683. doi:10.1080/00222340902837238.
[191] D. Turnbull, J.C. Fisher, Rate of Nucleation in Condensed Systems, J. Chem. Phys. 17 (1949) 71–73. doi:doi: 10.1063/1.1747055.
[192] N. (Ed. . Hannay, Treatise on Solid State Chemistry, n.d.
[193] J.D. Hoffman, J.I. Lauritzen, Crystallization of Bulk Polymers With Chain Folding : Theory of Growth of Lamellar Spherulites, J. Res. Natl. Bur. Stand. - A. Phys. Chem. 65 (1961) 1961. doi:10.6028/jres.065A.035.
[194] A.J.K. T. Suzuki, Temperature dependence of spherulitic growth rate of isotactic polystyrene. A critical comparison with the kinetic theory of surface nucleation, Polym. J. 1 (1970) 82–100. doi:doi:10.1295/polymj.1.82.
[195] L.H. Sperling, Introduction to Physical Polymer Science, 2005. doi:10.1002/0471757128.
[196] Z. Su, Q. Li, Y. Liu, G.-H. Hu, C. Wu, Multiple Melting Behavior of Poly(lactic acid) Filled with Modified Carbon Black, J. Polym. Sci. PART B-POLYMER Phys. 47 (2009) 1971–1980. http://gateway.isiknowledge.com/gateway/Gateway.cgi?GWVersion=2&SrcAuth=AegeanSoftware&SrcApp=NoteExpress&DestLinkType=FullRecord&DestApp=WOS&KeyUT=000270692400002.

[197] M. Nofar, W. Zhu, C.B. Park, Effect of dissolved CO2 on the crystallization behavior of linear and branched PLA, Polymer (Guildf). 53 (2012) 3341–3353. doi:10.1016/j.polymer.2012.04.054.
[198] D. Li, T. Liu, L. Zhao, X. Lian, W. Yuan, Foaming of Poly(lactic acid) Based on Its Nonisothermal Crystallization Behavior under Compressed Carbon Dioxide, Ind. Eng. Chem. Res. 50 (2011) 1997–2007. doi:10.1021/ie101723g.
[199] Z. Zhang, Y.P. Handa, An in situ study of plasticization of polymers by high-pressure gases, J. Polym. Sci. 36 (1998) 977–982. doi:10.1002/(sici)1099-0488(19980430)36:6<977::aid-polb5>3.0.co;2-d.
[200] T.S. Chow, Molecular Interpretation of the Glass Transition Temperature of Polymer-Diluent Systems, Macromolecules. 13 (1980) 362–364. doi:10.1021/ma60074a029.
[201] M. Takada, S. Hasegawa, M. Ohshima, Crystallization Kinetics of Poly(L-lactide) in Contact With Pressurized CO2, Polym. Eng. Sci. 44 (2004) 186–196. doi:10.1002/pen.20017.
[202] M. Nofar, A. Tabatabaei, A. Ameli, C.B. Park, Comparison of melting and crystallization behaviors of polylactide under high-pressure CO 2, N 2, and He, in: AIP Conf. Proc., 2014: pp. 320–323. doi:10.1063/1.4873791.
[203] Y. (Eds.). Neumann, A. W., David, R., Zuo, Applied surface thermodynamics (Vol. 151)., CRC Press: Taylor & Francis Group, 2010.
[204] C. Van Oss, R. Good, M. Chaudhury, C. Oss, Additive and nonadditive surface tension components and the interpretation of contact angles, Langmuir. 4 (1988) 884–891. doi:10.1021/la00082a018.